MASTER'S THESIS

Indirect Nanoplasmonic Sensing Study of Z907 Dye Molecules Interacting with TiO_2 Films for Dye Sensitized Solar Cell Applications

Emmanuel NKURUNZIZA

SUPERVISOR

Dr. Viktoria Gusak

Chalmers University of Technology

EXAMINER

Assistant professor Christoph Langhammer

Chalmers University of Technology

Department of Applied Physics

Division of Chemical Physics

Göteborg, Sweden, 2014

Indirect Nanoplasmonic Sensing Study of Z907 Dye Molecules Interacting with TiO_2 Films for Dye Sensitized Solar Cell Applications

Master Thesis within the Applied Physics Master Programme
Emmanuel NKURUNZIZA

Department of Applied Physics
Chemical Physics
Chalmers University of Technology
SE-412 96 Göteborg
Sweden
Telephone: +46(0)31-772 1000

Chalmers Reproservice
Göteborg, Sweden 2014

Abstract

In todays society, increasing demand to switch to renewable energy has triggered the scientific community to have a deep interest in the Dye Sensitized Solar Cell (DSSC), which is thought to be one of the future's reliable sources of solar energy because of its low cost and simple manufacture compared to conventional semiconductor photovoltaics (PV). Still, at the molecular level, many of the phenomena crucial for the DSSC optimum performance are not well understood and this has had a consequence of a very small improvement in the performance of the device in the last two decades (until a recent breakthrough by using solid - state sensitizers). Nanotechnology has provided plasmonics-based sensors such as Indirect Nanoplasmonic Sensing (INPS), which are effective for studying the dye adsorption process (one of the core phenomena for the functioning of a DSSC) with high sensitivity, *in situ*, and in real time.

In this thesis, INPS was used to investigate the real time adsorption and desorption of dye (Na/Z907) molecules on flat TiO_2 surfaces, which mimic the cathode of the DSSC. From the INPS real time adsorption/desorption kinetics, values of rate constants and equilibrium adsorption constants were obtained. They are in agreement with the ones obtained when Langmuir isotherms of the equilibrium coverage for different concentration were used. The existence of loosely bound dye molecules has been experimentally proven by a series of intermittent adsorptions and desorption cycles. These experiments showed a decreased desorption rate after each adsorption-desorption cycle, which is explained by removal of the loosely bound molecules during each rinsing step to promote the reorganization of the dye molecules on the surface and thereby increasing its stability. Finally, a method to calculate the number of dye molecules adsorbed/desorbed was successfully adapted, which allowed the interpretation of the achieved quality of the dye layer formed in terms of dye molecules per unit surface that would participate in electricity generation in a real DSSC.

Key words: Dye Sensitized Solar Cell (DSSC), Indirect Nanoplasmonic Sensing (INPS), Langmuir isotherms, loosely bound dye molecules, centroid shift.

Acknowledgements

During this project, there have been a number of inspiring and helpful people involve into it and others who helped me to achieve it, to whom I owe a sincere gratitude.

To begin, I would like to thank Dr. Viktoria Gusak who has been my day to day supervisor, for borrowing the experimental set up, spending a lot of time and using a lot of efforts manufacturing the nanosensors and being involved in different discussion regarding this project. Thanks to Assistant professor Christoph Langhammer for allowing this project to benefit from his collaboration with Professor Michael Grätzel Group, for general discussions and input on different aspects of the project. Thanks to Martin Wersäll for rewarding discussion which inspired me to initiate the quantitative studies involving the important systems used in this project and Adam Arvidsson for taking the time and read this report, for a nice discussion and corrections.

For sure, my family constantly motivated me, but also during this project, I got unwavering support from the following people:

Linnea Russo. The family of Daniel Wagner. The family of Emmanuel Nzatunga. The family of Michael Mwera. The family of Cesar Kisangani Makombe. The family of Paul Oladele Olayinka without forgetting “the family” of David Baugh.

This project has been done during my scholarship period at Chalmers University of Technology.

Thanks to Swedish Institute scholarship.

Emmanuel NKURUNZIZA, Göteborg 17/02/2014

Contents

1. **Introduction**.....1
2. **Theoretical background**……...……4
   2.1. Interaction of dye molecules with TiO_2 …… 4
      2.1.1. Basics of DSSC…….4
      2.1.2. Langmuir model and Kinetics of Adsorption and Desorption ……..……6
      2.1.3. The Kinetic model of Ruthenium Complex-Dye on TiO_2 ……...……8
   2.2. Plasmonic sensing ……..……..9
      2.2.1. Basics of Plasmon Physics ……..……..9
      2.2.2. Principles of Indirect Nanoplasmonic Sensing (INPS) ……..…….10
      2.2.3. INPS for Z907 dyes interacting with TiO_2 for DSSC Applications —our case study……..……12
3. **Experimental** ……..……14
   3.1. INPS Sample systems and design ……..……14
   3.2. Dye -Solvent systems ……..……..16
   3.3. Dye solution concentration determination by spectrophotometry ……...…….18
   3.4.INPS Experimental Setup ……..……21
4. **Experimental results and Discussion** ……..……..24
   4.1. Overview: dye-solvent-sample systems ……...…….24
   4.2. Results from the NaZ907MeCN: tbuOH-sput system ……..25
   4.3. Results from the NaZ907MeCN: tbuOH-ALD system ……...…. 30
   4.4. Results from the Na/Z907DMSO-ALD system ……..……...33
      4.4.1. The stability of the DMSO systems ……..……33
      4.4.2. Adsorption results of the NaZ907DMSO-ALD system ……34
      4.4.3. Suspected non- Langmuirian desorption of the NaZ907DMSO -ALD system ……..……42
   4.5.Theoretical estimation of the amount of molecules adsorbed/desorbed from INPS ……..……46
   4.6.Intermittent adsorption-desorption ……48
   4.7.Blue shift in the adsorption curve ……..……54

5. **Conclusions and outlook** ……..……..57
   5.1.Conclusion ……57
   5.2.Outlook ……..……59

Bibliography ……..……60

Appendices ……..63

Appendix 1. Plasmon Physics ……..……63

Appendix 2. Plasmon Peak fitting procedure for the extinction spectroscopy ……67

Appendix 3. Full-measurement-time of principal concentrations 70

1

Introduction

THE WORLD'S HUNGER FOR AND CONCERN ABOUT ENERGY is increasing, and so is the research in the field of energy related materials. In the last 20 years, tremendous efforts were put in finding a reliable and sustainable energy source for the future. Before the 1990's it was hard for researchers to believe in the possibility of a large-scale solar electricity production using a device based on molecular components, but in 1991, O'Regan and M. Grätzel [1] initiated the development of the Dye-Sensitized Solar Cells (DSSCs). The main part of a DSSC is a porous oxide (often TiO_2) film, covered with a monolayer of organic dye (or sensitizer), and immersed into an electrolyte. The dye molecules absorb light, and the generated excited electrons diffuse to the TiO_2 film, from where they eventually reach the external circuit to produce work. Contrary to the semiconductor photovoltaic technology, what is needed for DSSCs is very large material interfaces (oxide/dye/electrolyte interfaces; high material purity not required); there is no built-in electric field, but phenomena such as light harvesting, charge separation and charge transportation occur at the oxide/dye interface.

However, it is not completely clear how to form the optimal monolayer of dye on the oxide and how to improve its stability. Therefore, the objective of the work connected with this thesis is to use a Ruthenium (Ru)-dye molecule (Z907) in adsorption and desorption studies with the goal to achieve a good quality, dense monolayer of Ru-dye molecules on the TiO_2

flat films. This is one of the things of great importance for the optimal performance of DSSCs. Moreover, we address the question of whether a simple Langmuirian adsorption kinetics, which is commonly used for describing the adsorption process in dye-TiO_2 systems, holds for the system considered in this work. The work reported here is one of many efforts done to try to elucidate the nature of the interaction dye-TiO_2 and the dye stability at these interfaces.

In the last two decades the dye-sensitized solar cells (DSSCs) have become one of the competitors of semiconductor photovoltaics (PV), mainly for indoor applications. By improving the performance of the device from its nanoscale properties, it is believed that DSSCs will deliver electricity at large scale for less than $ 0.5 per Watt peak (Wp) whereas the current PV power production price is around $ 3/Wp. That is why many companies are developing interest in this new technology [2]. The DSSC consists of several material layers, and in a following chapter (section 2.2.1) we are going to explain the DSSC structure, the electron transfer processes through these layers and why among these components the dye layer is one of the most important ones.

Promising features of the DSSC have triggered the research community to gradually improve it as the future source of energy. Since its invention in 1991, it was reported to be a low-cost, high-efficiency solar cell [1]. Then it took a number of years for Wang et al, 2003 [3] to solve the problem of thermostability, which impeded the outdoor applications, by engineering the ruthenium amphiphilic dye Z-907. In the section 3.2 of the third chapter, we will motivate the choice of the Z907 (or DN520) and its sodium salt Z907Na dyes to be used in the experiment connected to this project, among the hundreds of the dye molecules, which could be used. The understanding of how this dye interacts with the TiO_2 sites and the way we interpret what happens upon adsorption and desorption is a result of a two-decade endeavor.

Since the breakthrough of B. O'Regan and M. Grätzel, the DSSC efficiency of 6.1% was boosted to the nowadays efficiency of 11-12%. To be able to do that, a progressive understanding of the chemical identity of the Z907—TiO2 interaction, among other things, was needed. Nazeeruddin et al. 2003 [4] published the commonly accepted chemisorption of Ru-based dye(such as Z907) on the TiO_2 surface using 2 carboxylate groups found on the peripheral ligands of the Dye molecule. Pérez et al. 2006 [5] also support this chemisorption through 2 carboxylate groups using either a monodentate ester-type linkage, a bidentate chelating or bridging linkage, or physisorption via single or double hydrogen bonding. Shklover et al. 1998 [6] studied the structural model of the sensitizer and its anchoring to the TiO_2. Their work supported the idea of chemisorption via 2 carboxylic groups and suggested that for the 2 adsorbed carboxylic groups, the most stable structure is when one of them is covalently bonded and the other is hydrogen bonded. Lee et al. 2010 [7] highlighted this idea

of the partial physisorption of the dye molecules by supporting the picture of one bidentate bridged and the other hydrogen bonded.

In some of the recent works it was found useful to study the gain a DSSC can have if the arrangement of dye molecules on the TiO_2 surface is optimized. Fillinger and Parkinson, 1999 [8] postulated a two-step dye adsorption mechanism where initial binding of dye is with one carboxylate, with subsequent binding of two or more carboxylate groups. De Angelis et al., 2010 [9] have shown that the adsorption geometry of dye molecules on TiO_2 affects the photovoltage and thus the efficiency of a DSSC. Many new dye molecules of various structures and different numbers of carboxylic acid, responsible for the binding, are being engineered,. A number of them are reported in Hagberg et al, 2008 [10]. Bazzan et al. 2011 [11] used Z-907 (designed with only two acid groups) in a series of desorption/adsorption cycling process repeated several times, and demonstrated an increase in the power conversion efficiency of up to 23%. This suggests the importance of understanding and controlling the dye adsorption geometry for the optimal solar cell performance. Also other studies like the one by Harms et al. 2012[12], where the Z907-dye adsorption and desorption were studied using the QCM-D, gave a motivation to the possibility to achieve a good quality, dense monolayer of Ru-dye molecules on the TiO_2 flat films using adsorption and desorption cycles.

The INPS (Indirect Nanoplasmonic Sensing) technique, which will be explained in sections 2.2.2 and 2.2.3, has been introduced by Langhammer et al. 2010 [13] and proven to be a versatile experimental platform for measurements of the kinetics and the thermodynamics of processes in /on nanomaterials and thin films, *in situ* and in real time. It can operate in a wide range of the electromagnetic spectrum, at various gas pressures and environments, and even at high temperatures. Gusak et al. 2012 [14] reported the possibility of detecting various maneuvers for optimizing the Z-907 dye desorption/adsorption and diffusion on TiO_2 surfaces (flat and mesoporous) in real time, using INPS as the experimental platform. INPS is also the sensing method that is used in the experiments presented in this work. The entire apparatus to make our experiments possible is presented in the third chapter. And the results (presented in the fourth chapter) answer important questions such as: (1) How could one reorganize a dye layer on the TiO_2 and thus have a more closely packed dye layer? (2) What are advantages and drawbacks of the material and methods used in this work? The fifth chapter will show the contribution this work makes in the research community in terms of energy production and propose the solutions the drawbacks of our used system. To get started, let's remind ourselves in the following chapter of the background which forms the basis of the work presented in this report.

2

Background

In this chapter two main things are discussed: (1) formation of a monolayer of ruthenium dye molecules on TiO_2 using Langmuir model; (2) Indirect Nanoplasmonic Sensing (INPS) as a tool for studying in real time and *in situ* the compactness and the stability of formed layer on the semiconductor surface.

We start with a motivation for our study by showing why a dense and stable layer of dye molecules is very important for the optimal performance of the DSSC. Our aim is to address the question of how the dye molecules adsorb on the TiO_2 surface, what types of adsorption sites are present on TiO_2, and how they change in different conditions. We will show how one can address this using the Indirect Nanoplasmonic Sensing (INSP) technique, developed in the Chemical Physics group at Chalmers University of Technology, on a model system of flat TiO_2 films.

In this chapter, we will also introduce, briefly, the physical phenomenon that gives rise to localized surface plasmons. We will conclude the chapter by showing what part our sample represents in the complete functional DSSC, and how it is used to study the reaction of the Ru-dye molecules with the TiO_2 surface.

2.1. Interaction of dye molecules with TiO_2

2.1.1. Basics of a DSSC

To harvest electricity from the sun using a dye-sensitized solar cell, the following processes have to take place. A photon strikes a dye molecule adsorbed on the TiO_2 and promotes the dye to an excited state. The molecule then de-excites by injecting an electron into the

conduction band of the TiO_2, provided that the involved energy levels are aligned properly. The electron then diffuses through the TiO_2 film and eventually reaches the back electrode where it is collected and then fed into the outer circuit to do its work. The electron then returns to the cell through the bottom-conducting layer (fig. 2.1, left). With the help of a catalyst, the electron enters back into the electrolyte, which finally transfers the electron back to the oxidized dye. In this way, the dye is reduced to its inactivated state, ready to receive a photon again.

In practice, we expect much more complex molecular interactions (based on the electron transfer processes) for the DSSC functioning [15]. Nevertheless for simplicity, Hagfeldt et al. 2010 [2] have classified all these phenomena into 7 categories (see figure 2.1, right). 5 out of these 7 core phenomena are directly related to the dye molecules adsorbed on the mesoporous TiO_2 and take place on the oxide/dye/electrolyte interfaces. Many of these phenomena are not fully understood, and their understanding is crucial for the DSSC optimum performance. We are not attempting to understand all these phenomena, but we strongly believe that understanding of the formation of the stable and dense dye monolayer on the oxide surface is an important part and will help increase the performance of a DSSC. For that reason this project is restricted to study how we would achieve this monolayer of the dye molecules on the semiconductor (TiO_2) surface and we don't discuss other important DSSC parameters such as efficiency, I-V curve measurements, the Incident photon to current efficiency (IPCE) and the absorbed photon to current efficiency (APCE), etc.

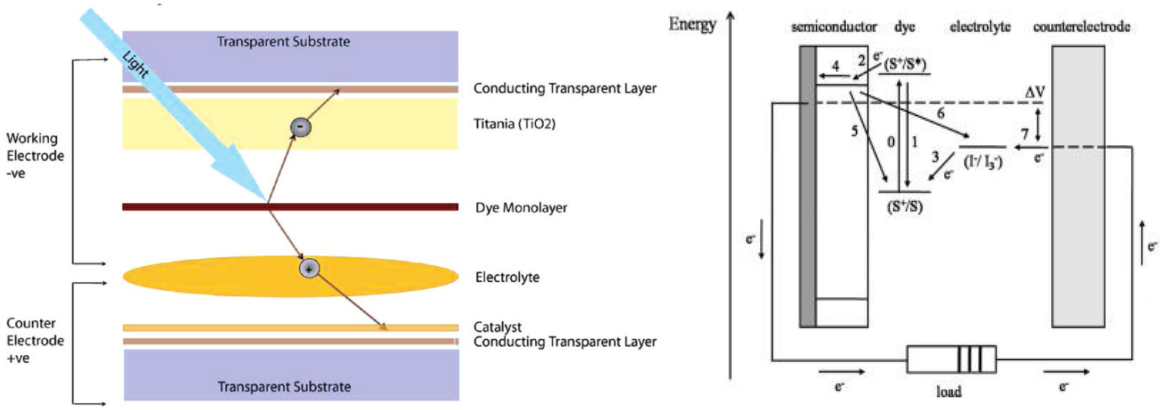

Figure 2.1 *(Left) A Schematic overview of the DSSC. (Right) Transition of the dye to the excited state (Phenomenon 1) is followed by the quick electron injection into the TiO_2 conduction band (Phenomenon 2). Phenomenon 3 is regeneration of the oxidized dye due to a reaction with the electron donor (in most of the cases I^-) present in the redox electrolyte. Phenomenon 4 is electron transportation through mesoporous TiO_2 (the phenomenon not fully understood so far). Phenomenon 5 and 6 are recombination, from the conduction band of the TiO_2 to the dye molecule and to the electrolyte, respectively.*

The study approach we have chosen is to simplify the real DSSC and remain with a model system where the adsorption/desorption of dye molecules can be traced in time under well-controlled conditions. Two main simplifications are done to the oxide/dye/electrolyte interfaces: (1) we consider only the interface oxide/dye; (2) the complex surface (of a mesoporous film) is reduced to a flat TiO_2 surface. Since in this work we have studied the

kinetics of adsorption and desorption of dye molecules, we need to introduce the Langmuir kinetics model, which is commonly used for description of such processes.

2.1.2. Langmuir model and Kinetics of Adsorption and Desorption

The Langmuir isotherm is a model, which can be used to describe the reaction of molecules in gas or liquid phase coming in contact with the solid surface at a fixed temperature.

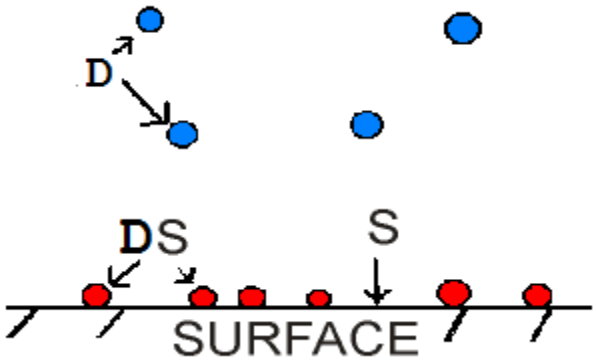

Figure 2.2 *A schematic of the adsorption process as described by the Langmuir model: D is the dye molecule in the liquid phase. S is the vacant surface site. DS is the occupied surface site.*

According to this simple model, the adsorption (the forward reaction) and the desorption (the backward reaction) can be represented by the equations:

$$S + D \underset{(d)}{\overset{(a)}{\rightleftarrows}} SD, \qquad (2.1)$$

where D is the dye molecule in the liquid phase, S is the vacant surface site, and DS is the occupied surface site. The model assumes that (i) each adsorption site can hold one molecule at most, (ii) all sites are equivalent, and (iii) there is no interaction between the adsorbed molecules.

Assuming a fixed number, N, of sites at the surface, at equilibrium, $K_a = \frac{[SD]}{[S][D]}$,

$K_d = \frac{[S][D]}{[SD]}$

With $[SD] \propto \theta$ which is the fraction of the adsorbed molecules $0<\theta<1$

$[S] \propto$ S, which is the number of vacant sites $(1-\theta)$

$[D] \propto C$, which is the concentration of dye molecules in the solution,

Assuming the Langmuir adsorption kinetics, the rate of formation of a monolayer of molecules on a surface is expressed as:

$$\frac{d\theta}{dt} = K_a(1-\theta)C - K_d\theta \qquad (2.2)$$

As mentioned above, θ is a unit less number expressing the fraction of monolayer formed, k_a and k_d are rate constants of adsorption and desorption, respectively. Integrating eq. (2.2) gives

$$\theta(t) = \frac{C}{C + K_a/K_d}(1 - e^{-(K_aC + K_d)t}) \qquad (2.3)$$

Simply written as: $\theta(t) = \theta_\infty(1 - e^{-\kappa_{ads}t})$ (2.4)

In the experiments I present in this thesis, we measure the fractional coverage θ as function of time, t, thus, θ_∞, and κ_{ads} are determined by fitting the experimental data to eq. 2.4. By repeating the experiments at different concentrations, and plotting κ_{ads} vs C, a line of slope K_a and y-intercept of K_d (see eq.2.3) can be obtained.

It is also possible to derive the adsorption and desorption rate constants by analyzing the initial stages of adsorption and desorption processes, respectively. At the onset of adsorption, when $\theta \approx 0$, eq. 2.2 simplifies to

$$\frac{d\theta}{dt} = K_aC \qquad (2.5)$$

By measuring the initial slope of an adsorption kinetic curve ($d\theta/dt$) for different dye solution concentrations C, and plotting it as the function of the concentration, one can obtain the adsorption rate constant K_a as the slope of the corresponding linear fit.

Moreover, eq. 2.2 also takes a simple form during desorption when $C \approx 0$:

$$\frac{d\theta}{dt} = -K_d\theta \qquad (2.6)$$

By plotting the desorption slope (in this work, the initial desorption slope was used) versus the coverage at the corresponding time, and fitting the data with a linear dependence, one obtains the value of K_d.

In studies of dye adsorption on TiO_2, often the equilibrium adsorption constant K_{eq} is used. It can be expressed as

$$K_{eq} = \frac{K_a}{K_d} = \frac{\theta}{(1-\theta)C} \Leftrightarrow \theta = \frac{K_{eq}C}{1 + K_{eq}C} \qquad (2.7)$$

The latter dependence is often referred to as the Langmuir isotherm. It relates the equilibrium coverage of adsorbed molecules to their concentration in the solution (or pressure, if

adsorption occurs from a gas phase). From fitting the coverage versus concentration data, it is possible to extract the equilibrium adsorption constant K_{eq}.

2.1.3. The Kinetics of Ruthenium Complex-Dye adsorption on TiO_2

Many authors investigating adsorption and desorption of molecules of Ruthenium complex dyes on TiO_2 surfaces are well aware that the assumptions of Langmuir model, such as equivalence of all sites and independence of the occupation of sites with coverage, are not fully valid for studies involving Ruthenium complex dyes on TiO_2 surfaces. Nevertheless, it is educative to approach studies of those complex systems with the simple Langmuir isotherm, and by doing so, interesting results have been found. In the following, I summarize 3 examples of studies of adsorption/desorption of Ru-dye from the literature, where the Langmuir model was used to obtain important results, however, with some restrictions.

(1) Lee et al. 2011[16] studied adsorption of the N719 done by dipping annealed TiO_2 films in a dye solution for some time. The amount of the adsorbed dye was determined from the absorbance measured with a spectrophotometer, and monitored over time. When plotted, the amount of adsorbed dye as function of adsorption time showed a Langmuir adsorption behavior, which was used to extract the coverage. The reaction of N719 dye adsorption on the used TiO2 was shown to be of pseudo 1^{st}-order adsorption kinetics.

(2) Lu et al, 2006[17] studied adsorption of N3 Ru dye on rutile and anatase single crystal TiO_2 electrodes. Upon dipping the electrodes into dye solutions of various concentrations. The adsorptions isotherms were deduced from photocurrent (IPCE) measurements, and modeled with the Langmuir isotherm. The data followed the Langmuir model reasonably well, although, as the authors point out, some of the assumptions of the model are not valid for the dye-TiO_2 system. Moreover, the authors found indications of possible re-organization of dye molecules on the TiO_2 surface, a process that cannot be accounted for by the Langmuir model in its simplest form..

(3) In Fillinger et al, 1999[8] where the adsorption was done by soaking a mesoporous TiO_2 film in N3 solutions in ethanol, the absorbance of the impregnating dye solution was measured as a function of time. The authors used the Langmuir model to fit the dye loading as the function of the dye solution concentration; although they also pointed out that some of its assumptions are not valid for their system. Additionally, they studied desorption of dye from films with the same dye loading that were impregnated at different concentrations and over different times. The authors observed more desorption from the films that were impregnated at higher concentrations (and during shorter times). This result suggests a 2-step adsorption mechanism, which could be adsorption using first carboxylate (fast, but less strongly bound), followed by the second carboxylate (slow, but strongly bound). Such a two-step adsorption is not accounted for by the simplest Langmuir model.

In the fourth chapter of this report, I will do the analysis of our results using the Langmuir kinetic model, and like in many studies involving adsorption and desorption, I expect deviations from that model. The question whether or not adsorption of dye molecules on TiO_2 follows the Langmuir model is one of the central aspects of our study. We employ a versatile

tool, based on plasmonic sensing, that is capable of measuring in situ and in real time the adsorption and desorption of molecules. Using this experimental platform, we will try to understand the phenomena leading to a dense and stable monolayer via adsorption and desorption.

To this point, a curious reader would want to know how the plasmonic sensing detects the adsorption and desorption of molecules on/from a surface. This is what the next section treats before we explain our experimental tools and methods in chapter 3.

2.2. Plasmonic sensing

2.2.1. Basics of Plasmon Physics

A localized surface plasmon is a quantum mechanical description of a collective oscillation of electrons in a noble metal nanostructure, induced by an electromagnetic wave (light with the energy in and around the visible range). The electrons in the metal nanostructure are spatially confined in a region that is much smaller than the wavelength of the used electromagnetic radiation. In such situation, the oscillating field $\vec{E}(\vec{r},t)$ interacts with the nanoparticle (e.g. in gold) and provokes a displacement of free electrons with respect to the stationary lattice ions. This displacement gives rise to a restoring force of $\vec{F}(\vec{r},t) = q\vec{E}(\vec{r},t)$ * (see figure 2.3).

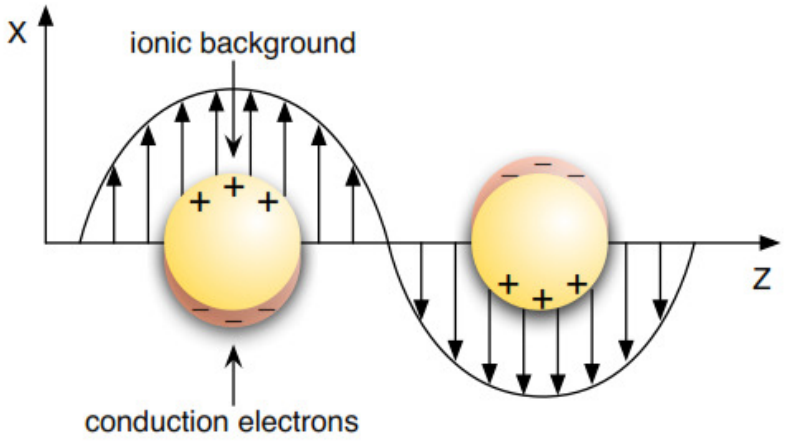

Figure 2.3 *A schematic illustration of the interaction between light and a gold nanoparticle.*

**** Since the plasmon sensing technique is just a tool in this work, in this section we only show the formulae, which describe the phenomena relevant to sensing, used to detect adsorption and desorption of dye molecules on TiO_2 surfaces. For the physics behind the formulae used here, we recommend the reader to see the appendix I entitled "Plasmon Physics")***

The dielectric function of a (free electron) metal (see eq. I5 in ***appendix I***) can be written as:

$$\varepsilon_{free} = 1 - \frac{\omega_{plasma}^2}{\omega^2 + i\kappa\omega} \tag{2.8}$$

For visible and infrared frequencies, $\omega_{plasma}^2 >> \kappa\omega$, so that (2.8) can be written as

$$\varepsilon_{free} = 1 - \frac{\omega_{plasma}^2}{\omega^2} \tag{2.9}$$

Then, using the expression of the Localized Surface Plasmon Resonance (LSPR) condition (see eq. I. 11 in the ***appendix I***) in equation 2.9, we obtain

$$\omega_{LSPR} = \frac{\omega_{plasma}}{\sqrt{1 + 2\varepsilon_{dielec}}} \text{ (Which is equation I.15 for } L_n = 0.5) \tag{2.10}$$

Using eq. I. 16 , the above eq. 2.10 can be written in terms of wavelengths as

$$\lambda_{LSPR} = \lambda_{plasma}\sqrt{2n_{dielec}^2 + 1} \tag{2.11}$$

Equation 2.11 shows a linear dependence of the LSPR peak wavelength on the change in the refractive index of the medium. This is the essence of the plasmonic sensing technique used in this work, and it has been used in this thesis to follow adsorption and desorption of dye molecules on TiO_2 films.

The nanoplasmonic sensing relies on the enhanced electric near field around a nanoparticle at resonance. This field decays exponentially from the nanoparticle surface, with the characteristic decay length on the order of 30 -50 nm (this depends on the dielectric properties of the medium around the particle, and also the particle size and material). Only the changes in the dielectric properties of the surrounding medium that happen within the extension of the near field will be sensed. Thus, the relatively short decay length provides a very local sensitivity of the LSPR sensing technique.

2.2.2. Principles of Indirect Nanoplasmonic Sensing (INPS)

Indirect Nanoplasmonic Sensing (INPS) is an experimental platform where metal (often gold) nanoparticles are covered with a dielectric space layer (of about 10nm), see figure 2.4. This dielectric space layer is thinner than the decay length of the near-field, and thus the plasmonic particles can still act as sensors. The shift of λ_{LSPR} (due to adsorption /desorption, and other type of reaction in the locally enhanced electric field) can be read-off remotely with high resolution, by means of rather simple optical transmission spectroscopy. Adding a dielectric spacer layer on the top of the gold nanostructures has made this method of nanoplasmonic sensing very versatile; it is possible to probe nearly any kind of reaction involving materials

of all phases. Moreover, the addition of the spacer layer also makes it possible to tailor the surface chemistry of the sensor according to the needs for a specific experiment. Here, for example, we can use TiO_2 for this purpose.

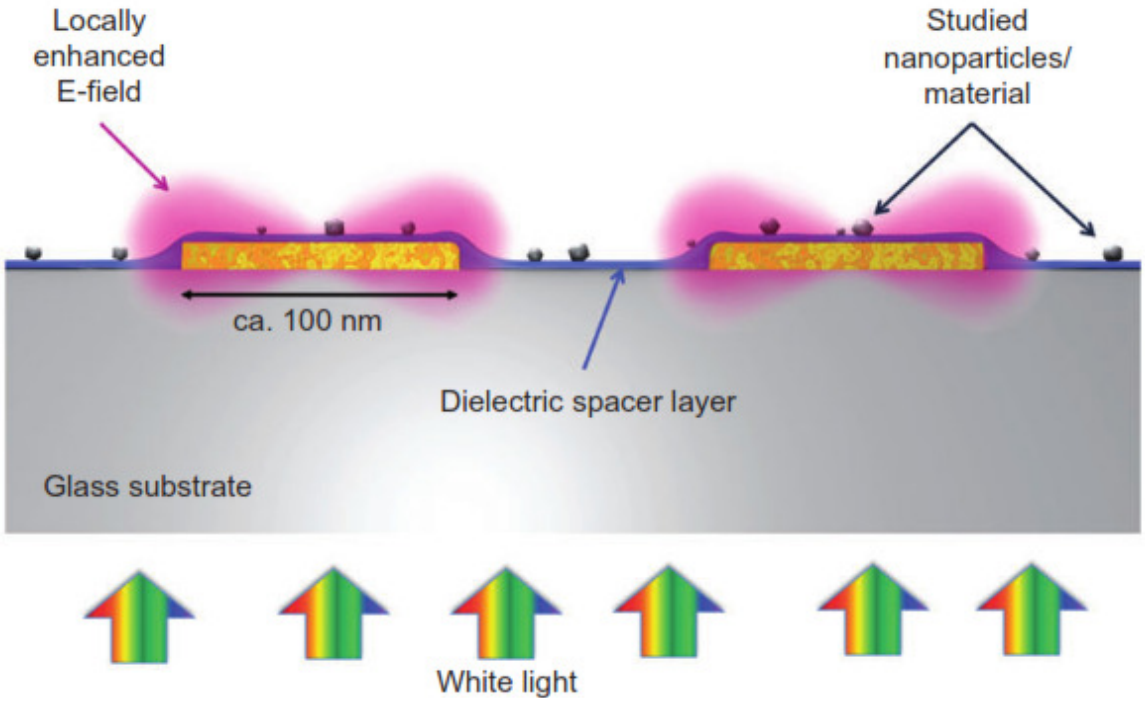

Figure 2.4 *A schematic illustration of the indirect nanoplasmonic sensing platform, INPS. A thin dielectric spacer layer on the sensors is used for protection of the plasmonic Au nanodisk sensors and tailoring of the surface chemistry of the sensor chip.*

To date, INPS has proved to be a useful tool for studying different material properties, for example, the glass transition of confined polymers, catalytic light-off on Pd nanocatalysts, and hydrogen uptake/release in Pd nanoparticles [13]. Other phenomena that can be studied by INPS, according to Larsson et al., 2012 [18], are: different phase transitions (such as melting/freezing transition, insulator/semiconductor/metal transition, ferroelectric/paraelectric transition), corrosion, nanoparticle sintering, recrystallization, molecular diffusion in materials. Moreover, a number of catalytic processes can be sensed with this experimental platform, in particular in the gas phase.

Even in the field of Ru-dye molecules adsorbing on TiO_2 surfaces for DSSC application, INPS has been used to selectively follow dye adsorption locally in the hidden interface region inside of the thick porous TiO_2 DSSC photoelectrode [14]. Thus the technique used in our experiments has been tested and found to be reliable for the measurements to be carried out in this project.

2.2.3. INPS for Z907 dyes interacting with TiO_2 for DSSC Applications – our case study

For our specific case of studying the Ru-dye Z907, the gold nanodiscs have the diameter of 120-150 nm and a constant height of 20 nm. The dielectric spacer layer tailoring the surface sites for dye adsorption is TiO_2 ~ 12 nm thick and the enhanced field volume around the particle will be calculated in chapter 4 of this report. It is estimated to be a couple of tens of nm (see section 4.5).

INPS is able to generate adsorption and desorption curves based on the phenomena explained by eq. 2.9. Upon dye adsorption on the sensor, the lines of the generated nearfield traverses the medium with a larger dielectric constant, and every increase in ε_{dielec} is coupled with an increase in the in λ_{LSPR}; which means that the $\lambda_{LSPR}(t)$ increases to $\lambda_{LSPR}(t+\Delta t)$ $(\lambda_{LSPR}(t+\Delta t) > \lambda_{LSPR}(t))$. This interpretation is also in accordance to the fact that when more dye is adsorbed, its absorption peak shifted to the red, as published in Katoh et al, 2010 [19]. Upon desorption, we observe a reverse situation compared to the adsorption. As the desorption time increases, the peak position shifts to the blue, $\lambda_{LSPR}(t+\Delta t) < \lambda_{LSPR}(t)$.

The structure of the DSSC, represented in figure 2.5, will help the reader to understand what the sample under study represents in the general functioning of the DSSC. It also shows the INPS sample used in the study reported here.

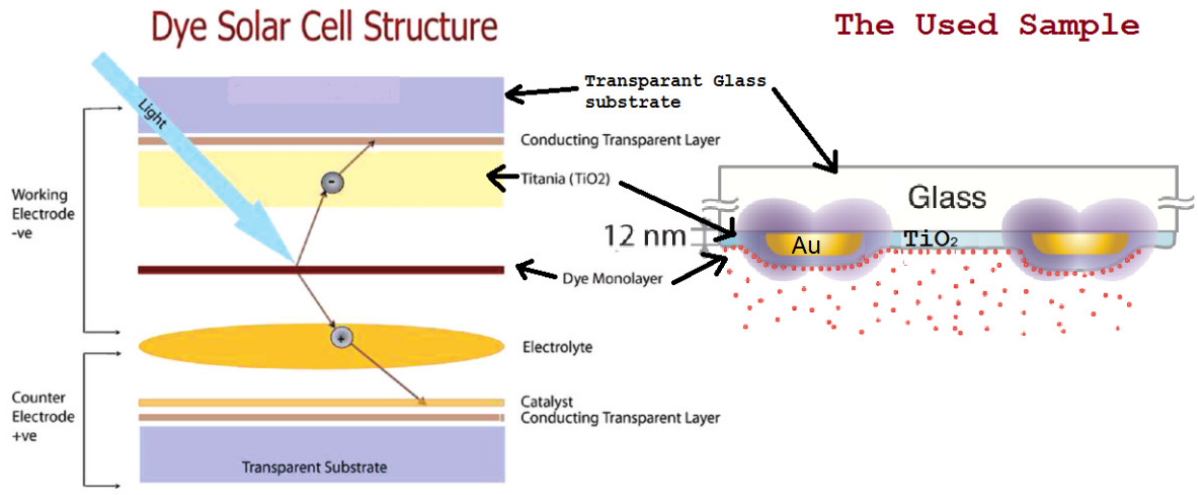

Figure 2.5 *(**left**); Nanoscopic processes taking place in the DSSC, enabling to harvest electricity from the sun. (**right**)What the used sample mimics in the DSSC structure.*

To this point, having the background of the project and knowing the motivation, one would wish to see the results. But still before we present the results obtained, there are questions

such as: Which organic solvents to be used? Of hundreds of existing dye systems, which is to be used, and why? Why the choice of TiO_2 and how are the INPS sensors fabricated? The answers to these questions and some additional reasons for the choice of our experimental system are the subject of the next chapter.

3

Experimental

In this chapter, the aim is to give the reader a thorough explanation of how our experiments of studying the adsorption and desorption of dye molecules look like. I will not only discuss the tools such as samples, dye or experimental set up, but also to some extent the principle behind their function or fabrication. This will help in understanding of the data obtained and it is a good preparation for a better understanding of the way I will analyze and discuss the obtained results in the next chapter.

3.1. INPS sample systems and design

As it has been said in the previous sections, the used nanoplasmonic sensors are comprised of gold nanodiscs of dimensions in the range 100 - 200nm of diameter (see also ***Appendix I—section I.c***). These sensors have been fabricated in the MC2 clean room by a fabrication method called Hole-mask colloidal lithography (HCL). This fabrication method was presented in detail by Fredriksson et al, 2007 and 2009 [20 and 21]. Thus, here, I just mention briefly the most important steps of this fabrication process, see figure 3.1.

The INPS technique introduced above also requires the deposition of an additional layer, the so called the dielectric spacer layer, on the top of the gold nanodiscs. One critical function of this dielectric spacer layer is to provide a sample surface where the surface chemistry can be

tailored according to the requirements for a particular experiment. Moreover, the spacer layer also serves as a protection of the nanodiscs against direct contact with the environment. Here I used a 10 nm thick film of TiO_2 as spacer layer to mimic the surface of the mesoporous TiO_2 photoelectrode layer in a real DSSC.

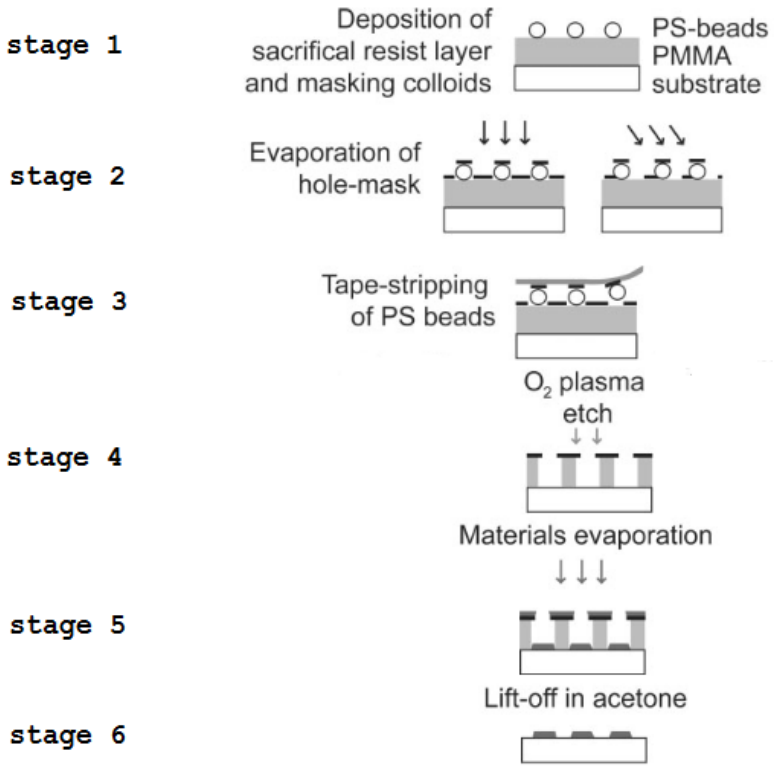

Figure 3.1. *Hole-mask colloidal lithography, image adapted from Fredriksson et al, 2007[20]: (stage 1) First a circular transparent glass (borofloat) substrate, onto which the nanodiscs are going to be grown, is cleaned by step by step sonication in acetone, isopropyl alcohol (IPA) and then methanol. Then, polymetylmetacrylate (PMMA) is spin coated on the top of the substrate in a controlled manner to adjust the PMMA thickness. Then, a 5 second etching in oxygen plasma is applied to reduce the hydrophobicity of PMMA. Then, water (Milli-Qr) suspended polyelectrolyte (poly-diallyldimethylamonuim (PDDA) is layered on the top of PMMA for a short time. Finally, a colloidal solution containing negatively charged polystyrene (PS) particles is layered on the top of the polyelectrolyte layer formed on the PMMA surface. Then, controlled by the coulomb attraction between PDDA and PS, the PS particles self-assemble into a sparse array with no long-range order on the PMMA surface. (stage 2) Evaporation of the hole-mask by depositing a thin metallic film onto the sample covered with the PS particles. (stage 3) Stripping of the PS particles using tape. (stage 4) Application of oxygen plasma etching for removal of the exposed PMMA. (stage 5) Gold deposition. (stage 6) Lift-off: the sample is placed in acetone, which will remove the whole of the PMMA remaining.*

Right from the birth of DSSCs, mesoporous TiO_2 has been used as the support for the monolayer of the sensitizer [1]. TiO_2 was chosen for a number of reasons: it is a stable, nontoxic oxide, abundant, and has a high refractive index (n=2.4-2.5). Naturally its crystalline form can be rutile, anatase or brookite. The anatase phase is thermodynamically the most

stable form and has a larger bandgap than rutile (3.2 vs 3.0 eV). Moreover, it also matches well with many of the conducting layers for electron collection. In addition, it can be synthesized/deposited easily into different forms of mesoporous structures, as well as flat TiO_2 surfaces, which was done in this work. In this report, I will thus report on the dye anchoring on flat TiO_2 anatase surfaces grown onto the INPS Au sensor nanodiscs either by RF-sputtering [22] (in the MC2 Clean room) or by Atomic Layer Deposition (ALD) [23]. The ALD deposition was carried out in collaboration with Prof. Michaël Grätzel and Leo-Philipp Heiniger at the Laboratory of Photonics and Interfaces, Institute of Chemical Sciences and Engineering, École Polytechnique Fédérale de Lausanne in Switzerland. The difference in the stability of the dye monolayer formed on these 2 types of samples will be discussed in the next chapter.

The choice of the specific dye molecule system to use is tricky because there exist hundreds of them, which all have been tested for the DSSC. Therefore, in the next section I will try to motivate our choice.

3.2. Dye-solvent systems

In a recent review, Hagfeldt et al, 2010 [2], present hundreds of dyes that have been designed and tested successfully for use in a DSSC. Among this multitude, dyes based on Ruthenium (Ru) complexes display interesting properties. Apart from having the common properties of dye to be used in a DSSC (e.g. an anchoring group (-COOH) and an optimized molecular structure to prevent the aggregation of the dye at the surface of the semiconductor (see figure 3.2), it has a broad adsorption spectrum, suitable excited state energy levels (higher in energy than the conduction band (CB) of TiO_2 to enable efficient electron transfer from the excited dye to the CB of TiO_2, a long excited state life-time, and a good electrochemical stability. These desirable properties, collectively, lead to DSSC efficiencies around and above 10%.

Due to the importance of the Ru complex based dye systems, much effort was put in improving their ligands to further optimize the photosensitization. For that purpose, Wang et al [24-26] worked to adjust the ancillary 2, 2'-bipyridyl ligand of the commonly used carboxylated bipyridine ligands with different substituents with the aim to increase the molar extinction coefficient, suppress dye aggregation on the semiconductor, and to optimize the redox potential of the photosentizer. In that process, the amphiphilic heteroleptic ruthenium sensitizer, Z907, was engineered, characterized by the introduction of two hydrophobic alkyl chains on the bipyridyl ligand (see figure 3.2). Since its introduction, Z907 has become a real "classic" and was therefore also used in this work.

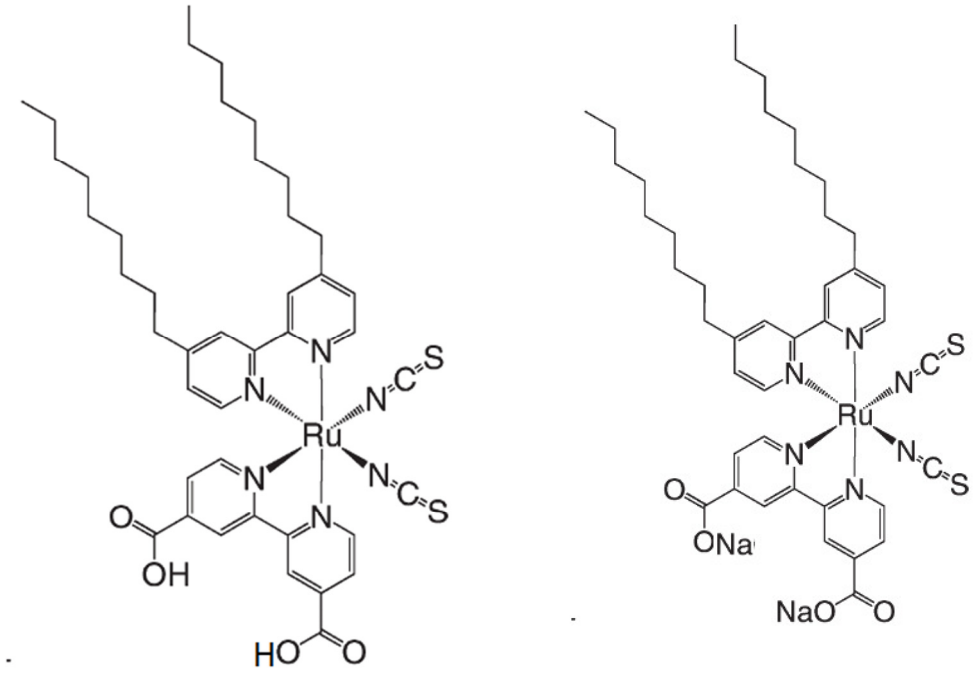

Figure 3.2. *(**Left**): dye Z907 or Ruthenizer 520-DN. (**Right**): its sodium salt or Z907Na*

The dye powders used to make dye solutions in all measurements are thus either standard dye Z907, also called Ruthenizer 520-DN (commercial name), or its sodium salt, Z907Na. Ruthenizer 520-DN was purchased from Solaronix (Switzerland) and is a dark purple powder with molecular formula $C_{42}H_{54}O_6N_6S_2Ru$, molar weight: 903 g/mol, chemical name: cis-disothiocyanato-(2,2'-bipyridyl-4,4'-dicarboxylicacid)-(2,2'-bipyridyl-4,4'-dinonyl) ruthenium(II), and chemical structure as displayed in the figure3.2 (left). Its sodium salt, dye Z907Na, has the molecular formula $C_{42}H_{52}O_6N_6S_2RuNa_2$, molar weight: 947 g/mol and chemical name NaRu(2,2′-bipyridine-4-carboxylic acid-4′-carboxylate)(4,4′-dinonyl-2,2′-bipyridine)-$(NCS)_2$. It was synthesized by the Grätzel research group and we received the necessary amount of such dye via our collaboration.

The organic solvents used to prepare the dye solutions were either a mixture MeCN:tBuOH, 1:1 (acetonitrille:Tert-Butanol) or DMSO (dimethyl sulfoxide). To motivate the choice of two solvent systems – which was imposed by problems of insolubility of some of the used dye in some of the used solvent – in section 4.1 of the next chapter I will define the dye-solvent-sample systems used in experiments in detail. Nevertheless, already here, in Table 3.1, I briefly summarize a number of key characteristics of the used organic solvents.

Table 3.1. *Summary of key properties of the solvents used in this work. Among the properties of a good solvent is its chemical stability, low viscosity to minimize transport problems, good dissolution of the dye powder, but still reasonable for not causing dissolution of the adsorbed dye to the semiconducting material of the electrodes. Moreover, it should be hydrophobic and non-volatile to avoid losses due to evaporation.*

Properties / **Solvent**	**Molecular formula**	**Molar mass [g mol^{-1}]**	**Viscosity (dynamic) 25 °C [mPa·s]**	**Density[mg mL^{-1}]**	**Melting point/boiling point at 1 atm.(°C)**	**Refractive index (n_D)**	**Vapourizability**	**Polarity**
Acetonitrille	C_2H_3N	41.05	0.34	786	46-44 / 81-82	1.344	Non-volatile	Polar aprotic
Tert-Butanol	$C_4H_{10}O$	74.12		0.775	25-26/ 82-83	1.387	Volatile	Soluble in water
Dimethyl sulfoxide(DMSO)	C_2H_6OS	78.13	1.996	1.1004	19/189	1.479	Non-volatile	Polar aprotic

3.3. Dye solution concentration determination by spectrophotometry

When using a spectrophotometer (Varian Cary 5000) to determine the concentration of a species in solution, light in the UV-vis-NIR spectral range is incident to the sample and the transmission of light through it is measured. Typically this is done by using a (double) beam arrangement as indicated in the figure below (fig 3.3)

The phenomena happening at the molecular level in the sample are the following. When the energy of a photon impinging on a molecule in the solution is the same as that of an allowed electronic transition in that molecule, it will be transferred to an excited state by absorbing the photon. In other words, an excitation of an electron of that molecule from the Highest Occupied Molecular Orbital (HOMO) to the Lowest Unoccupied Molecular Orbital (LUMO) is taking place. Among the many possible electronic transitions so-called n —π* and π*— π* transitions usually occur in the 400-800nm band and they characterize many of the organic functional groups, thus acting as the fingerprints of that functional group in absorption spectroscopy.

For our case of a Ruthenium-based dye solution, in UV/Vis spectroscopy, one typically observes two main absorption bands: the metal-to-ligands charge transfer (MLCT) transitions, where the molecular orbitals HOMO and LUMO are located in the d-orbital of the Ruthenium, and the π* orbital of the ligands giving rise to 4d - π* transitions in the visible region (500—600nm). There is also ligand-centered charge transfer (LCCT) transitions (π - π*)—in the near UV (450—250nm)[27, 28]. That is why for our specific case of Z-907 dye (see figure 3.4), the absorption bands at lower energies represent the MLCT transitions (with a typical extinction wavelength 550—520 nm) and the transitions at higher energies correspond to LCCT transitions.

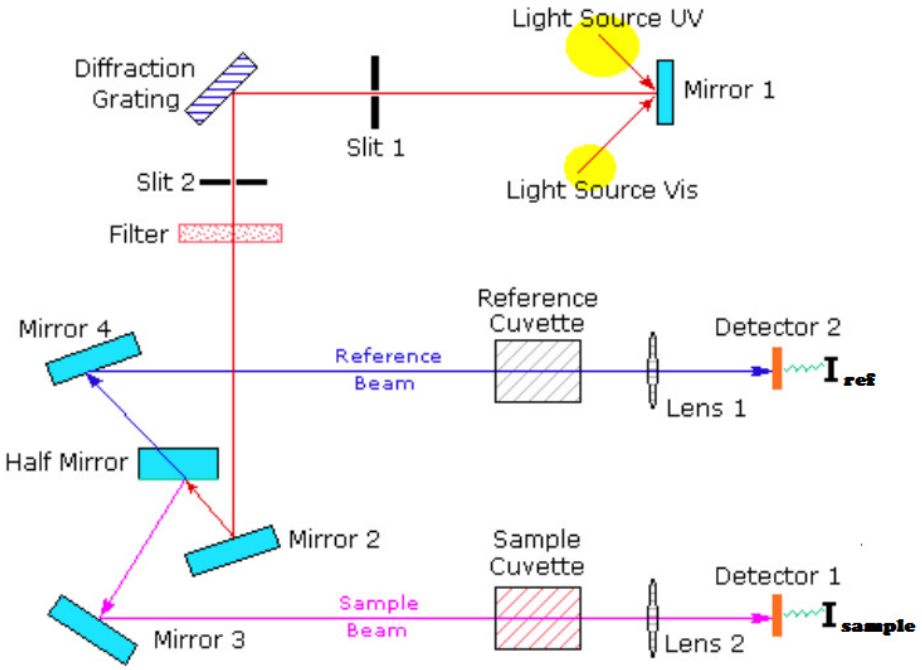

Figure 3.3 *Simple schematic drawing of the double beam light path used in UV-vis absorption spectroscopy.*

The absorption bands at lower energies, the MLCT transitions, are of particular interests not only for entity characterization, but also for determination of the concentration of the Ruthenium-based dyes solution by using the Beer-Lambert law which can be expressed as,

$$A_{\lambda_{extinction}} = \varepsilon_{\lambda_{extinction}} \times C \times l \,. \qquad (3.1)$$

For this analysis the parameter $A_{\lambda_{extiction}}$ is assigned to describe the MLCT peak in absorbance - see figure 3.4 - and can be expressed as

$$A_{\lambda_{extiction}} = \log_{10}(\frac{I_{ref}}{I_{sample}}) \,, \qquad (3.2)$$

where I_{ref} is the intensity of the reference beam and I sample the intensity of the light that has passed through the sample.

Since $\frac{I_{ref}}{I_{sample}} > 1$, then $A_{\lambda_{extiction}}$ has to be always positive.

$\varepsilon_{\lambda_{extinction}}$ is the molar absorptivity constant, or extinction coefficient [in 1 mol^{-1} cm^{-1} or Mcm^{-1}] and according to Wang et al, 2005 [29] it has the value of ~12200 Mcm^{-1} for Z907, C is the dye concentration and l is the optical path length, i.e. the thickness of the cuvette (1 cm in our case). Thus, measuring the optical absorbance spectra of our dye solutions (see figure 3.4 for some examples), we have been able to determine the nature of the used dye (if it is really the Z-907 dye), and, using equation 3.2, we have been able to derive the values of the concentrations of dye solutions used in this work.

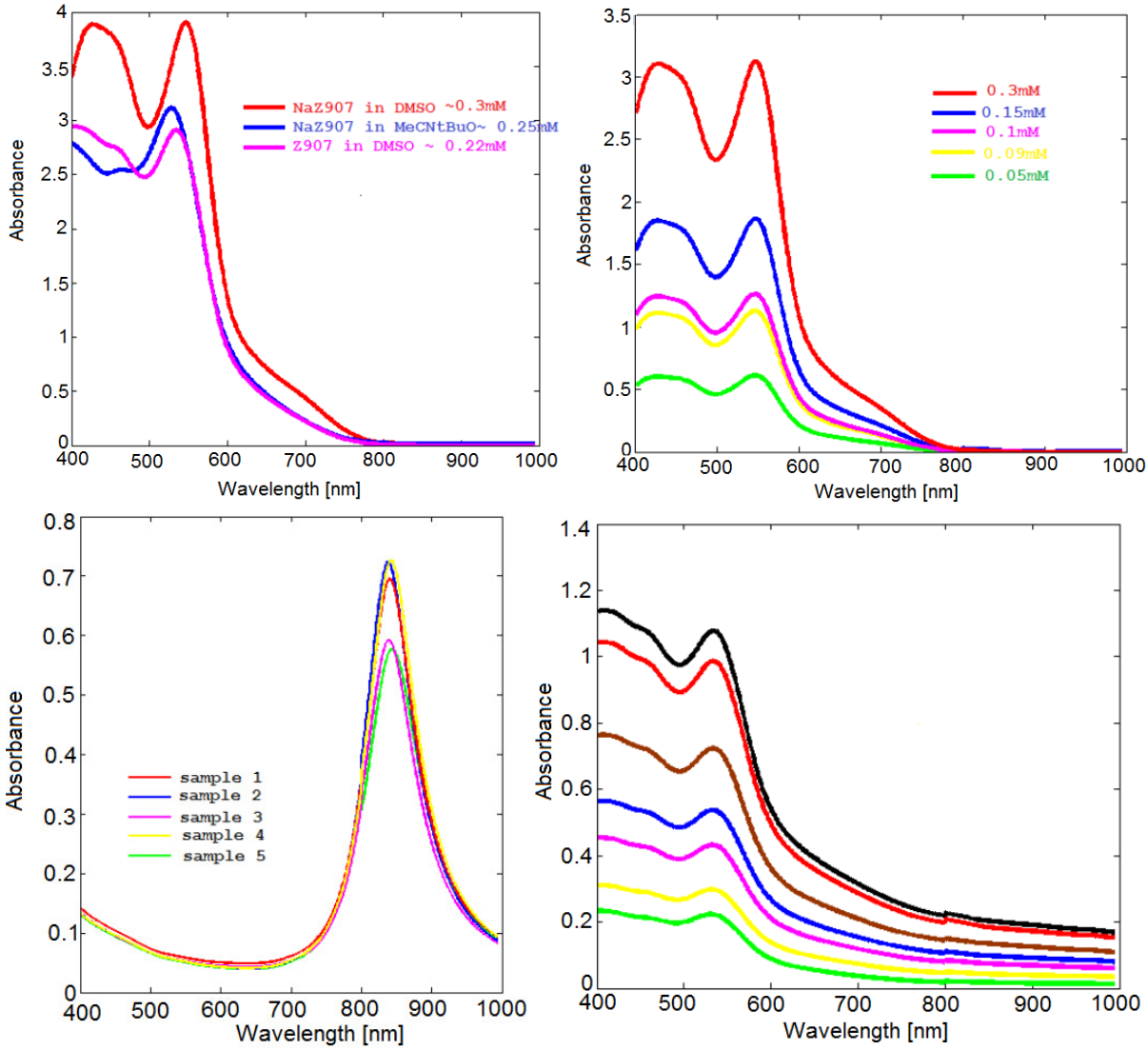

Figure 3.4. *UV-vis analysis of dye solution concentration.* ***(Top left):*** *Characteristic absorbance spectra of the 3 types of dye and solvents commonly used in our measurements.* ***(Top right****): Absorbance spectra of the NaZ907 in DMSO at different concentrations.* ***(Bottom left):*** *Absorbance spectra of the used INPS samples.* ***(Bottom right):*** *the non-dissolution of the Z907 in MeCNtButOH shown by its absorption spectra at different concentrations.*

In the above figure 3.4, I took the opportunity to show how the UV-vis analysis, supports our experimental proceedings when it comes to recognition of the dye type, its solubility in the chosen solvent, and how the dye (non/)dissolution would affect the plasmon peak and its shift. The 3 main types of dye solutions (NaZ907 in DMSO, Z907 in DMSO, and NaZ907 in MeCNtButOH) can be recognized from their absorbance spectra (see figure 3.4, top, left) and it should be noticed that the absorbance signal for both fig. 3.4 (top, left) and fig. 3.4 (top, right) goes to zero at ~770nm which testifies the perfect dissolution of these dyes in their solvents. This indicates that the LSPR peak which is observed at ~850 nm (see figure. 3.4, bottom, left) will not overlap with the dye-absorbance signal. Therefore the spectral reading can be trusted, because in the plasmon peak shift signal, there is no dye adsorption signal interfering (the absorption that we are observing for the samples at short wavelengths, corresponds to the absorption of TiO2, as its bandgap is in the UV). The situation looks different in the case of absorption spectra of Z907 in MeCNtButOH shown in fig. 3.4 (bottom right). Here, the absorbance signal does not go to zero at 770nm, this shows the non-dissolution of Z907 in MeCNtButOH. For this case, the LSPR peak at 850 would overlap with the dye absorbance, which would lead to an erroneous interpretation of the plasmonic peak shift due to its interference with the dye absorbance at that wavelength.

3.4. INPS Experimental Setup

One of the attractive features of the INPS-based experiments carried out in this work is the simplicity of the experimental set up. What is needed is a light source, i.e. a standard halogen lamp (AvaLight-HAL, Avantes), a fiber coupled spectrometer (Avantes AvaSpec-1024) and two optical fibers connected to properly aligned parallel collimators located on both sides of a flow cell (figure 3.5). This arrangement allows the light to cross the sample, excite the plasmons, and detect any change of the refractive index by tracking the spectral position of the plasmon peak by spectrally analyzing the transmitted light.
For the INPS experiment, the sample, i.e. a glass support patterned with plasmonic gold nanodiscs and a layer of TiO_2 on top (explained in section 3.1 of this chapter), is mounted in the flow cell. The dye solution is then pumped through the latter to allow the dye molecules to interact with the adsorption sites of the TiO_2 layer (see figure 3.5 and the real pictures of the experimental set up are depicted on figure 3.6), thereby changing the local refractive index of the medium surrounding the Au nanodiscs and inducing a small spectral shift of the plasmon resonance – which is what we detect. The physics that is at the origin of this detection procedure was explained in chapter 2.

During the INPS experiments, a spot of ~0.2 cm^2 was illuminated in the middle of the flow cell. The transmitted light intensity is conveyed by the optical fiber to the spectrometer. In this way extinction spectra were acquired with a rate of 1spectrum/3seconds up to 1spectrum/150 seconds (depending on the total length of the measurement) and analyzed in

real time by a MATLAB code to extract the plasmon peak position as a function of time. The used peak fitting procedure is documented in ***appendix II*** of this report.

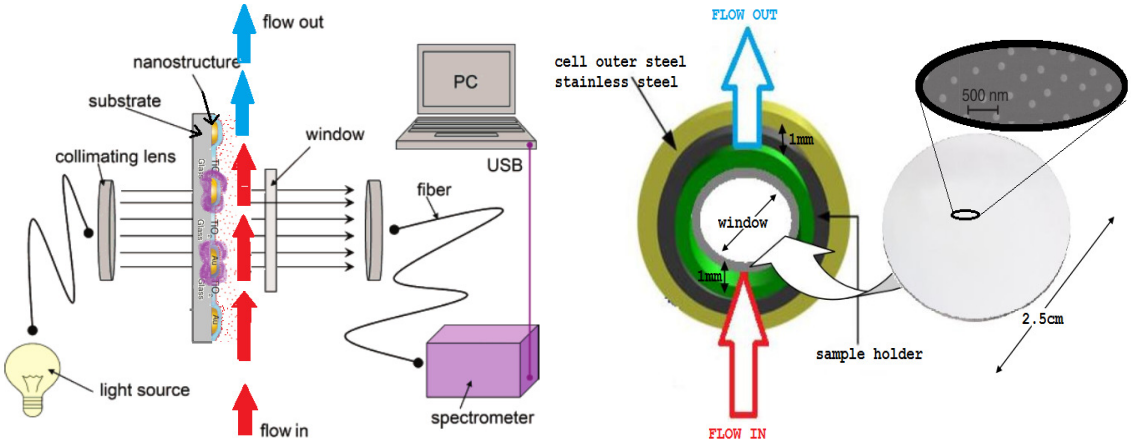

Figure 3.5. *(**Left**): Sketch of the set up used for the INPS measurements. (**Right**): Schematic of the sample (with an SEM image showing the nanodiscs embedded between the glass substrate and the TiO_2 layer). The right image also shows the shape of the flow cell and directions of the flow.*

To be able to follow the dye adsorption/desorption in real- time and *in situ* a peristaltic pump was used to pump the dye solutions through the flow cell at a flow of 7.35µL/s.

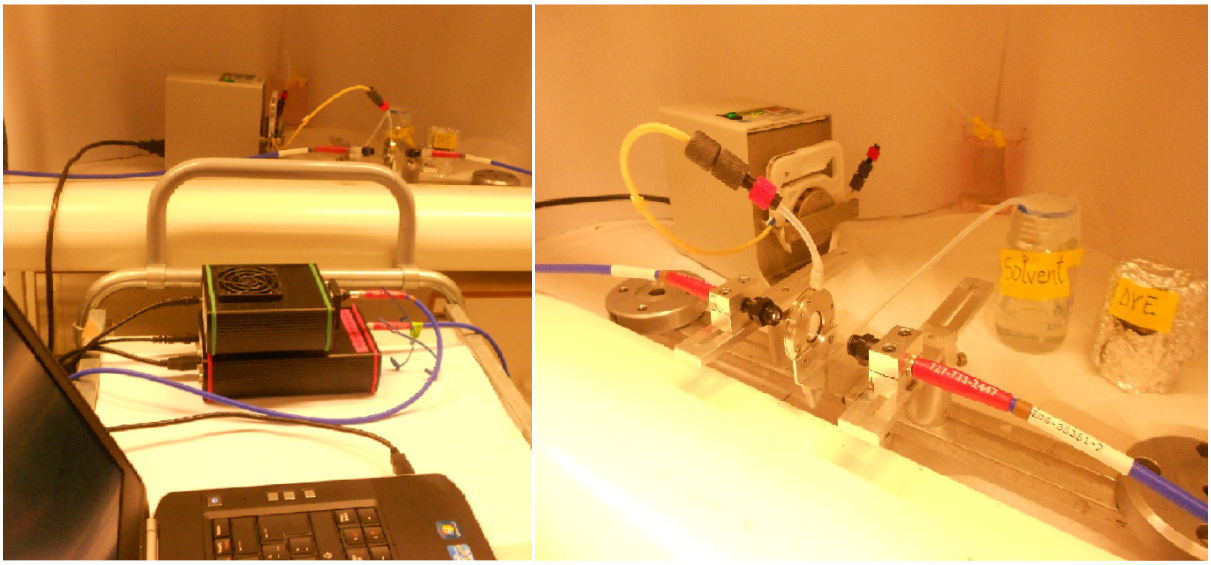

Figure 3.6. *Pictures showing the used experimental apparatus. **(Left):** picture of the whole set up. (**Right**): picture focusing on the liquid circulation system: flow cell, dye/solvent container, connecting pipes, optical fibers, pump and sink.*

The actual INPS experiment is the carried out in the following way. First a baseline is measured by measuring an extinction spectrum of the flow cell filled with solvent. Then the INPS sample is placed in the flow cell and its extinction spectrum exhibits a peak around 900

nm (Figure 3.7, top). When the dye solution is introduced, in addition to the plasmon peak, we also observe the dye absorption peak around 520-550 nm (Figure 3.5, bottom). Thus the dye extinction peak is located between 2 other peaks: that of the TiO_2 itself and that of the Au-plasmon peak. This was achieved by carefully engineering the size of the Au disks to shift the plasmon resonance to wavelengths where it is not overlapping with the dye and TiO_2 extinction signals. During the measurement, the position of the plasmon peak is tracked and plotted as a function of time, as also seen in figure 3.7

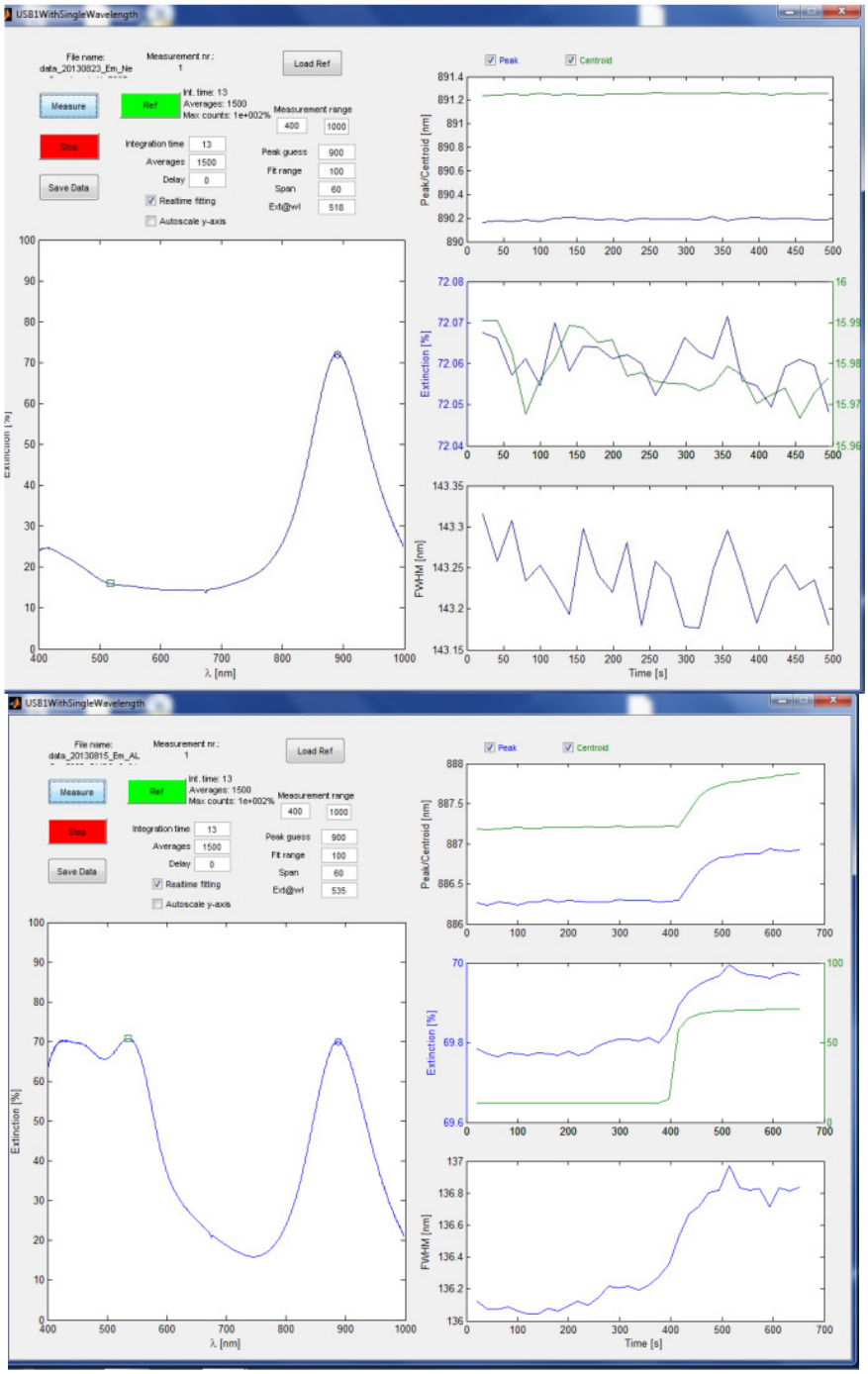

Figure 3.7. *Screenshots from the MATLAB program used to register the experimental data.* ***Top****: the recording of the baseline at the beginning of the measurement showing the extinction spectrum of the INPS sensor without dye solution in the flow cell.* ***Bottom****: The corresponding extinction spectrum with dye solution in the flow cell. Note the additional peak around 500nm due to light absorption by the dye.*

4

Experimental Results and Discussion

In this chapter, the prior knowledge that we have developed concerning our experimental platform INPS, different tools and methods, are to be used to be able to decipher, interpret and quantify the phenomena involving the adsorption/desorption of the used Ruthenizer-dye on the TiO_2 surface. After defining the systems that we used to classify results, we use the Langmuir approach of adsorption and desorption to analyze the obtained date. As the last step we also try to discuss and interpret the observed deviations from the Langmuir framework. Then we will conclude this chapter by summarizing the problems/drawbacks that we encountered when trying to achieve the goals that were set for this project. We start out by making a certain convention on how our results are to be grouped.

4.1. Overview: dye-solvent-sample systems

As mentioned previously, our attempts to form dense and stable monolayers of Ru-dye molecules (Z907) on TiO_2 were done on 2 types of samples (the sputtered and ADL deposited, see section 3. 1), 2 types of dyes molecules were used (Z907 and NaZ907, see section3.2), and 2 types of solvent were used (MeCNtbutOH and DMSO, see section 3.2). Combining all together we would have 2^3=8 systems where investigations have to be done! Classifying all the results that we have obtained into dye-solvent-sample systems has proven to be the most pedagogical way of grouping the measurements and obtained results. Each of these results stands for the group in which it belongs. When defining the groups 2 things have to guide us: (1) the solubility dye in the solvent, (2) the detection limit of the INPS technique. According to the 1st guiding point we observed that the dissolution properties of the used dyes Z907 (520-DN) and its sodium salt of Z907Na are different in different organic solvents (see fig. 3.4 (bottom right) where the non-dissolution is observed as the absorbance signal > 0 at longer wavelengths).

Table 4.1. *This table summarizes the dissolution properties of the used dyes in the used solvents as well as explains the used sample nomenclature. Note that the black squares in the table indicate that this particular dye, solvent-TiO_2 combination was not explored.*

Dye	**Solvent (Dye Dissolution in)**		**Sample type**	**Dye-solvent-sample systems**	
	MeCN:tBuOH	**DMSO**		**MeCN:tBuOH, as solvent**	**DMSO as solvent**
Z907Na	good	good	Sputtered	NaZ907MeCN:tbuOH-sput	NaZ907DMSO-sput
			ALD	NaZ907MeCN:tbuOH-ALD	NaZ907DMSO-ALD
Z907	bad	good	Sputtered		Z907DMSO-sput
			ALD		Z907DMSO-ALD

The information summarized in this table2.1 above leads to the definition of the 4 meaningful systems on which our investigations were done. These are:

(1) NaZ907MeCN:tbuOH-sput: Z907Na dye in acetonitrile and tert-butanol as solvent, on INPS samples where TiO_2 was deposited by RF-sputtering.
(2) NaZ907MeCN:tbuOH-ALD: Z907Na dye in acetonitrile and tert-butanol as solvent, on sample where TiO2 was ALD-deposited .
(3) Z907DMSO-sput: Z907 dye in DMSO as solvent, on sample where TiO_2 was deposited by RF-sputtering.
(4) Z907DMSO-ALD: Z907 dye in DMSO as solvent, sample where TiO_2 was ALD-deposited

This definition of the systems being done, in the rest of the result part of this report, we are going to present the adsorption and desorption results grouping them in the above defined systems.

4.2. Results from the NaZ907MeCN: tbuOH-sput system

The quantity of adsorbed NaZ907dye is monitored in real time by measuring the INPS sensor plasmon peak position using the centroid shift formalism. As it was mentioned before (section

2.1.3) we start treating the analysis of the dye adsorption using the Langmuir real-time kinetic model. Figure 4.1 indicates that the 3 first minutes of the NaZ907MeCN: tbuOH-sput system can almost perfectly be fitted by equation $\theta(t) = K(1-e^{-\kappa_{ads}t})$ (or eq. 2.4), where $\theta(t)$ is the dye coverage, proportional to the centroid shift (Δλ). I used the dye concentrations 0.007, 0.02, 0.11, and 0.25mM.

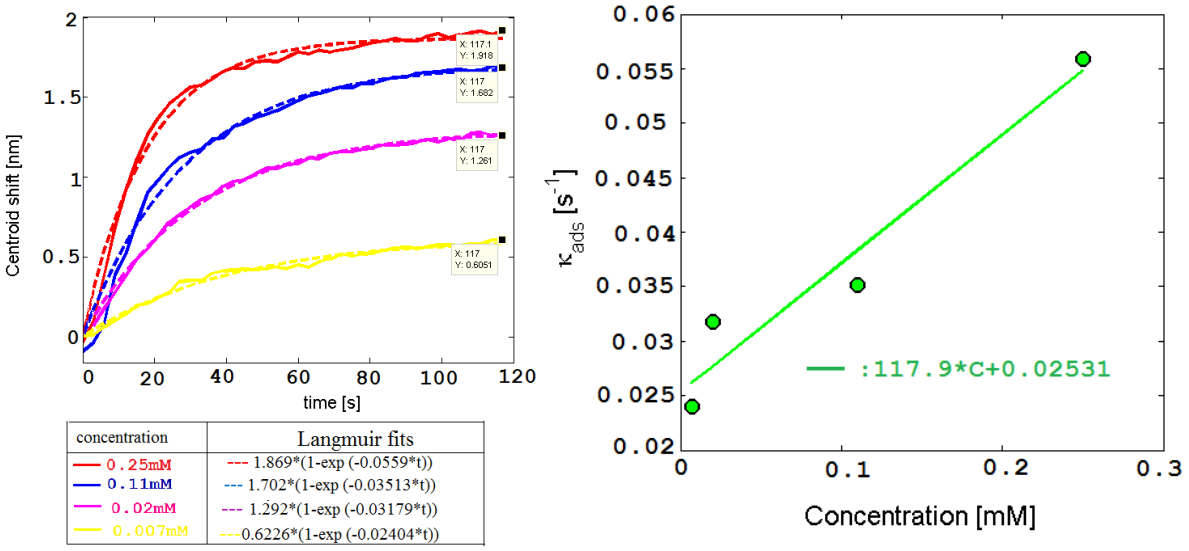

Figure4.1 ***(left)****: few first minutes of adsorption of the NaZ907MeCN:tbuOH-sput system* ***(right)****:determination of the value of* K_a*=117.9* $M^{-1}s^{-1}$*:the slope of the* κ_{ads} *vs concentration curve. For* K_d *(the intercept) we find 0.02531*s^{-1}.

As mentioned in section 2.1.2, in the Langmuir adsorption framework of this real-time kinetic model(see eq.2.3)., plotting K_{eq} vs. C is expected to yield a line of slope K_a =111.9 $M^{-1}s^{-1}$ and y-intercept of K_d =0.02531s^{-1} as shown in the Figure 4.1 (right). Knowing k_a and k_d, in the Langmuir theory, we can now define the adsorption equilibrium constant as $K_{eq} = K_a / K_d$ = **0.44212×10^4** M^{-1}. This represents the binding affinity between the dye molecule and the TiO_2 surface. This can be understood as that it expresses how many attempts a dye molecules needs to do (in its interaction with an adsorption site on TiO_2) before it gets adsorbed. We can thus also call it the sticking probability.

In this analysis, the parameter that corresponds to the surface coverage of the adsorbates as shown in the figure 4.2, is the shift of the centroid since it – in a first approximation – is proportional to the latter. Thus monitoring the centroid shift as function of the dye concentration will give us a reasonable measure of the amount of adsorbed dye at each of the used concentrations. A more quantitative analysis will be presented later.

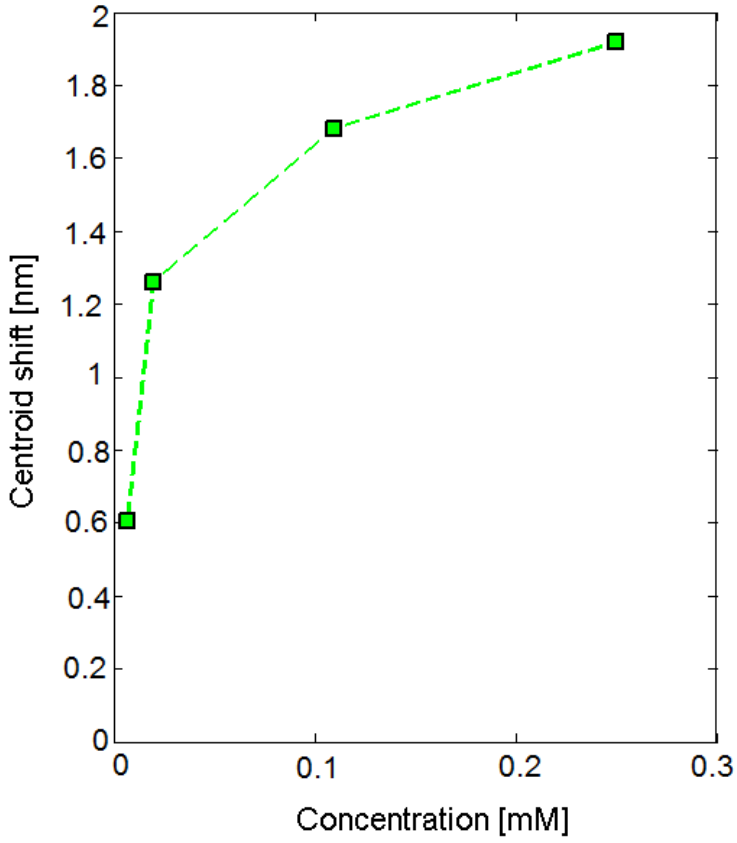

Figure 4.2. *The centroid shift (which is proportional to the amount of the adsorbed dye-molecules) vs. concentration as obtained for the NaZ907MeCN: tbuOH-sput system*

The curve of the amount of dye adsorbed as function of the concentration is expected to be of the form of eq. 2.4 at equilibrium. Nevertheless, the behavior that is on figure 4.2 is not in contradiction to the expectation as we keep in mind that this has been registered only at the 3rd minute of the adsorption, i.e. when the equilibrium dye coverage is not completely reached.

The values of the K_a , K_d and K_{eq}, can also be found for the initial conditions (few first seconds) of Langmuir model of adsorption and desorption. 2 things have to be done on the data of figure4.1 (left), as indicated in the figure4.3 (left): (1) to convert the peak shift into the coverage θ done by dividing all the kinetic curves by the peak shift of the highest concentration (2.5mM) at saturation. This assumes that, at this concentration, the highest possible coverage (θ =1) was reached. (2) The initial adsorption/desorption slopes are determined by linearly fitting the few first seconds of the measured adsorption and desorption kinetics.

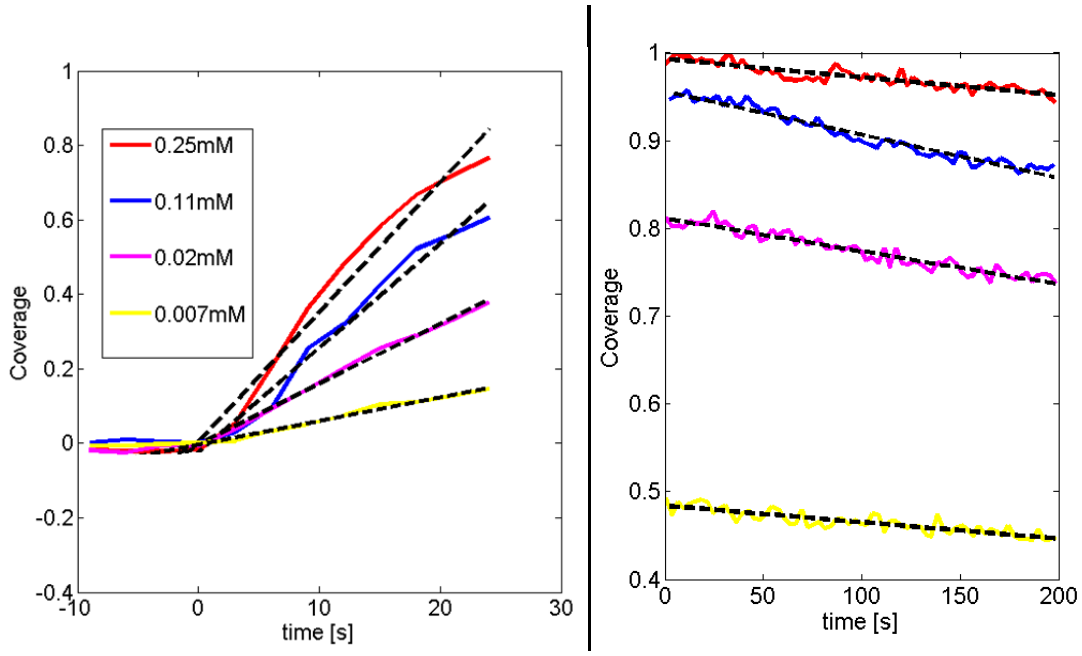

Fig 4.3*: Initial adsorption (left) and desorption (right) kinetics for the measurements for the NaZ907MeCN: tbuOH-sput system and their linear regression fits to find the initial adsorption/desorption slopes (black dashed lines).*

This means that I just consider the trivial case of eq.2.2 near *(θ=0), $d\theta/dt=K_aC$*), (eq.2.5) and extracting the initial adsorption slopes *$d\theta/dt$* and plotting the slopes versus the concentration, in the figure4.4 (left). And during desorption, *C=0*, and *$d\theta/dt=-K_d\theta$*(eq. 2.6). The desorption rate constant K_d can thus be extracted from desorption slopes, *$d\theta/dt$* , plotted versus the coverage θ. figure4.4 (right)

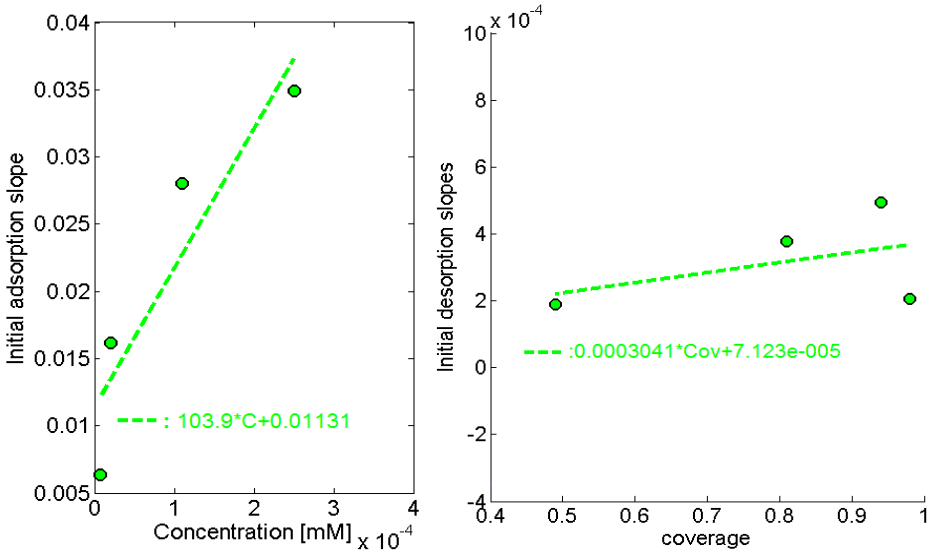

Fig4.4*(**left**):Values of the initial adsorption slopes plotted versus the dye solution concentration for the NaZ907MeCN: tbuOH-sput system slopes extracted from the fits of fig. 4.3-left* ***(right)****: Initial desorption slopes as a function of the coverage in the beginning of desorption for the NaZ907MeCN: tbuOH-sput system slopes extracted from the fits of fig. 4.3-right*

The linear fit of the slopes of adsorption vs concentration (figure 4.4 (left)) provides the value of K_a = 103.9 M^{-1} s^{-1} and the linear fit of the initial slopes of desorption vs, coverage (figure 4.4 (right)) provides the value of K_d= 0.0003041 s^{-1}.Then $K_{eq} = K_a / K_d$ =**3.4166×10^{5}M^{-1}**

Also, the value of K_{eq} can be found by assuming that for the points of figure 4.3 (right), at t=0 (i.e. prior to starting desorption), the coverage is close to saturation coverage. Then we use the Langmuir equation 2.5 to fit these points when they are plotted as function of concentration, as presented in the next figure, figure 4.5.

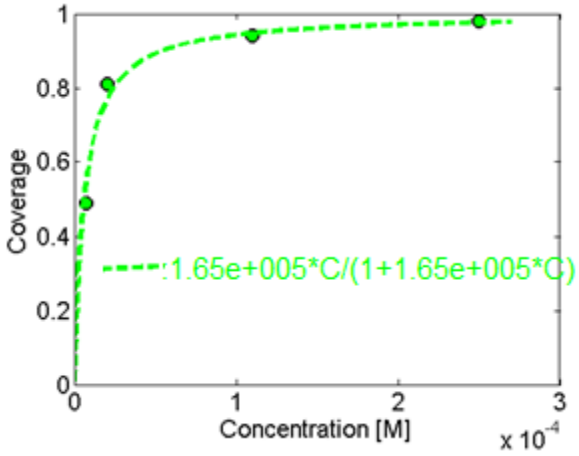

***Fig.4.5**. A Langmuir adsorption isotherm based on measurements in Figure 4.1. The dye-solvent-sample system is NaZ907MeCN: tbuOH-sput and the used data are supposed to be at maximum coverage and fitted with the Langmuir equation 2.7.*

the value of K_{eq} found with this analysis method is **1.65×10^{5}M^{-1}**

Remember, that the measurements for this system (NaZ907MeCN: tbuOH-sput) are done for a short time period 2 minutes according to figure4.1 (left). One of the reasons that we recorded data for such short time for this system is that, for times longer times, for example 3 minutes or more, the INPS signal starts to blue shift (i.e. shift in opposite direction as attributed to the dye adsorption), see figure 4.6, the possible reasons for this observed phenomenon will be discussed later.

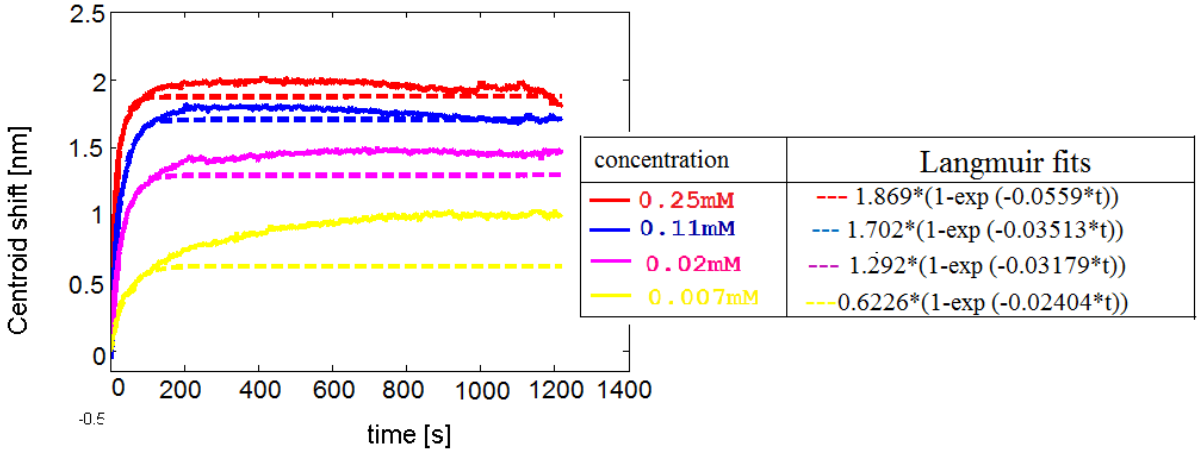

***Figure4.6:** 20 first minutes of adsorption of the NaZ907MeCN:tbuOH-sput system*

In the trials of eliminating (reducing) the blue shift, we noticed that the stability of the INPS sensors in the dye solution environment is necessary to be able to have stable longer time measurements. Therefore, in the next section, I study a different type of TiO_2 deposited by Atomic Layer Deposition (ALD).

4.3. Results from the NaZ907MeCN: tbuOH-ALD system

To be able to continue our study with the aim of forming a dye monolayer of improved quality and study its stability one needs to have a stable experimental platform providing a stable surface. As a first hypothesis to eliminate the blue shift we assume that a TiO_2 layer deposited by RF magnetron sputtering is not of good enough quality (in density and purity) to provide the stable surface that we need. Knowing that it is only a layer of 12nm that covers the gold nanodiscs it is reasonable to think that the preparation of the sample (cleaning the TiO_2 surface in tetrabutylammonium hydroxide TBAOH (30 min), then in MilliQ water at ~100 °C (30min), the ethatnol (5min), then anneal at 400°C for 1 hour) either may damage (create artifacts) in the adsorption sites or, if the TiO_2 film is affected by this procedure, it may even affect the geometry of the nanodiscs. The latter could change the nature of the adsorption signal. For these reasons, I did the rest of the measurements with samples where the TiO_2 layer has been deposited using Atomic Layer Deposition (ALD)

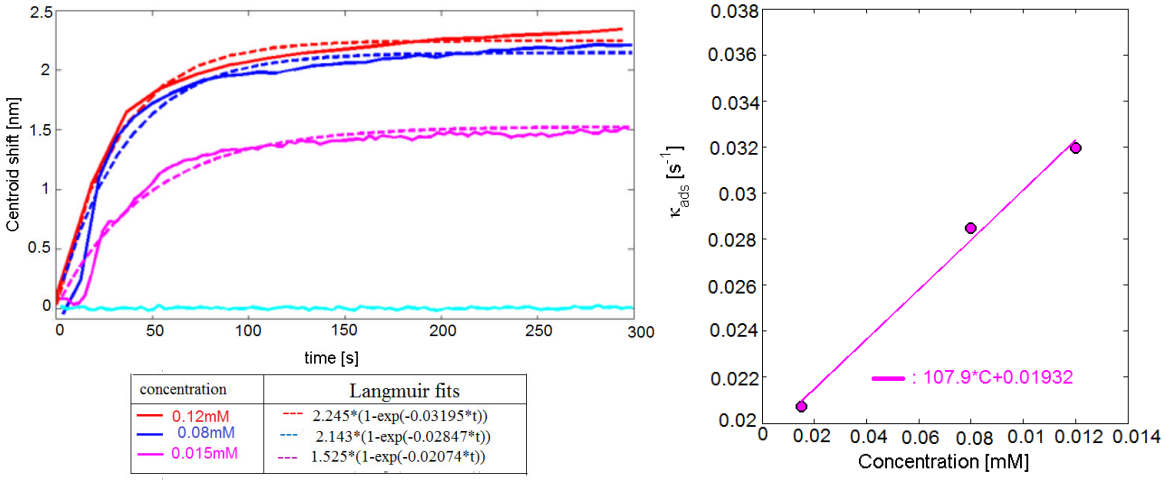

Figure 4.7. *(**left**): few first minutes of adsorption of the NaZ907MeCN: tbuOH-ALD system (**right**): determination of the value of K_a=107.9 $M^{-1}s^{-1}$:the slope of the κ_{ads} vs concentration. For K_d (the intercept) we find 0.01932s^{-1}.*

In terms of stability of the INPS signal, it is obvious (by comparing figure 4.1 and 4.7) that the measuring time was improved to 5min without a blue shift. Moreover, I observed higher values of the centroid shift for identical concentrations for the ALD sensors compared to the

sputtered ones. The most likely reason for this observation is the expected higher refractive index of the dense ALD TiO_2 compared to the less-dense sputtered one.

As before also for these samples a Langmuir real-time kinetic analysis was done by fitting equation 2.4 to the measured time dependency of the centroid shift for this dye-solvent-sample system (see figure 4.7, left) for 3 concentrations: 0.015 mM, 0.08 mM and 0.12 mM. the deduced value of K_a is $107.9 M^{-1}s^{-1}$ an that of K_d is $0.01932 s^{-1}$ (figure 4.7, right). Then $K_{eq} = K_a / K_d = \mathbf{0.55849 \times 10^4 M^{-1}}$

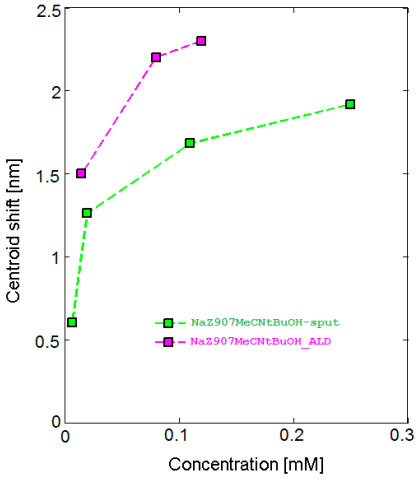

Figure 4.8. *The centroid shift (which is proportional to the amount of the adsorbed dye-molecules) vs. concentration as obtained for both NaZ907MeCN: tbuOH-sput and NaZ907MeCN: tbuOH-ALD systems. The higher centroid shift values on the ALD samples observed for identical concentrations are partly attributed to the higher refractive index of the dense ALD TiO_2 layer. A part of it may, however, also be caused by a larger number of adsorbed dye molecules per unit area.*

Compared to the previous case of the NaZ907MeCN:tbuOH-sput system, the NaZ907MeCN:tbuOH-ALD systems show generally higher values of K_{eq}. This is a good indication that the ALD surface promotes the dye adsorption compared to the sputtered ones and thus yields a higher coverage at a given concentration. This conclusion is also supported by the observed higher centroid shift of the Plasmon peak at a given concentration compared to the sputtered surfaces.

With reference to what I did in the previous dye-solvent-sample system, this system can also be analyzed using the Langmuir isotherm equation (eq.2.7). But to inform the reader, in the real time kinetic measurements that I have done for this system (fig4.7-left), I had in mind the study of the dense layer formation and the stability of the formed layer for longer time periods. So there was no short time measurements of the system that I performed myself to be able to do the analysis of linearly fitting the few first seconds of the desorption which would help in the obtention of the K_{eq}; but the thorough analysis for this system for short time periods has been done in the research paper (Gusak, et al, 2014) yet to be published.

Still, to obtain the value of the K_{eq} by using the Langmuir equation, one has to use the values of the centroid shift found as shown on fig 4.7.(left), convert them into coverage values

assumed to be close to saturation coverage fig 4.9(left) - then fitted with the Langmuir equation (eq.2.7) as presented in the fig4.9(right).

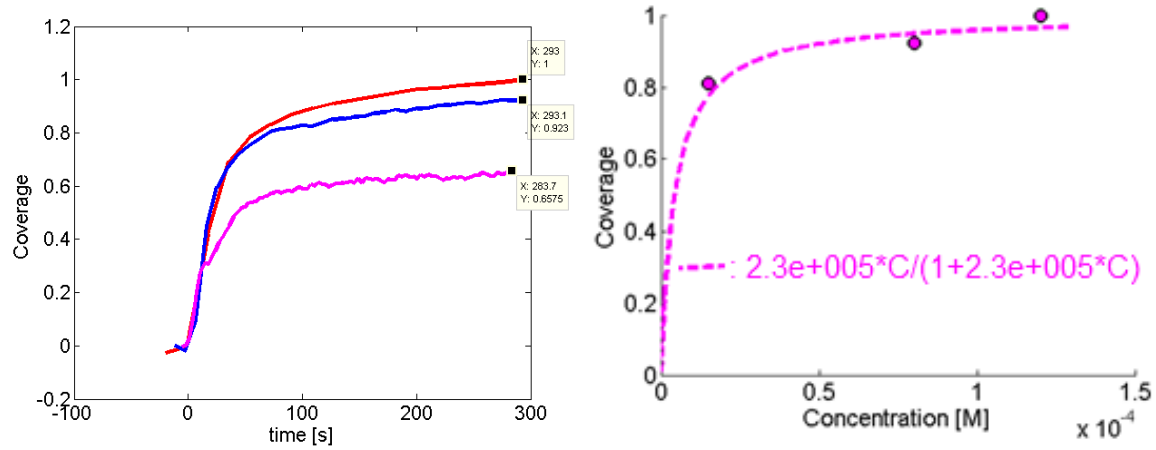

***Fig4.9**: (left) coverage as function of time for the 5 first minutes of the NaZ907MeCN: tbuOH-ALD system (right): An adsorption isotherm based on measurements in (left), fitted with the Langmuir equation 2.7.*

The value of K_{eq} found with this method is $2.3\times10^{5}M^{-1}$, and as noticed in the previous system, the values of K_{eq} found by fitting with the Langmuir equation continue to be a bit higher (~10 times) compare to those found using the Langmuir real time kinetic model.

The following figure 4.10 shows the deviation of this NaZ907MeCN: tbuOH-ALD system from the ideal conditions for much longer times, and this justifies why the analysis was done on the first 5 min of the adsorption only.

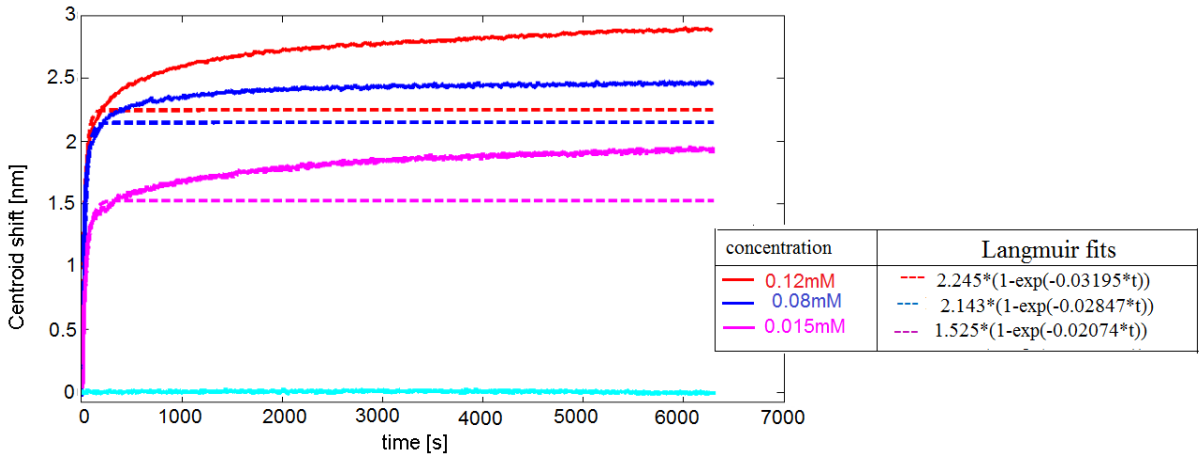

***Fig. 4.10** adsorption kinetics of the NaZ907MeCN: tbuOH-ALD system measured for ~100 minutes*

As shown in figure 4.10, the NaZ907MeCN:tbuOH-ALD system shows a reversed behavior compared to the previous system(NaZ907MeCN:tbuOH-Sput), i.e. instead of a blue-shift we observe continuous red-shifting of the INPS signal for 100 minutes or more. Moreover, after a couple of minutes, the adsorption kinetics can no longer be accurately fitted with a simple Langmuir adsorption isotherm. Thus this red shift, which goes far beyond the equilibrium saturation indicated by the "ideal" Langmuir adsorption isotherms, probably indicates an artifact in the experimental procedures. An example for the latter possibility that could give rise to a continuous red shift of the INPS signal may be the slow evaporation of the volatile

tert-butanol component in the solvent mixture, which would lead to the increase in $\Delta\lambda_{LSPR}$ according to $\Delta\lambda_{LSPR} = \Delta n_{effect} \times \delta(\lambda_{LSPR} / \delta n)$ where $(\lambda_{LSPR} / \delta n)$ is the bulk sensitivity of the INPS sensor.

In the next section we are going to show how we dealt with this issue in order to have a more stable experimental system where solvent evaporation artifacts can be ruled-out.

4.4. Results from the Na/Z907DMSO-ALD system

4.4.1. The stability of the DMSO systems

Dimethyl sulfoxide (DMSO) was shown in table 3.1 to have interesting properties that make it a good solvent for both Z907 and Na Z907. Moreover, since it was thought that the previous system showed a red shift in the adsorption mainly due to the change in bulk refractive index caused by evaporation of one of the constituents in the solvent mixture, the non-volatile DMSO is supposed to help us solve this issue. Clearly, as can be seen in figure 4.11, the use of DMSO appears to further improve the measurements.

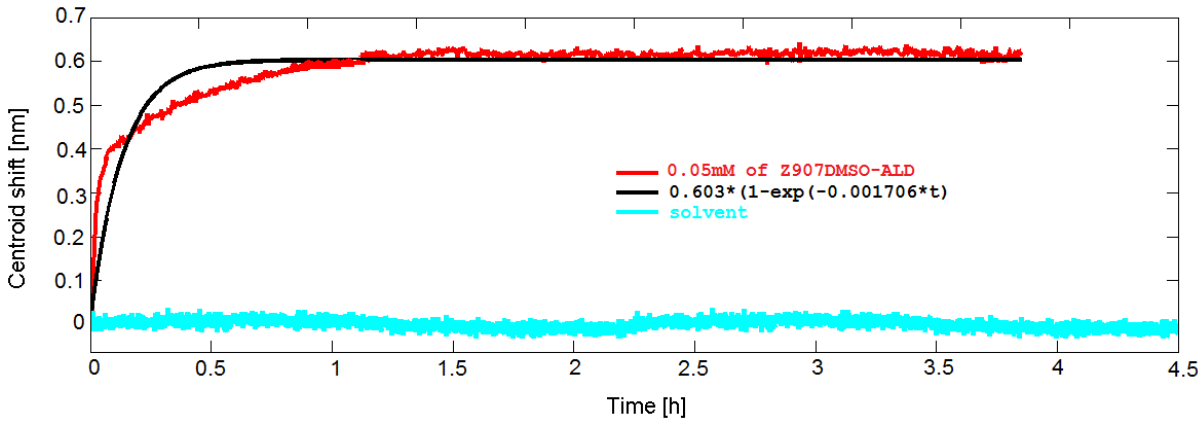

Figure4.11 *adsorption kinetics of the Z907DMSO-ALD system after nearly 4hours (red) and corresponding Langmuirian fit (black).*

Having the objective of forming a stable, dense monolayer of Ru-dye on TiO_2, the DMSO-ALD system turns out to be the most interesting system for our study due to its good stability over a reasonably long time interval. Figure 4.12 compares the stability of the 3 systems investigated so far for a relatively similar concentration (~0.05mM) under the same time interval. The centroid signal is normalized to 1 for better comparison.

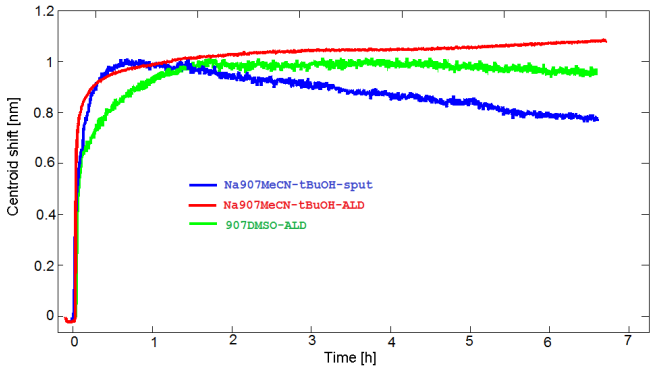

Figure4.12. *Comparison of the dye adsorption kinetics measured by INPS for the Z907DMSO-ALD, NaZ907MeCN:tbuOH-sput and NaZ907MeCN:tbuOH-ALD systems (the curves are normalized for comparison). We observe that Z907DMSO-ALDis the more stable system and shows its stability compare to the other systems*

Having this (Na)Z907DMSO-ALD as a stable system, the next interesting thing to do (see the next section) is to analyze its dye adsorption kinetics in the Langmuir framework, as we have done for the other systems.

4.4.2. Adsorption results of the NaZ907DMSO-ALD system

Figure 4.8 shows the time dependency of the dye layer formation on the NaZ907DMSO-ALD system in the first 30 minutes of an adsorption step with corresponding fits of eq. 2.4.

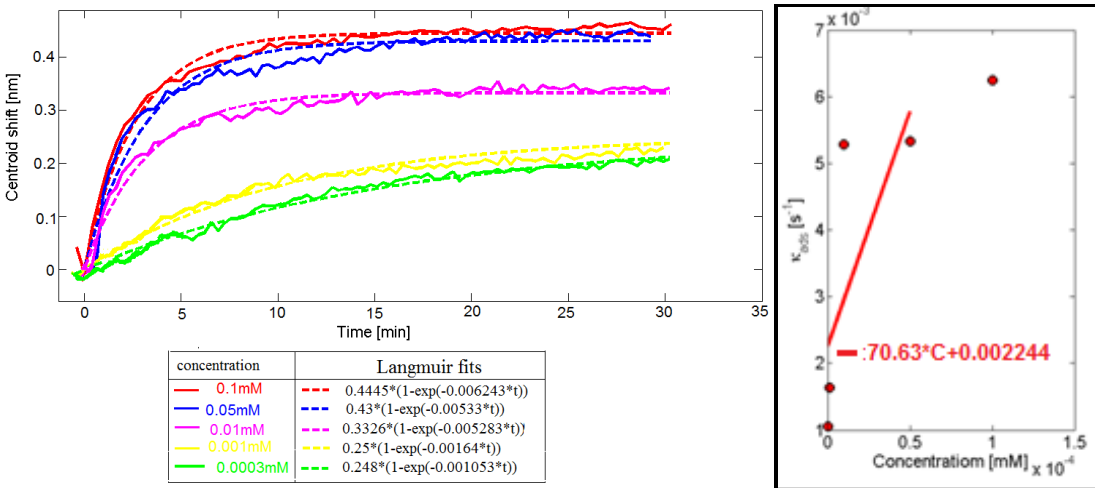

Figure4.13. ***(left)*** *the time dependence of the adsorption signal of the NaZ907DMSO-ALD system with corresponding Langmuir curve fitting.* ***(Right)****: determination of the value of* K_a=70.63 $M^{-1}s^{-1}$ *the slope of the* κ_{ads} *vs concentration. For* K_d *(the intercept) we find 0.002244* s^{-1}.

As I did previously, K_a =70.63 $M^{-1}s^{-1}$ corresponds to the slope of the κ_{ads} vs. C and is easily extracted for the 4 lower concentrations among the 5 used concentrations that we used. The reason for excluding the highest concentrations comes from the fact that at that concentration the adsorption is influenced by the finite cell filling time, i.e. the time it takes to exchange liquids in the measurement cell (from solvent to dye solution) is longer than the typical adsorption time at this concentration. For K_d=0.002244 s^{-1} and the adsorption equilibrium coefficient K_{eq}= 3.1475×10^4 M^{-1} is found. The higher values of the sticking probability for this system compared to other values that we obtained in the 2 previous systems under this Langmuir real-time kinetic analysis (see also in table4.2) can be attributed to the fact that in longer time adsorptions more dye molecules end up finding the corresponding good site for an effective adsorption, than for shorter times used in the previous measurements.

The following figure, fig.4.14, summarizes the centroid shifts as function of concentration for all the 3 dye-solvent-sample systems put together.

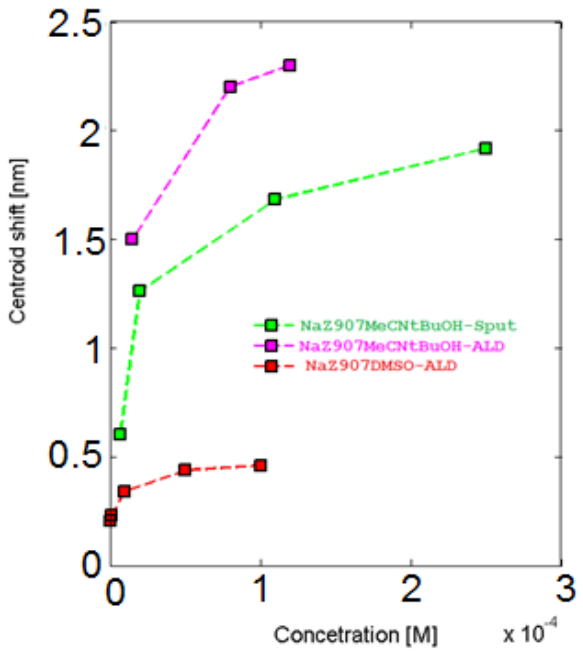

Figure 4.14. *the centroid shift vs. concentration as obtained for NaZ907MeCN: tbuOH-sput /NaZ907MeCN: tbuOH-ALD / NaZ907DMSO-ALD systems*

The above figure 4.14 was inserted to make it clear the usefulness of using the coverage as we do the Langmuir analysis. For the more interesting case of NaZ907DMSO-ALD, where I have been able to follow the adsorption for a much longer time, thus reach the required saturation, its centroid shift is lower compare to other systems. This is because of the change in refractive index between a dye monolayer and DMSO is small compared to that of between the dye monolayer and MeCN:tBuOH. The quantitative analysis done in section 4.5 will confirm that the higher the K_{eq}, the higher is the number of dye molecules adsorbed in that system.

As it has been the case for the 2 previous dye-solvent-sample systems, this system can also be fully analyzed using the initial conditions of the Langmuir isotherms. I start by fitting

(similarly as in fig. 4.3) the few first seconds of the coverage vs. time of the measurement in fig.4.13(left). The results are found in the following figure 4.15.

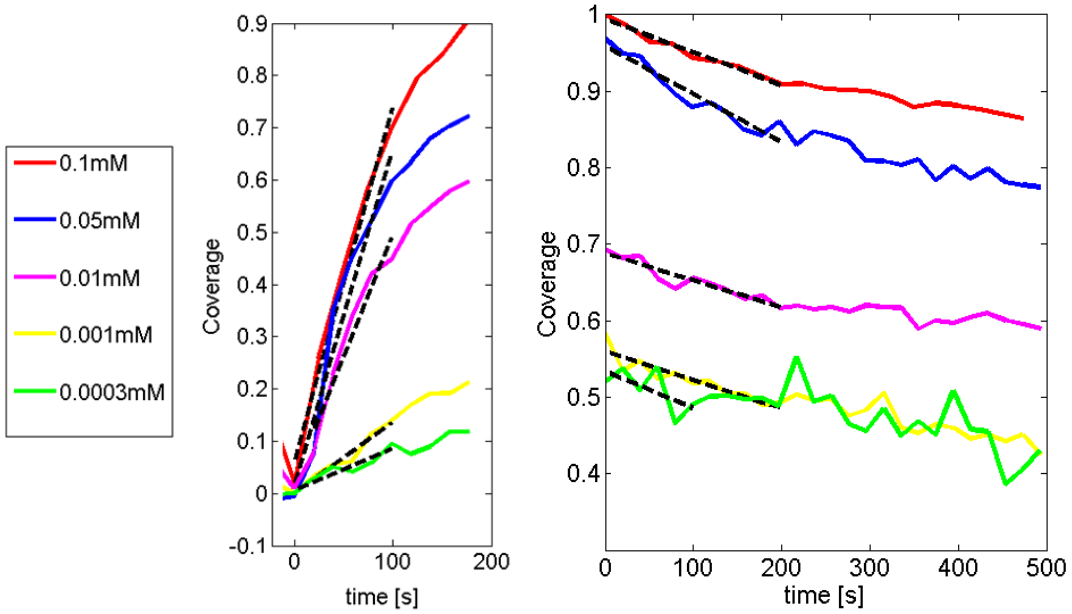

Fig4.15 *Initial adsorption (left) and desorption (right) kinetics for the measurements for the NaZ907DMSO-ALD system and their linear fits to find the initial adsorption/desorption slopes (black dashed lines).*

Then in figure 4.16(left) the initial slopes of adsorption are plotted as function of concentration and in fig.4.16 (right) the initial slopes of desorption are plotted as function of coverage are shown.

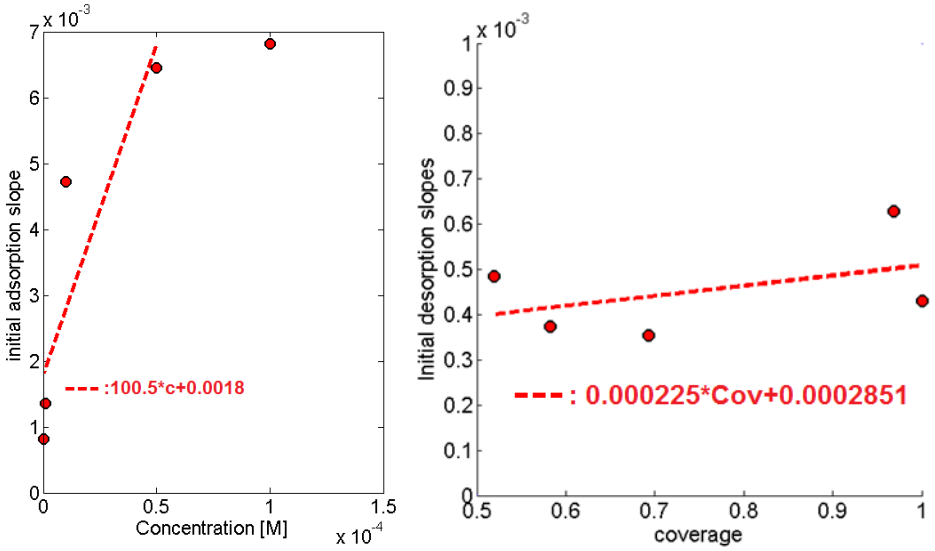

Fig4.16*(**left**):Values of the initial adsorption slopes plotted versus the dye solution concentration for the NaZ907DMSO-ALD system slopes extracted from the fits of fig. 4.15-left* ***(right)****: Initial desorption slopes as a function of the coverage in the beginning of desorption for the NaZ907DMSO-ALD system. The slopes are extracted from the fits of fig. 4.15-right.*

As it was done previously, one gets the value of K_a = 100.5 M^{-1} s^{-1} from the slopes of the linear fit of initial adsorption slopes vs low concentration. Only the low concentrations are used for the analysis because, as previously, the adsorption is influenced by a finite cell filling time for the highest concentration (figure 4.16 (left)). From the initial slopes of the desorption kinetics we find K_d= 0.000225 s^{-1}, and thus K_{eq}= K_a/K_d= **$4.4667\times10^5 M^{-1}$**

Now, also with this NaZ907DMSO-ALD system, we can plot a Langmuir isotherm by taking the initial points prior to desorption (fig4.15 right at t=0) as saturation coverage and fit them with eq.2.7, (see fig. 4.17). The value of K_{eq} found with this method is **$5.33\times10^5 M^{-1}$**

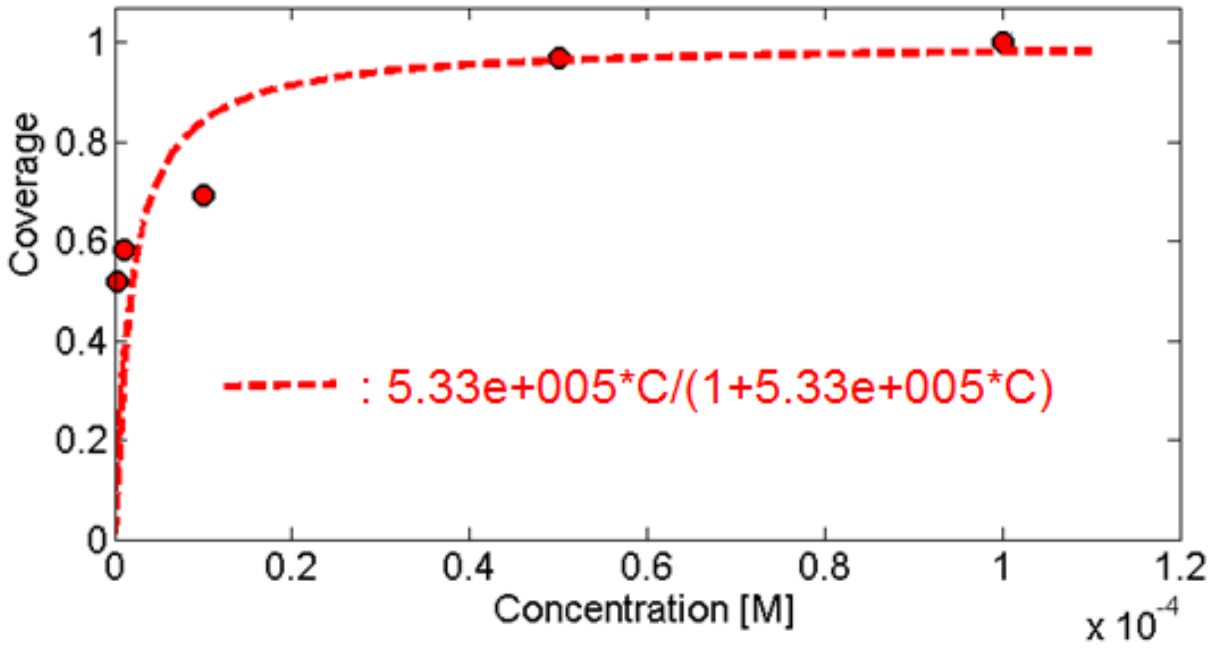

Figure4.17: *An adsorption isotherm based on measurements in Figure 4.13. the dye-solvent-sample system is NaZ907DMSO-ALD and the used data are supposed to be at maximum coverage and fitted with the Langmuir equation 2.7.*

All the values of the kinetic constants (K_{eq}, K_a, and K_d) obtained in all the 3 dye-solvent-sample systems used (NaZ907MeCN: tbuOH-Sput, NaZ907MeCN:tbuOH-ALD, and NaZ907DMSO-ALD) and analysed by the 3 methods based on Langmuir kinetics (real-time kinetics, linear fitting of the initial values of adsorption/desorption and by using the fit to the Langmuir adsorption isotherm) are shown in the following table.

Table 4.2 *summary of all the kinetic constants (K_{eq}, K_a, and K_d) obtained by different methods used in the analysis above for the 3 systems used in this report (NaZ907MeCN: tbuOH-Sput, NaZ907MeCN:tbuOH-ALD, and NaZ907DMSO-ALD.)*

System / Analysis method	NaZ907MeCN: tbuOH-Sput	NaZ907 MeCN: tbuOH -ALD	NaZ907DMSO-ALD
Real-time kinetic model	K_a =111.9$M^{-1}S^{-1}$ K_d =0.02531 S^{-1} K_{eq}=0.44212×10^4 M^{-1}	K_a =107.9$M^{-1}S^{-1}$ K_d =0.01932 S^{-1} K_{eq}~0.55849×10^4 M^{-1}	K_a = 70.63 $M^{-1}S^{-1}$ K_d = 0.002244S^{-1} K_{eq}~3.15×10^4 M^{-1}
Linear fittings of the initial values	K_a =103.9$M^{-1}S^{-1}$ K_d =0.0003041 S^{-1} K_{eq}=3.4166×10^5 M^{-1}		K_a =100.5 $M^{-1}S^{-1}$ K_d =0. 000225S^{-1} K_{eq} =4.4667×10^5 M^{-1}
Fit with Langmuir adsorption isotherm	K_{eq}=1.165×10^5 M^{-1}	K_{eq}~2.3×10^5 M^{-1}	K_{eq}~5.33×10^5 M^{-1}

What one has to notice in that table is that the results are reasonable within each of the systems and the slight difference that we see in the above tabulated values (see table 4.2) probably stems from the fact that the kinetics of our systems are not perfectly Langmurian.

The set of results as a whole is reasonably in agreement with those reported in the literature. For example, Harms et al [12] reports the adsorption equilibrium constant K_{eq} of 5)×10$^6M^{-1}$ determined by QCM-D measurements for Z907 dye adsorbed on a compact TiO_2 film surface. This value is nearly 10 times higher compared to the values presented in the above table4.2 where K_{eq} is ranging between (1.6-5.3)×10^5 M^{-1}. The probable reason of my lower values of K_{eq} is the very low pumping speed (7.35µL/s) for liquid exchange (dye/solvent) in the system compare to the 40 µL/s used in Gusak et al, 2014, which is thought to lead to a slow adsorption kinetics.

Otherwise, other values of K_{eq} found in the literature for systems similar to the ones I used are 4×10^4 M^{-1} determined from electrochemistry measurements for dye Z907 on mesoporous TiO_2 films [30] and K_{eq} =3×10^4 M^{-1} for dye N3 on mesoporous TiO_2 films [8]; the values which are comparable to ones I obtained (0.4×10^4 - 3.15×10$^4M^{-1}$ – see table4.2) when analysing using the real-time kinetic model.

This analysis becomes more clear when the above values of the adsorption equilibrium constant K_{eq} obtained (as tabulated above, table 4.2) are plotted (see next figure 4. 18) as function of dye-solvent –sample systems they do belong to, and shown (in a color code: green, purple, red) for the analysis method used (real-time kinetics, fitting with isotherm, and linear fitting respectively).

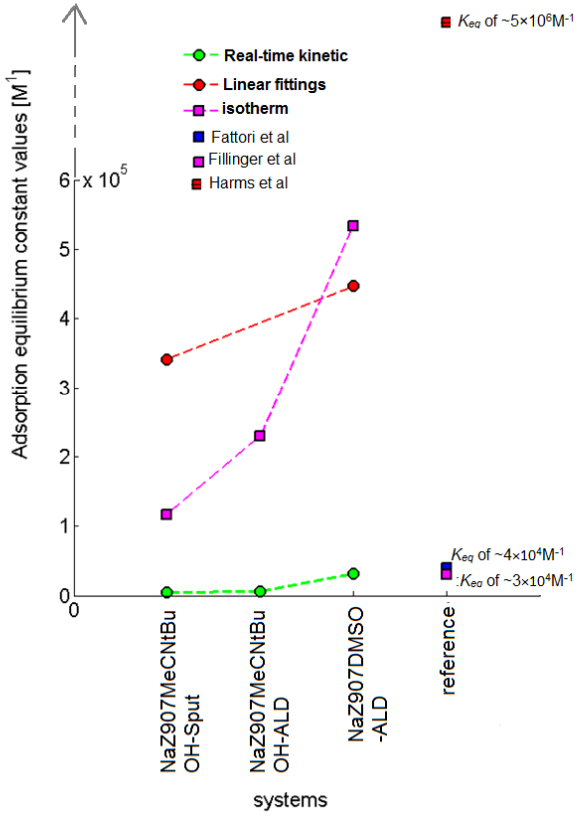

***Fig. 4.18**: Plot of the experimentally fund values of K_{eq}. They are plotted as function of dye-solvent-sample system used to obtain them, and the color code used (green, purple, red) represents the data analysis method used (real-time kinetics, fitting with isotherm, and linear fitting). My preferable system has been the NaZ907DMSO-ALD, as we can see the higher values of the K_{eq} compared to other systems. As mentioned above in the text, I could follow the real-time kinetics with that system for a longer time period. The figure also shows 2 red points as I did not correct the desorption data for the NaZ907MeCNtBuOH-ALD system, thus not been able to fit the experimental data of K_{eq} by the linear fitting method. The points for the reference column are taken from the literatures.*

From our data analysis, we conclude that the dye adsorption process is non-perfectly Langmuirian. This hypothesis, which has been supported by numerous experimental observations presented in the following pages of this report, can be explained by the possible existence of initially physisorbed NaZ907 molecules which have possibility to rotate (due to various influences) and end up in a chemisorbed—binding by the correct anchoring ligands on TiO2 sites. I will call molecules, in this transition state “loosely bound molecules”. In view of their existence, what do the 3 different ways to analyze the data introduced above mean?

(i) the linear fit to the initial slope (red points on figure 4.18): in this regime the surface is basically empty and the rearrangement of first loosely bound molecules is not hindered. Thus what we measure with INPS (which predominatly records new molecules adsorbing and probably does not detect if molecule rearranges on the surface) is only the first adsorption which, in this regime can be considered Langmuirian. (ii) fit with the isotherm at saturation: The fact that in this regime the only used parameter is the final coverage, the details about how the layer was formed are irrelevant since there is no consideration on how this coverage was obtained . (iii) the real-time kinetic analysis: in this regime, by really fitting the kinetics, one is sensitive to the temporal evolution of the process and - if the adsorption and loosely bound molecule rearrangement process happen simultaneously and start to influence each other because the coverage is no longer close to zero (as during the initial seconds) the kinetics are not perfectly Langmuirian and yield a different K_{eq} than the other two analysis methods.

We now turn our attention to the reproducibility of our experiments. For this NaZ907DMSO-ALD system, good reproducibility is observed between measurements of 30 min adsorption and 60 min adsorption, as shown in figure 4.19.

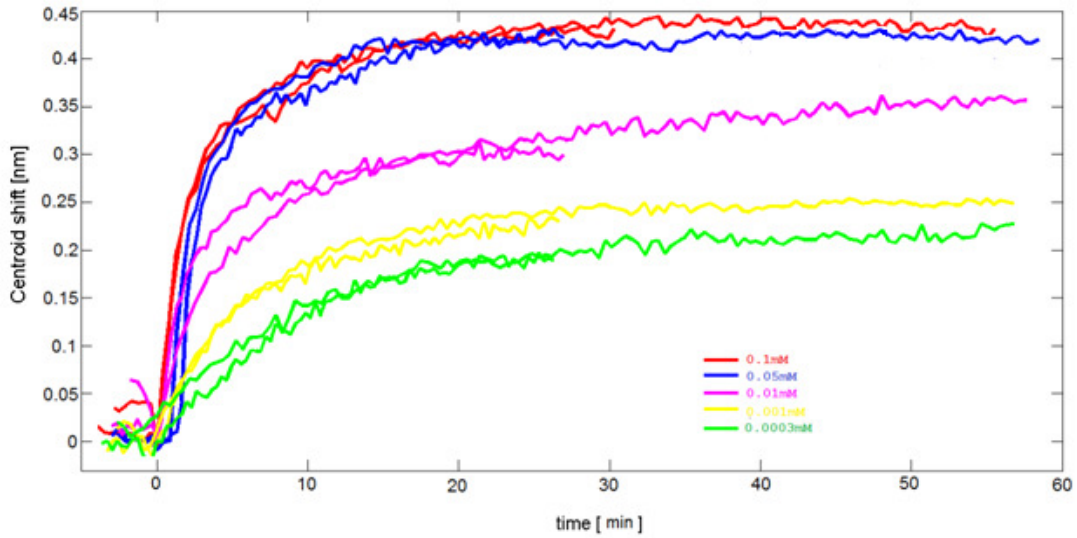

Fig 4.19: *adsorption 30 min and adsorption 60 min plotted together for the NaZ907DMSO-ALD system: Note the good agreement between two repeated measurements under the same conditions.*

From figure 4.19 we notice also that within 1 hour we are still observing the stability of the dye layer formed for high concentrations (at least for 0.1mM). To highlight this fact we plot the Plasmon shift at maximum adsorption time vs concentration for only the cases of dye layer formation monitored in Fig.4.19 and present that in the following figure4.20.

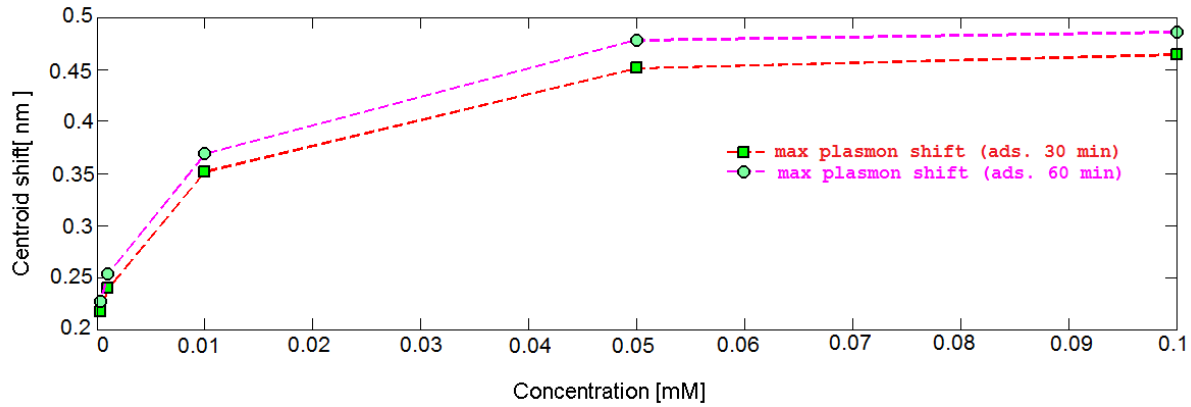

Fig 4.20 *Maximum centroid shift vs Concentration for NaZ907DMSO-ALD system as measured for 30 min and 60 min adsorption times, respectively.*

What is observed in fig4.19 and 4.20 is thought to show a slight deviation from the Langmuir adsorption. If we reasonably assume that all the adsorption sites are occupied after 30 min of adsorption, we would not expect any further adsorption as Langmuir stipulates a 1 to 1 (molecule – adsorption site) adsorption for a limited number of adsorbates (as well as adsorption sites), which don't interact with each other. But the observation on figure 4.19 and 4.20 present a different story. In the time interval between 30 min and 60 min there has been a slight increase in the number of molecules from the dye solution to be adsorbed on the TiO_2 surface. Mechanistically, this can be attributed to the possibility of a dye molecule to undergo different rotations in different attempts of "fixing" the non-symmetrically distributed anchoring ligands of the NaZ907 molecule (-COOH) to an adsorption site on the TiO_2. This means that it may take time for a dye molecule, which "lands" on the TiO_2 surface with its anchoring ligands not pointing towards the TiO_2 (it is thus in a physisorbed state) to "rotate" into a the right position and bind to the surface. Moreover, for this rearrangement of the molecule to be possible, it may be necessary that neighboring sites on the TiO_2 are empty. Thus, the tentative explanation of the observed long-term slow adsorption is that after long enough time, the molecules initially disorganized (physisorbed or "loosely bound"), reorganize so as to form a more favorable adsorption state (chemisorbed) where the molecules are closely packed.

4.4.3. Suspected non- Langmuirian desorption of the NaZ907DMSO-ALD system

As it was explained in the section 2.2.3 and shown in *appendixIII,* upon desorption, we expect to see a blue shift in the centroid signal, which corresponds to dye (of higher refractive index) being replaced just by solvent (DMSO in this case) of lower refractive index. If this desorption process would perfectly obey the Langmuir model, it would obey eq.2.2 assuming

K_a =0 (there is no more adsorption). Integrating this equation leads to a simple form of an exponential decay in time $(K_d)^{-1}$, which is concentration *independent*. The concentration independent Langmuir desorption is different to what we are observing in the figures 4. 21 and 4.23 where desorption seems to be concentration dependent. But, in fact, we get more desorption at higher concentrations because the coverage is higher, so there is more dye to start with. But the fraction of desorbed dye is very similar for all concentrations, and it is about 60% (see the full measurenments on *appendix III*). So this effect of higher coverage and steeper desorption itself doesn't suggest re-organization of dye molecules for this system. In the experiment connected to figure 4.21 I monitor desorption kinetics for 1 hour after an adsorption step of 30 min (previously shown in fig. 4.13).

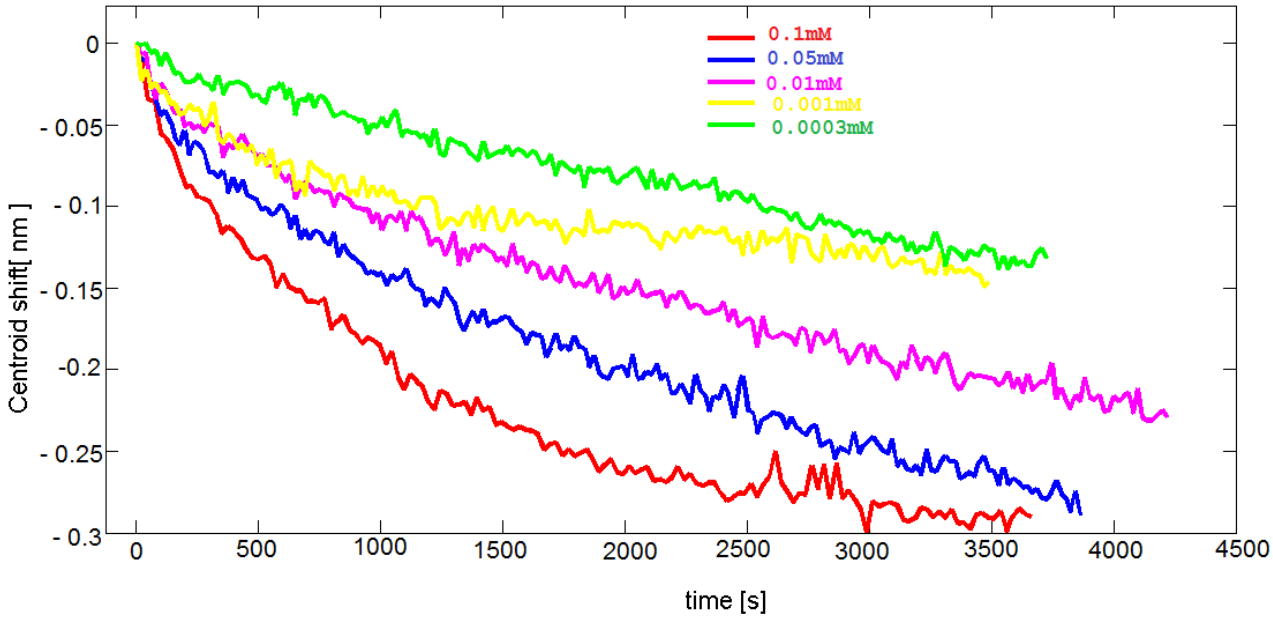

Figure 4.21. *60 min desorption kinetics of the NaZ907DMSO-ALD in different dye concentrations measured after a 30 min of adsorption step shown in fig 4.13.*

And I have monitored the higher initial desorption slopes in higher concentrations than in lower ones, as observed in Figure 4.22.

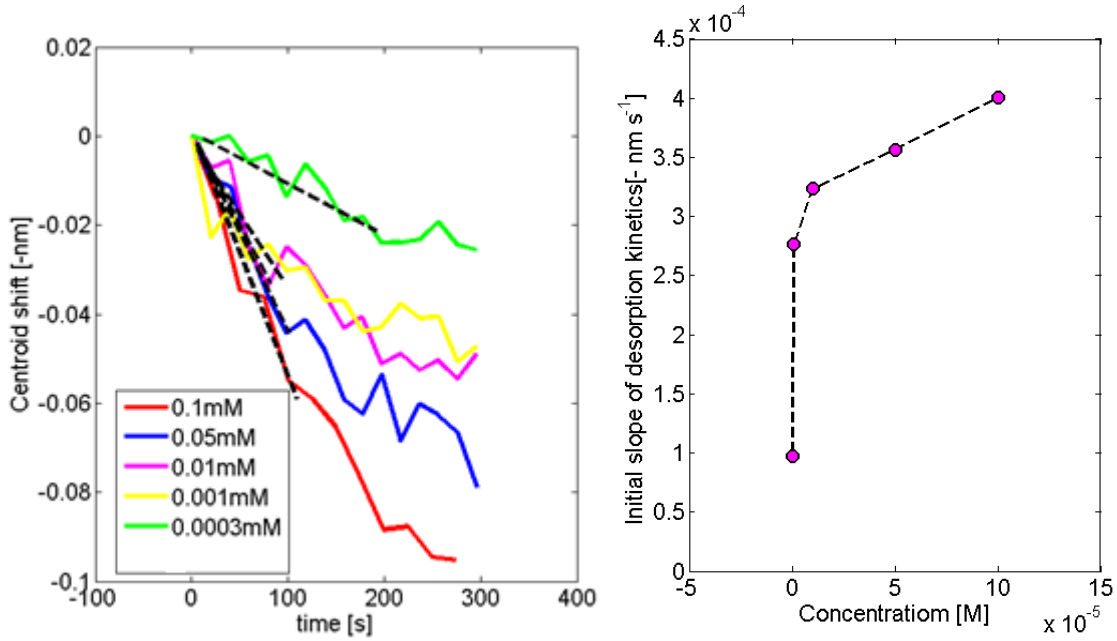

Figure4.22.*Case of the NaZ907DMSO-ALD, treatment of the desorption after 30 min of adsorption. (left): determination of the initial slope of desorption by linearly fitting the initial stage of the desorption. (right): initial slope of desorption kinetics vs concentration.*

For the desorption of in the NaZ907DMSO-ALD that follows a longer time of adsorption of 60 min,, the same effect of higher coverage and steeper desorption for high concentrations leads to this allusion of a concentration dependent desorption as depicted on figure4.23.

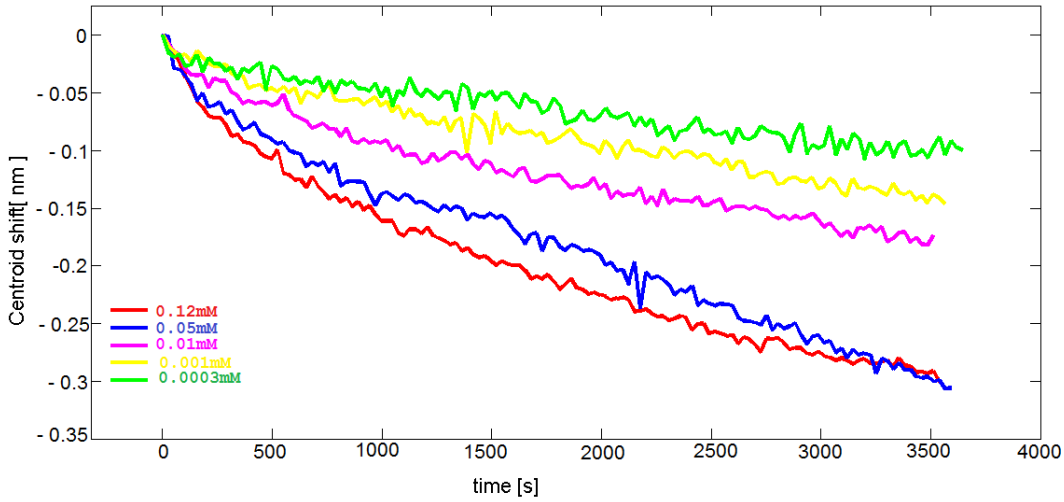

Figure4.23. *60 min desorption kinetics measured after a 60 min adsorption step in different dye concentrations.*

As previously, the initial slope during the few first seconds of desorption (see fig 4.24) indicates steeper slopes for higher concentrations than in lower ones.

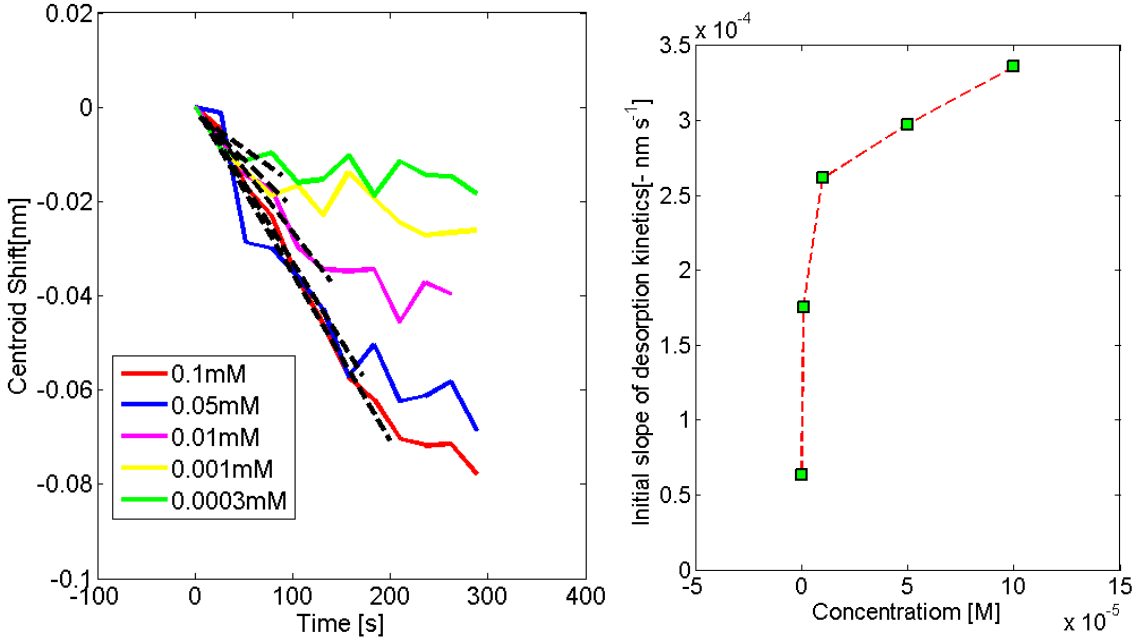

Figure4.24. *Case of the NaZ907DMSO-ALD, treatment of the desorption after 60 min of adsorption. (left): determination of the initial slope of desorption by linearly fitting the inital seconds of the desorption. (right) : initial slope of desorption kinetics vs concentration.*

It is now interesting to plot together (in the same graph) the desorption curves measured after 30 and 60 minutes of adsorption, respectively, as shown in the following figure 4.25(left).

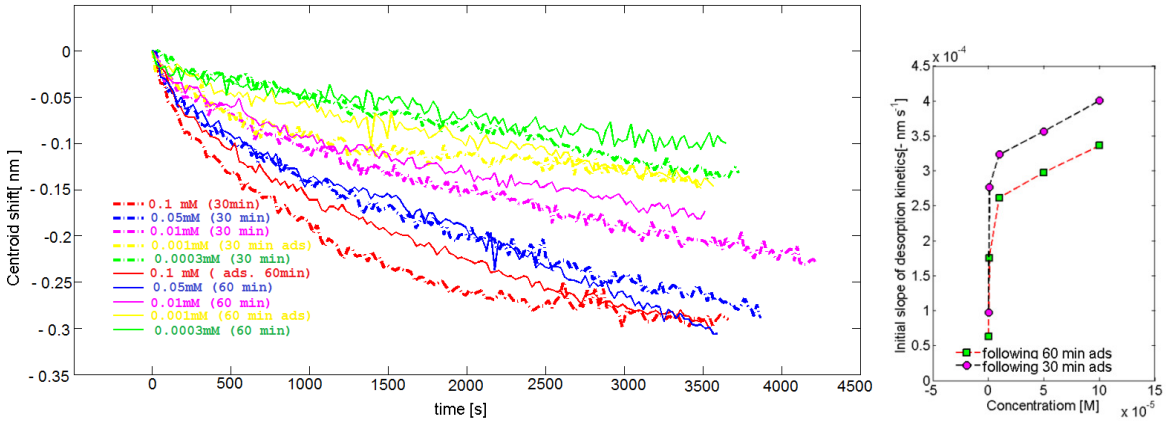

Figure4.25.*Case of the NaZ907DMSO-ALD:* ***(left)*** *the desorption kinetic curves measured after 30 min of adsorption (dashed lines) and after 60 min of adsorption (solid lines). (right): initial slope of desorption kinetics vs concentration derived from the desorption kinetics shown to the left. Clearly, the initial desorption rate is lower for samples which were exposed to 60 min adsorption compared to 30 min adsorption.*

What we see here is a clear difference in amplitudes of desorption because for all the 5 concentrations, more desorption was observed for desorption, which follows 30 min of adsorption compared to desorption after 60 min of adsorption. This very interesting result can be explained by what I mentioned in connection to figure 4.19 and 4. 20, i.e. that the more time we expose the dye solution to the sample surface, the more we allow dye molecules to reorganize on the surface, the more they will be strongly bound, and the less will be the physisorbed (loosely bound). In other words, if the molecule does not "land" with the anchoring ligands pointing towards the TiO_2, it might stay on the surface in a "loosely bound"

state until it either desorbs or rearranges itself on the surface to eventually form a stronger bond via the ligand; and it is intuitively correct to say that such re-arrangement need more time that a simple adsorption. Thus the fraction of the loosely bound molecules, which are the ones to be washed away at the beginning of desorption, is smaller after 60 min of adsorption compared to 30 min. that is why the figure 4.25 (right) puts together fig 22(right) and fig. 24(right) to explain the same phenomena, which we can put simply in this way:

For longer adsorption times we record for desorption, (of all concentrations) a higher initial desorption rate $\Delta\lambda/\Delta t$ compared to the ones of lower adsorption times (for all concentrations). Reasonably, this observation can be attributed to the existence of the loosely bound molecules, which need to be organized over the time to have an improved quality of the dye layer.

4.5. Theoretical estimation of the amount of molecules adsorbed/desorbed from INPS

To do this estimation, we adopt a quantitative interpretation of the response of surface plasmon resonance sensors to adsorbed films developed by Jung et al, 1998 [31]. This quantitative interpretation aims to convert the plasmon peak (or, in our case, centroid) shift signal at saturation $\Delta\lambda_{saturation}$ into a number of dye molecules adsorbed at the surface.

This estimation postulates that the plasmon wavelength shift ($\Delta\lambda_{\mu}$) is directly proportional to the change in the bulk index of refraction (Δn) of the medium in the vicinity of the sensors:

$$\Delta\lambda_{\mu} \propto \Delta n \Rightarrow \Delta\lambda_{\mu} = \mu\Delta n = \mu(n_{final} - n_{initial}), \quad (4.1)$$

where μ [nm/Refractive index unity or (RIU)] is the sensitivity of the sensor, which can be determined experimentally. For our sensors, the calibration was done by measuring the plasmon shift when a sensor was exposed to solvents with known refractive indices . The value of μ is ~110nm/RIU.

I consider a simple case of a single adlayer of thickness d and refractive index n_a, and above the adsorbate layer there is a solvent of index n_s (in our case, n_{DMSO}=1.48, and $n_{MeCNtBuOH} = (n_{MeCN} + n_{tBuOH})/2$=1.37). We use an effective index of refraction n_{effect} that is a weighted average of n_a and n_s, to estimate the response due to adsorption, as

$$\Delta\lambda_{saturation} = \mu(n_{effect} - n_s) \quad (4.2)$$

The evanescent electromagnetic field around the sensor nanoparticles, which determines the sensing volume, decays exponentially with a characteristic decay length l_d. It is the intensity of light (which is equal to the square of the field strength) that is "responsible" for the sensing, and thus the proper weighting factor in calculating n_{effect} is

e^{-2z/l_d} and the averaged value, n_{effect}, is calculated as

$$n_{effect} = \frac{2}{l_d}\int_0^\infty n(z)e^{-2z/l_d}dz \tag{4.3}$$

where $n(z)$ is the refraction index at height z.

The boundary conditions of our system, $n(z) = n_a$ for $0< z < d$, and $n(z) = n_s$ for $d < z < \infty$, help us to simplify the depth integral in calculation of n_{effect} so as to have

$$n_{effect} = n_a(1-e^{-2d/l_d}) + n_s e^{-2z/l_d} = n_s + (n_a - n_s)(1-e^{-2d/l_d}) \tag{4.4}$$

Then substituting eq.4.4 into eq.4. 2 gives:

$$\begin{aligned} &\Delta\lambda_{saturation} = \mu(n_{effect} - n_s) = \mu(n_a - n_s)(1-e^{-2d/l_d}) \Leftrightarrow \\ &d = -(\frac{l_d}{2})\ln[1-\frac{\Delta\lambda_{saturation}}{\mu(n_a - n_s)}] \end{aligned} \tag{4.5}$$

In eq. 4.5, we have 3 unknowns: d, l_d and n_a. The decay length l_d of the electric field around the sensing nanoparticles used in this thesis was numerically calculated by Tomasz Antosiewicz. For the Au nanodiscs coated by a 10 nm of TiO_2, the decay length in DMSO is 22.6 nm, and in MeCN:tBuOH is 23.1 nm.

In order to estimate the thickness of the adsorbed dye layer, one can assume that the corresponding thicknesses are the same for the layers formed in DMSO and in MeCN:tBuOH. (This is only an approximation, since there is more desorption in DMSO than in the other solvent, so the effective thicknesses will likely be somewhat different.) One could then equate the thicknesses in the two solvents as found from eq. 4.5:

$$(\frac{22.6}{2})\ln[1-\frac{0.5}{110(n_a - 1.48)}] = (\frac{23.1}{2})\ln[1-\frac{1.7}{110(n_a - 1.37)}]$$

Where 0.5nm and 1.7nm are the centroid shift at saturation ($\Delta\lambda_{saturation,}$ for the same dye concentration, 0.1mM) in DMSO and MeCN:tBuOH respectively. This above equation is a transcendental equation, which can be solved graphically to find n_a=1.525 as shown in figure 4.26. The thickness of the adsorbed dye layer is approximately 1.2 nm.

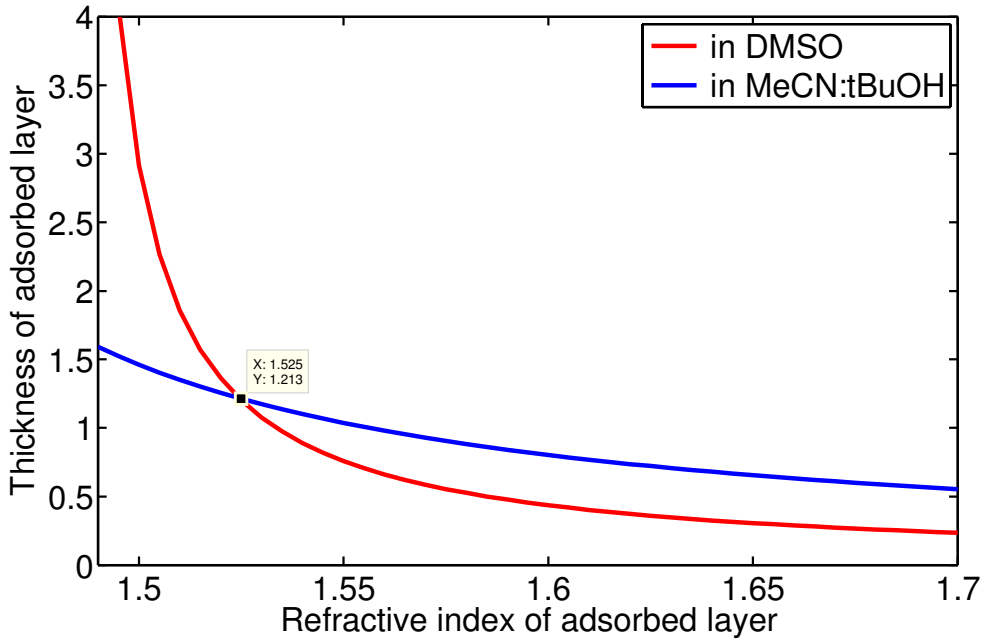

Figure4. 26. *Graphical determination of the refractive index of the Ru-dye*

The next step is to estimate the adsorbate coverage θ (in molecules/cm^2):

Adsorbate coverage θ (in molecules/cm^2)= d (in cm) × N (in molecules/cm^3), (4.8)

where N is the bulk number density of the adsorbate, which can be calculated as

$$N\left(\text{in molecules}/\text{cm}^3\right)=\frac{\text{bulk density of adsorbate}\rho\left(\text{in g}/\text{cm}^3\right)}{\text{molecular weight }\left(\text{g}/\text{mol}\right)}\times\text{Avogadro's number }\left(\text{molecules}/\text{mole}\right) \quad (4.9)$$

Shklover et al[6] reported a calculated density of 1.2 g/cm^3 for a similar dye molecule. Using this value of the density, the bulk number density of the dye becomes:

$$N=\frac{1.21\ (\text{g/cm}^3)}{947\left(\text{g}/\text{mol}\right)}\times 6.022\times10^{23}\ \left(\text{molecules}/\text{mole}\right)=7.69\times10^{20}\left(\text{molecules}/\text{cm}^3\right)$$

Using this above mentioned value of N in eq. 4.8, one gets the adsorbate coverage as $\theta=1.2\times10^{-7}\times7.69\times10^{20}=9.2\times10^{13}$ molecules/cm^2 . This corresponds to an area per adsorbed dye molecule of approximately 1.1 nm^2, which is in good agreement with the value of 1.3 nm^2 reported for the same dye by Harms et al. [12].

The above presented method of estimating the amount of dye adsorbed on TiO_2 gives more meaning to the adsorption and desorption signals that we have presented in the previous sections. The estimation is not very accurate, but it gives a quantitative idea and reasonable results.

Therefore, our kinetic measurements for adsorption and desorption provide two important types of information: (1) real-time detection of the dye layer formation, and (2) an estimation of the number of adsorbed dye molecules. In the next section, we are going to investigate the stability of Na/Z907 dye molecules, and attempt to improve it using adsorption and desorption processes.

4.6. Intermittent adsorption-desorption

As mentioned in section 4.4.3, there is a possible re-organization of dye molecules after sufficiently long adsorption times, and this has been shown by steeper initial desorption slopes for shorter adsorption times than for the longer time adsorption. This brought about a suggestion that the longer adsorption followed by the desorption would promote the formation of a compact dye layer due to the removal of more loosely bound molecules, which then opens a way to new sites for molecular binding upon subsequent adsorption steps. To overcome the factors, which limit the total number of strongly bound dye-molecules on the TiO_2 surface; in this section we are going to show different attempts made to try to form a more dense monolayer of Ru-dye on the TiO_2 surface.

I start with making a number of cycles of adsorption and desorption for dye solutions of the same concentrations for the NaZ907DMSO-ALD system, having in mind that, if really the desorption opens new adsorption sites, we would still see the increase in number of molecules adsorbed for subsequent cycles. Figure 4.27, shows the result of an experiment performed for 3 cycles of subsequent adsorption and desorption in a 0.001mM dye solution in DMSO. What is clear in this figure is that I observe a reduction in the number of molecules desorbing after each adsorption cycle (fig. 4.27, right). The latter can be quantified based on the calculations in the former chapter as that $-\Delta\lambda$~0.02nm or ~ $3.5181\times10^{12}\,(molecules/cm^2)$ desorbed at each 30 min of rinsing. Moreover, I observe a small increase in the total amount of adsorbed dye molecules after each consecutive adsorption step (figure 4.27, left). Of course all the desorbed molecules don't correspond to the number of adsorption sites made available upon intermittent rinsing because, there might be a multilayer formation, probably due to H-bond formation. Logically it is the dye molecules trapped in the multilayers, which are desorbed the first, and then some of the molecules at the surfaces will follow later.

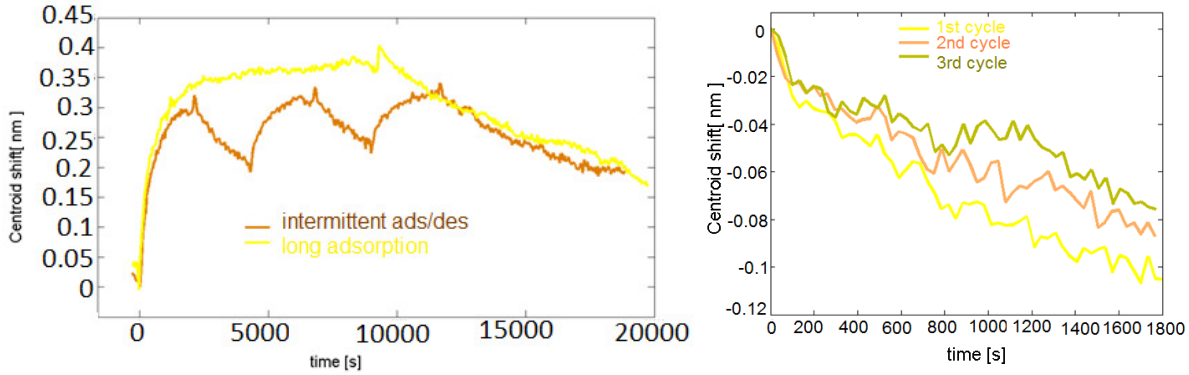

Figure4.27. *intermittent adsorption and desorption for a dye solutions of the same concentrations (0.001mM) of the NaZ907DMSO-ALD system. (**Left**): 3cycles of adsorption and desorption. (**Right**): only desorption cycles plotted together.*

The observed relatively large fraction of desorbed strongly bound dye molecules is mainly attributed to the fact that NaZ907 dissolves very well in DMSO. This means that for 30 min desorption even some of the tightly bound molecules are washed away, and upon 30min adsorption nearly a similar dye layer of nearly the same number of molecules is formed again. This, in turn, may mean that we have to replace the number of previously bound molecules washed out during the 30 min desorption because the estimated coverage remains at the expected ~ 5.4328×10^{13} $(molecules/cm^2)$ or $\Delta\lambda$~0.3nm which is also observed for a single adsorption taking place over the same total time interval as the sum of the intermittent adsorption steps (Figure 4.27 left).

I repeated the same experiment also at a higher dye concentration in DMSO solution. By increasing the concentration to 0.1mM carrying out a series of 15 min adsorption and desorption cycles, as shown on figure 4.28(left), we can see that there is an improvement in the number of adsorbed molecules after each adsorption cycle.

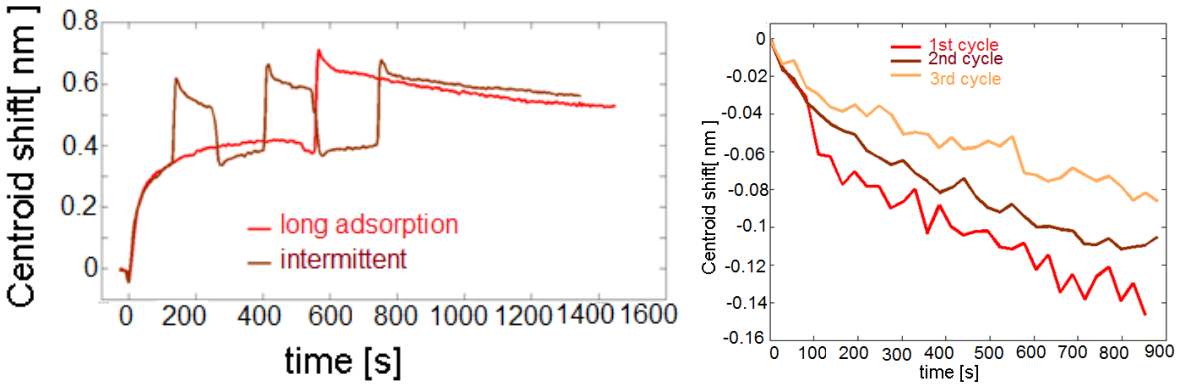

Figure4.28. *intermittent adsorption and desorption for a dye solutions of the same concentrations (0.1mM) of the NaZ907DMSO-ALD system. (**Left**): 3cyles of adsorption and desorption. (**Right**): only desorption cycles plotted together.*

For desoprtion, as can be seen in fig. 4.28, right, $-\Delta\lambda$~0.01nm or ~10^{12} $(molecules/cm^2)$ is the reduced number of molecules to be desorbed after each subsequent cycle. What one can deduce from this observation is that, by increasing the concentration (0.1mM and 0.001mM

were chosen for this investigation), if one could maximize the adsorption and try to reduce the desorption time by just sweeping away the loosely bound molecules one can make free a number of new adsorption sites to be occupied by additional dye molecules and thus form a more dense dye-layer for each successive adsorption.

If I go through this procedure systematically, I may start (**1st step**) by studying what results from the intermittent adsorption and desorption by just increasing the concentration at the next adsorption step. This experiment is carried out in the Z907DMSO-ALD system (a system that behaves nearly in the same manner as the Na Z907DMSO-ALD system) and the results are depicted on figure 4.29.

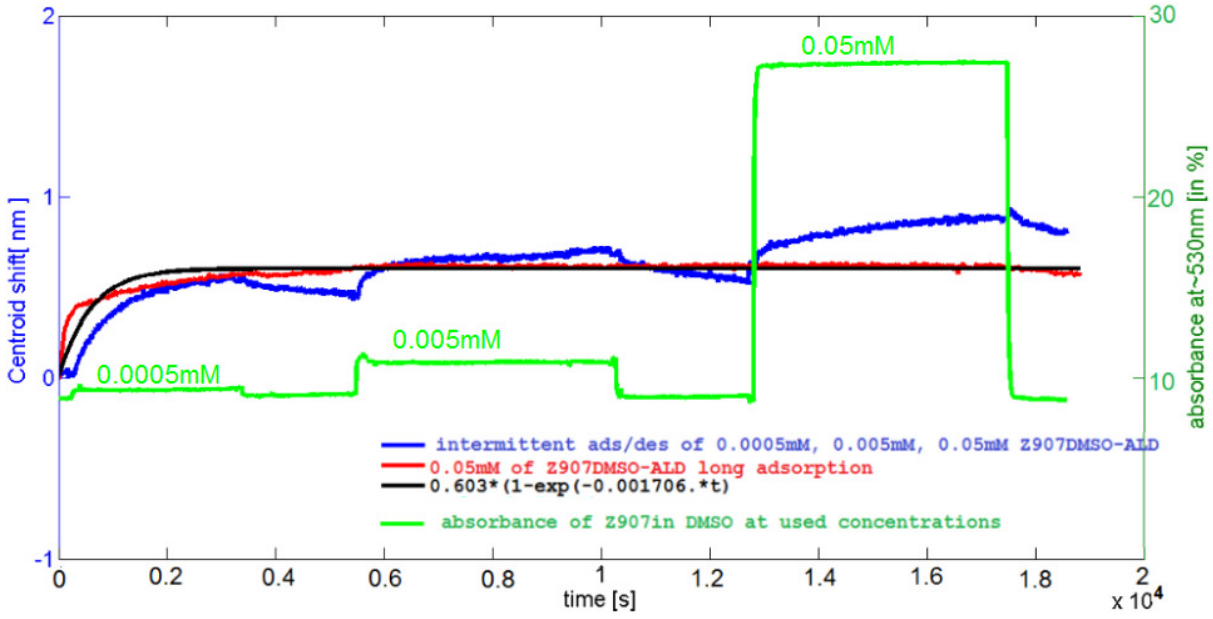

Figure4.29 *intermittent adsorption and desorption for a dye solutions with increasing concentrations of the Z907DMSO-ALD system.*

The result in figure 4.29 shows what we were expecting and is very interesting, i.e. I find an increasing number of molecules adsorbed after each cycle, because the more molecules that are in a unit volume of solvent (=higher concentration), the higher the chance of any of them to hit an available adsorption site after rinsing off loosely bound molecules in the preceding step. Consequently, I find that this approach of intermittently increasing the concentration during adsorption cycles leads to a total amount of molecules adsorbed that is significantly larger than what we would get during a single long adsorption at the highest concentration, which covers the whole 5 hours of the 2 experiments presented in fig. 4.29.

In the next step (**2nd step**) of this process of formation of the dense layer, I use the same concentrations of the NaZ907DMSO-ALD as above, but this time I maximize the adsorption steps and shorten the desorption step to only few minutes (~15min), just to try to sweep away only the loosely bound molecules; this situation is presented on figure 4.30.

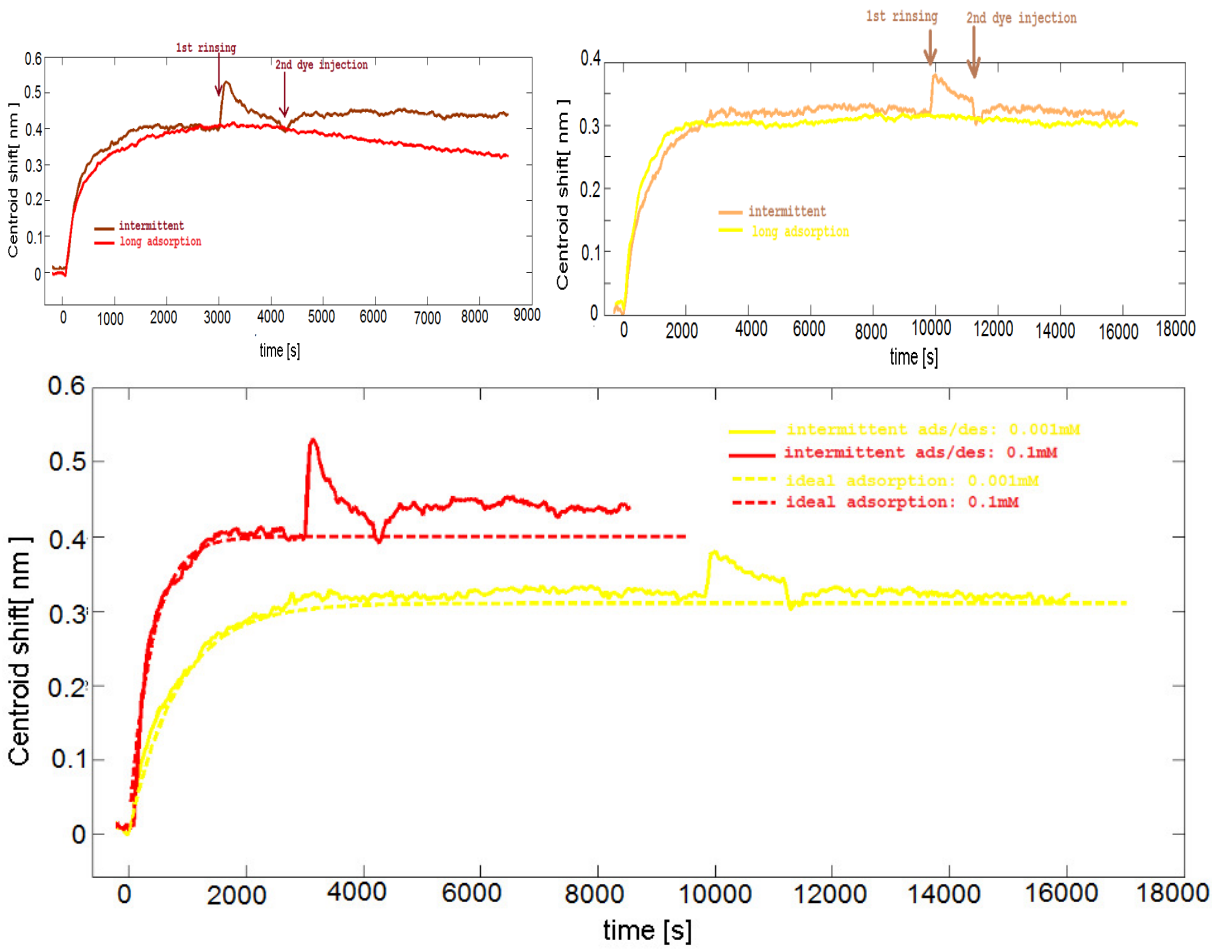

Figure4.30. *Intermittent adsorption and desorption for a dye solution of the same concentrations for the NaZ907DMSO-ALD system above. (**Top Left**): 2 cycles of adsorption and 1 short desorption for 0.1mM. (**Top Right**): 2 cycles of adsorption and 1 short desorption for 0.001mM. **(Bottom):** Comparisons of the results found on the top with the ideal long adsorptions for both concentrations.*

For the concentration 0.1mM (fig.4.30, top, left) the 15min sweep (desorption) has proved to be effective in removing the loosely bound molecules to make empty adsorption sites available, which then can be occupied by new dye molecules upon the next adsorption. The usefulness of having swept out loosely bound molecules and do the next adsorption is obvious when comparing the 2 types of adsorptions that we see in fig.4.30 (top, left). And even when one compare the increase in the adsorption signal with the horizontal of the ideal adsorption curve fig.4.30(bottom), one notice that there have been an increase of ~8.8221×10^{12} $(molecules/cm^2)$ (or $\Delta\lambda$ ~0.05nm) which is a non-negligible amount of additional dye molecules adsorbed upon well planned intermittent adsorption and desorption cycles.

The observation that there is no significant effect of using the "sweep" for the low concentration (see fig. 4.30. top, right and bottom) is presumably due to the fact that most of the molecules of the layer formed at lower concentrations are tightly bound already due to the fact that they are given more time to "organize" via diffusion to neighboring empty sites, before the latter are occupied by further adsorbed molecules. Thus, at low concentrations a "sweep" and subsequent adsorption of the same concentration will produce only a very small increase in molecules compared to the initially formed dye layer.

In the **3rd step** of the attempt of formation of the dense layer, I combine the first 2 steps. But it is clear that the time frame that we need for performing such an experiment is as high as ~20hours. Moreover, we have to aim at having a saturated adsorption at each step, which corresponds to nearly 2 hours for each adsorption step. Unfortunately, I have not yet been able to perform such an experiment for the NaZ907DMSO-ALD system, because of the blue shift observed during the adsorption. The latter occurs typically at ~1 hour for 0.1mM, and at 2 hours for 0.001mM dye solutions (see figure 4. 30). A solution to this problem is to use a long-pass filter to remove the visible part of the spectrum of the incident light and thus excite the plasmon with just the infrared (IR) without exciting the dye molecules that absorb light in the visible region. The reason for this procedure is going to be explained first in the next section in detail. Nevertheless I am going to show here an experiment done using the long-pass filter to eliminate/reduce the blue shift in order to be able to perform a meaningful **3rd step** attempt. The result is shown in figure 4.31 (red curve) where we now observe a dye layer formed by 0.1mM, which is stable up to 4 hours before it starts to blue shift.

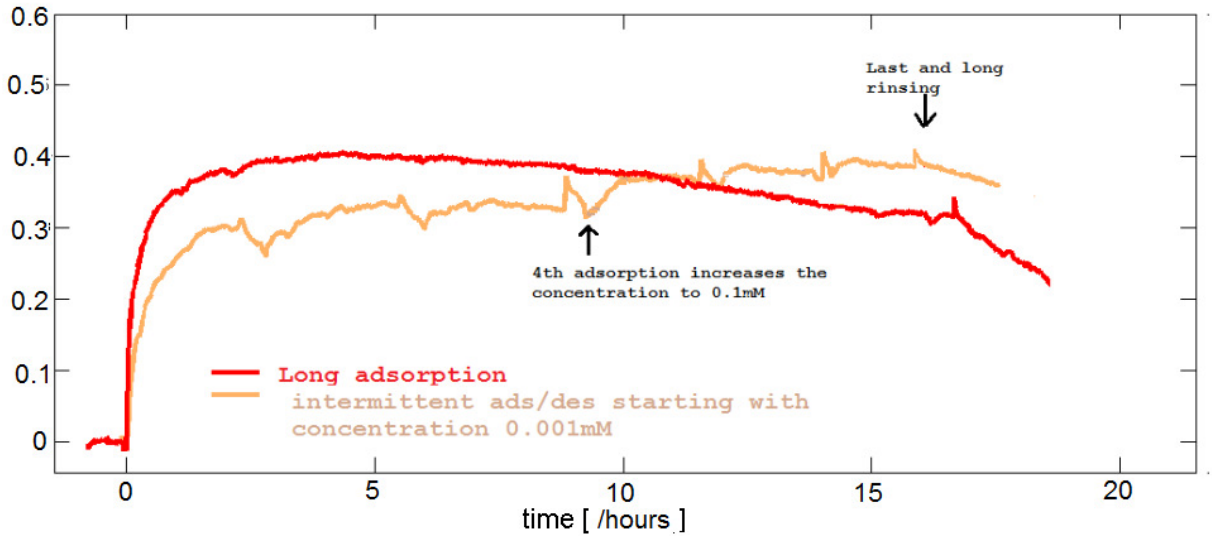

Figure 4.31. *Composed intermittent adsorption and desorption starting first in a dye solutions of 0.001mM concentration followed by intermittent adsorption and desorption at 0.1mM of the NaZ907DMSO-ALD system.*

For the intermittent case (orange curve in figure 4.31), the stability of the dye layer formed went up to the 10th hour before a blue shift appeared. At the 4th adsorption stage, I increased the concentration to 0.1mM and the number of molecules in the layer (resulting in the intermittent) increased and even went higher of the number of dye molecules in the layer of a single long adsorption (see figure 4.31)., At the 17th hour the layer (resulting in the intermittent) count an additional of ~ $1.2376\times10^{13}\,(molecules/cm^2)$ (or $\Delta\lambda$ ~0.07nm)

This gain of ~ $1.2376\times10^{13}\,(molecules/cm^2)$ is again associated to the fact that we have been "sweeping" away the loosely bound molecules and thereby exposing empty adsorption sites to the dye solution over and over again. Increasing the concentration has increased the probability of dye molecules to interact with the empty sites. Unfortunately, despite the increase in adsorbed dye molecules during intermittent adsorption, we still observe that the saturated value of the centroid shift intermittently formed dye layer after 17 hours is about the same as that of to the layer formed in a single long adsorption after 4 hours.

Would that mean that it is useless to investigate this type of adsorption for such a long time? Absolutely not! Because ***the stability*** in time of the formed dye-layer is of ultimate importance in the DSSC device, and it should be experimentally monitored. Also the solvent used (DMSO) seems to have played an important role in this intermittent process. As it was mentioned before, the NaZ907 dye seems to form not only H-bond with DMSO molecules but also this dye is susceptible of forming ions (due to electropositivity of the Na atoms) making this dye more soluble in DMSO. This "DMSO-phile" character of the used dye makes our sweeps (short desorption steps with DMSO), though short, to not only "brush away" the loosely bound molecules but also wash away some of the strongly bound molecules. Therefore it is interesting to repeat the above experiment using the same dye (NaZ907) but this time in the acetonitrile and Tert-Butanol mix as solvent? Figure 4.32 shows the outcome of this experiment.

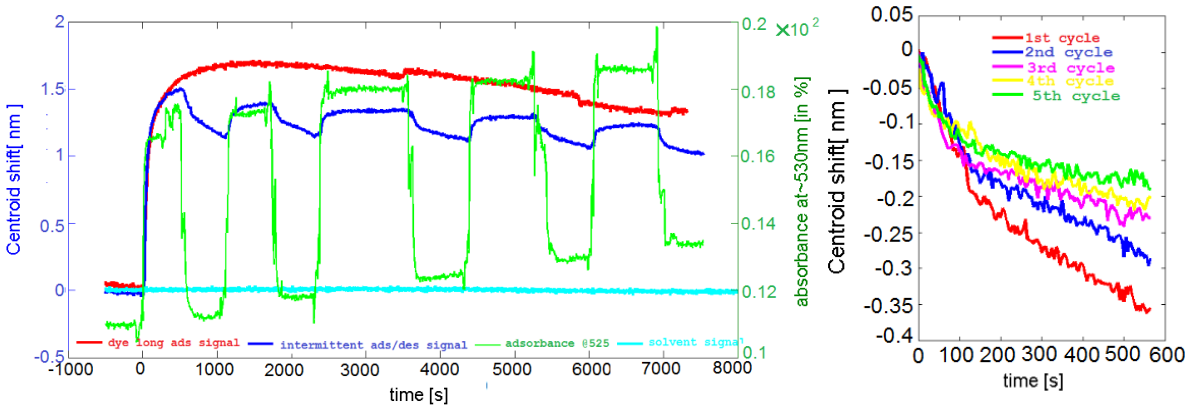

Fig. 4.32. *Intermittent adsorption and desorption for a dye solution of the same concentrations (0.1mM) of the NaZ907MeCN:tbuOH-sput system. (**Left**): 5cycles of adsorption and desorption. (**Right**): only desorption cycles plotted together.*

Now the situation that we have, even though the blue shift is more pronounced is that we observe a reduction in the number of molecules desorbed during each rinsing cycle (fig. 4. 32, right) by $-\Delta\lambda$~0.0167nm or ~8.7039×10^{11} $(molecules/cm^2)$. This situation is quite similar to the one that we observed in fig 27(right) and 28(right). This allows us to claim that what we thought happens to the system NaZ907DMSO-ALD - where the desorption was proven to be concentration dependent (see fig. 4.21, fig. 4.23 and fig. 4.25(right)) - may also be observed for the NaZ907MeCN:tbuOH-sput system.

In the experiment presented in figure 4.32, the sputtered sample used, displayed a very pronounced blue shift (starting as early as 10min). This blue shift, mentioned at numerous occasions above, has been a problem throughout all our experimental procedures. For this reason, a number of experiments have been done to try unearthing the origin of this unwanted blue shift in the hope to find a way to eliminate it. The latter is very important for future studies since it opposes the objective that we have in our work.

4.7. Blue shift in the adsorption curve

The blue shift, which has interfered with all our measurements, might be explained by the fact that dye molecules exposed to electromagnetic radiation can end up photobleaching! The fundamentals such photobleaching is not yet understood fully. Nevertheless it is an inspiring result of Pennec et al [32], who investigate the aftermath of the electronic excitation of the Ruthenium dye molecule called N3, which is of the same family as our used dye molecules, Z907. The only difference is that the 2 anchoring ligands of the N3 have been replaced by two hydrophobic alkyl chains on the bipyridyl ligands (see fig.3.2). In their experiments [32], it was found that the incident light can stimulate 2 processes: (i) at *longer wavelengths:* induction of an electronic transition from HOMO to delocalized LUMO immediately followed by an electron charge transfer to the TiO_2 conduction band. (ii) at *shorter wavelengths*: time-dependent change in the local chemical environment due to local charge distribution in the HOMO, followed by a photoemission (usually in non-visible range). The latter induces polarity in the dye molecule, independent if the molecule is adsorbed on TiO_2 or in solution.

The results of the experiments shown in figure 4.33 and 4.34 can be rationalized with the predictions by Pennec et al [32]. In figure 4.33 a high concentration (0.27mM) of NaZ907MeCN: tbuOH, forms (in the first few minutes) a layer on sputtered TiO2 sample, followed by severe blue shift of the centroid signal. Consequently, it appears that up to the 30^{th} minute of the adsorption nearly half of the initially adsorbed dye is again washed away from the surface under "light switched on" conditions. Interestingly, however, during the next 3 hours of the experiment a number of intermittent "lights on/off cycles" were made, and, as it can be seen in figure4.33 (top), half of the washed away dye is apparently recovered.

As a tentative explanation, the observations made can potentially be understood by invoking both the "longer wavelength" and the "shorter wavelength" processes explained above since; during an INPS measurement the dye is illuminated with white UV-vis-NIR light. Thus we induce charges both in the dye on the surface and in the solution in the illuminated spot in the used flow cell. If this is repeated over and over again, by circulating the dye solution as typically done in our experiments, we, over time, induce an electrostatic potential at the vicinity of the interfaces, which will act against the adsorption process. The consequence is a "washing away" of the previously adsorbed molecules. Thus by intermittently switching off the light during the INPS measurement, the system can "relax" from the radiation stress, and no more charges are created, which means that fresh dye molecules now can occupy available adsorption sites.

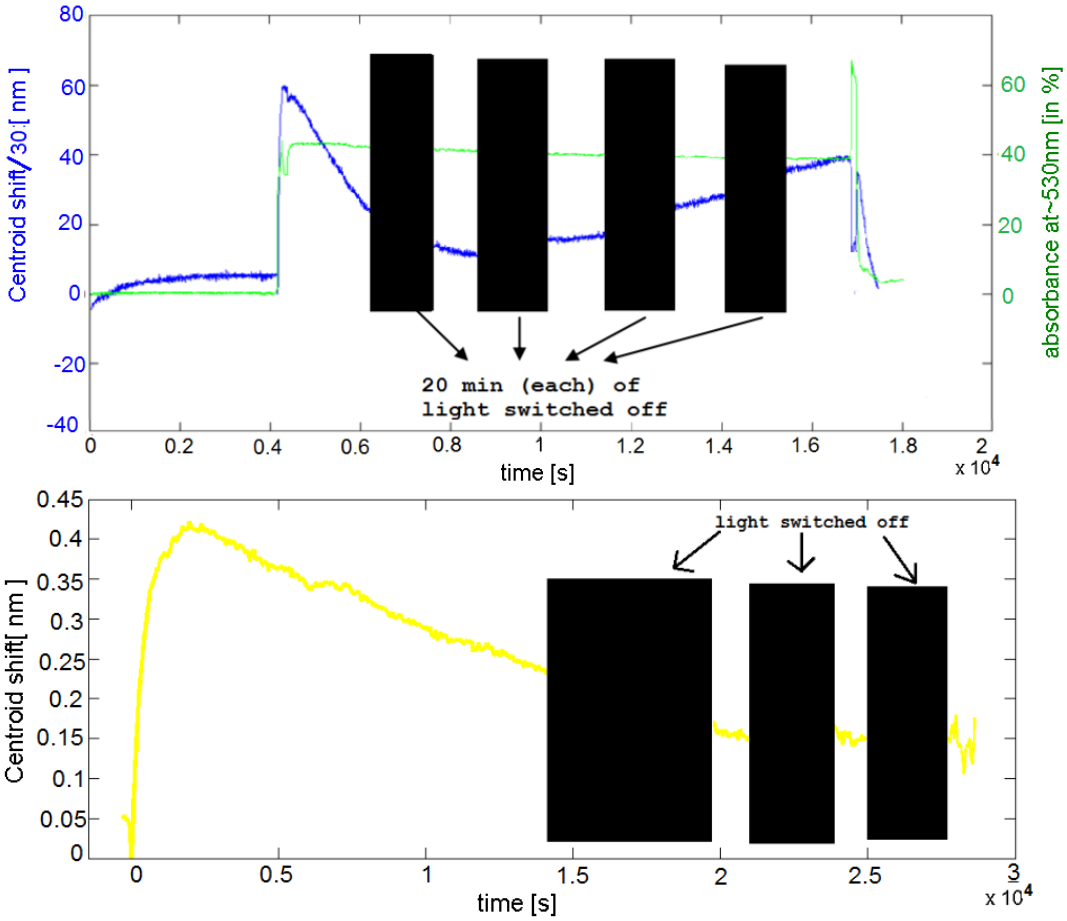

Fig. 4.33*. The observed trend of blue shift recovery.* ***(top****): the intermittent light on/off cycles for continuous adsorption in a 0.27mM solution of the NaZ907MeCN:tbuOH-sput system.* ***(Bottom)****: the intermittent light on/off cycles in 0.1mM dye solution of the NaZ907DMSO-ALD system.*

A similar intermittent light-off experiment as the one described above was also done in a 0.1mM solution with the NaZ907DMSO-ALD system (see figure 4.33, bottom): the adsorption took ~40 min before it started to blue shift, which continued to the 4th hour, then, a certain intermittent has stopped this blue shift, and the explanation of this is as explained in the previous paragraph, with the only difference that the sample used an ALD TiO_2 surface rather than a sputtered one.

In order to check the validity of our suggested explanation of the blue shift, a final experiment was conducted for the NaZ907 DMSO-ALD system with a dye solution concentration of 0.001mM (see fig 4.34). This system is typically not prone to a blue shift, at least up to 2 hours, which means that, according to our hypothesis, during this 2h period, the radiation stress on the dye molecules is minimum thus relaxing it by turning of the light would have no effect – precisely what is seen in the figure 4.34.

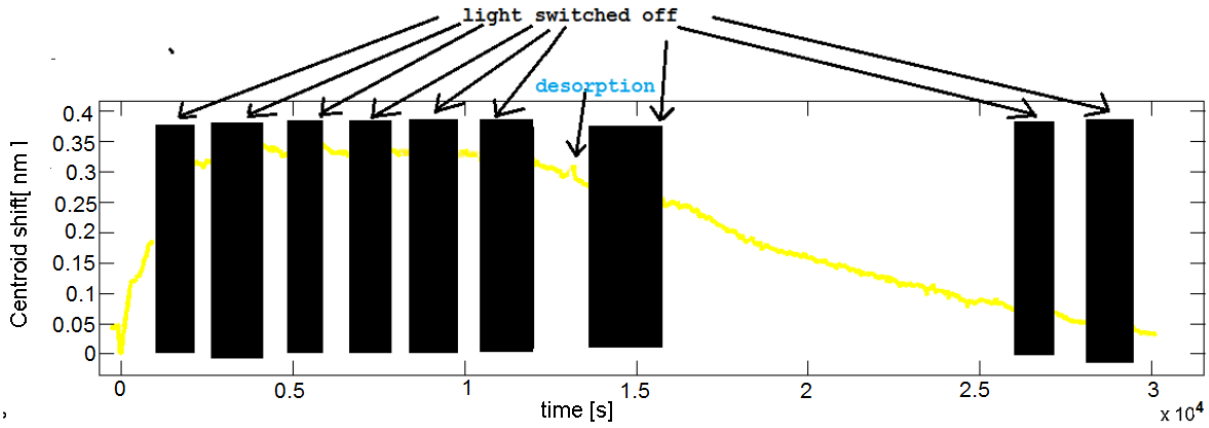

Fig. 4.34*. charge induction test for the system NaZ907 DMSO-ALD at a concentration of 0.001mM.*

So, what can we finally conclude from our dye-adsorption/desorption studies? This is going to be the object of the following and concluding chapter of this report.

5

Conclusions and outlook

In this concluding chapter, the main question to answer is if I have achieved the objective that we had at the beginning of the work associated to this thesis. As it is going to be in the first part of this chapter, the answer is "yes" and "no!" Yes, because as we have shown in the section 4.6 of the previous chapter, I have been able to use the adsorption and desorption studies to form a Ru-dye layer which is of improved quantity and stability compared to the one we usually have for a single adsorption/desorption processes. But still there have been impediments, which prevented to have considerable improvements in the quality of conventional single adsorption. Then the end part of this report will suggest what could be done in future studies on the dye molecule adsorption process on TiO_2 surfaces for DSSC applications.

5.1. Summary and Conclusions

In the study presented in this report, as I used Ruthenium dye molecules (Na/Z907) interacting with 2 types of TiO_2 surfaces (or deposited using the 2 different deposition methods, the RF-sputtering and the ALD), I have been able to re-affirm the high values of affinity between TiO_2 sites and Na/Z907 molecules. For the interaction between RF-sputtered TiO_2 and NaZ907 an adsorption equilibrium coefficient K_{eq} ranging between 0.4×10^4 M^{-1} and 3.4×10^5 M^{-1} (on different solvent and analysis method used) was found. For the interaction between ALD TiO_2 and NaZ907 in DMSO medium the values found of K_{eq} were higher (in different analysis methods) and were ranging between 3.4×10^4 M^{-1} and 5.3×10^5 M^{-1}

In this report, I have been able to adapt a method to calculate the number of molecules adsorbed/desorbed on/from the surface from the centroid shift signal measured in the INPS

experiments. The calculations are based on an assumed exponential decay of the enhanced field around the plasmonic gold sensor particles, and an assumption that the same dye at the same concentration would form layers of the same thicknesses irrespective to the media they are immersed into (whether DMSO or MeCN:tBuOH). Using this approach we calculated, for example, the number of molecules per square centimeter needed to saturate each of the 2 main systems used, i.e. NaZ907 DMSO-ALD, and NaZ907MeCN:tBuOH-Sput, for the same dye concentration of 0.1 mM (centroid shift of 0.5 and 1.7 nm respectively)to be ~9.2×10^{13} *molecules/cm*^{2}. And this calculation, though approximate, it has been useful in analyzing quantitatively the reorganization of dye molecules and their stability.

In this project I was also interested to in finding the state of the adsorbed molecules on the TiO_2 surface. From the design of the Na/Z907 molecule with just 2 anchoring ligands, close to each other, it is reasonable to think that such molecules would not form an organized layer at the surface at once. This because different molecular interactions would prevent the 2 (-COOH) anchoring groups of many molecules to be bind to the appropriate TiO_2 adsorption sites *directly* after first contact with the surface. Such molecules not bound strongly with their tailored anchoring ligands (only physisorbed) are called loosely bound molecules. As one of the results of this work we found that at higher dye molecule concentrations in the solution we have more loosely bound molecules than at lower concentrations. Moreover, the existence of these loosely bound molecules was confirmed by the concentration dependence of desorption, where we observed that higher concentrations have higher values of the molecules desorbed compared to lower concentrations. For example, for the same dye (NaZ907 in DMSO on ALD TiO_2) and after 1 hour of rinsing, but for a concentration of nearly 3 orders of magnitude different (~1000 times different: 0.1mM vs. 0.0003mM), we have desorbed

$$\theta^{0.1mM}_{NaZ\,907\,DMSO} = 5.43\times10^{13}\ molecules/cm^2 > \theta^{0.0003mM}_{NaZ\,907\,DMSO} = 1.77\times10^{13}\ molecules/cm^2 .$$

We have also made attempts using intermittent rinsing to “sweep out” only the loosely bound molecules to make room for more dye molecules to adsorb properly. These attempts have been hampered by the nature of the solvent we used the most, DMSO, which in fact washed away both the loosely and many tightly bound molecules. This made it challenging to use DMSO “sweeps” to form a dye monolayer of good quality (dense) by using the intermittent adsorption and desorption approach.

In our endeavor trying to form a dye layer of good quality, we encountered another difficulty – the notorious blue shift. As the possible origin we identified electrostatic forces (issuing from the excitation of the adsorbed dye molecules and produced electrons which become stagnant at the TiO_2 surface) opposing the dye adsorption potential. It proved to be that there is no way to get rid of this blue shift completely. Nevertheless by trying to identify the origin of this phenomenon (which is the incident light, meant to excite the plasmon, but also it excites the dye) we identified that exciting only the plasmons by using just the IR radiation (removing the visible part of the spectrum of the light where the dye is excited) increases the time interval where we can do measurements without this blue shift.

5.2 Outlook

As it was mentioned in the previous paragraph, we would advice the researcher who would continue this project first to find a way to deal with the problem mentioned in the previous section of the excess dissolution of NaZ907 in DMSO. When it comes to switching to a solvent different from DMSO, why not start the trial with acetonitrile and Tert-Butanol at equal proportions (MeCN:tbuOH-sput,1:1)?

Regarding the problem of the blue shift, the use of a long-pass filter to reduce the photobleaching of dye molecules during the INPS experiments is probably a good solution. In this way the sample is only irradiated by IR light (to which the LSPR of the INPS chip is tuned by adjusting the Au nanodisk size accordingly), which is not absorbed by the dye molecules.

Finally, after understanding the formation of a good quality and stable dye monolayer layer on the flat TiO_2 surface model system used in this study, for practical purposes, the next step would be to extend such studies to mesoporous samples. Doing so is relaxing the hypothesis of surface simplification of the system. Many of the parameter, procedures and methods that have been used in our work (for flat surfaces), like Langmuir adsorption/ desorption, quantitative study, the red/blue shift, among others will no longer be valid, or will have their corresponding values in the mesoporous case. Another motivation for this is that some investigations of dye (Z907) adsorption /desorption on a mesoporous TiO_2 using the INPS, have already been performed [14] and the results are very encouraging. It may seem like this project of trying to pack as much dye molecules as possible in the pores of on the mesoporous TiO_2 would be very ambitious, but it may be worth all efforts, because in practice semiconductors where dye have to be adsorbed in DSSC device are not flat TiO_2, but mesoporous structures with large specific surface areas.

Bibliography

[1] O'Regan B., Grätzel M., *A low-cost, high-efficiency solar cell based on dye-sensitized colloidal TiO_2 films*, Nature, 353 (6346) (1991): 737–740, doi:10.1038/353737a0.

[2] Hagfeldt A., Boschloo G., Sun L., Kloo L., Pettersson H., *Dye-Sensitized Solar Cells*, Chemical Reviews 110 (11) (2010): 6595–6663, doi:10.1021/cr900356p

[3] Wang P., Zakeeruddin M., Moser J. E., Nazeeruddin, M. K.; Sekiguchi T., Grätzel M., *A stable quasi-solid-state dye-sensitized solar cell with an amphiphilic ruthenium sensitizer and polymer gel electrolyte*, Nature Materials 2 (6) (2003): 402–7, doi:10.1038/nmat904.

[4] Nazeeruddin M. K., Humphry-Baker R., Liska P., Grätzel M., *Investigation of Sensitizer Adsorption and the Influence of Protons on Current and Voltage of a Dye-Sensitized Nanocrystalline TiO_2 Solar Cell,* J. Phys. Chem. B 107 (8981)(2003)

[5] Perez Leon C., Kador L. , Peng B. , Thelakkat M., *Characterization of the Adsorption of Ru-bpy Dyes on Mesoporous TiO_2 Films with UV-Vis, Raman, and FTIR Spectroscopies*, The Journal of Physical Chemistry *B* 110(17) (2006): 8723-8730

[6] Shklover V., Ovchinnikov Y. E., Braginsky L. S., Zakeeruddin S. M., Grätzel M., *Structure of Organic/Inorganic Interface in Assembled Materials Comprising Molecular Components. Crystal Structure of the Sensitizer Bis[(4,4'-carboxy-2,2' bipyridine) (thiocyanato)] ruthenium(II),*Chem. Mater. 10(2533)(1998)

[7] Lee K. E., Gomez M. A., Elouatik S., Demopoulos G. P., *Further Understanding of the Adsorption Mechanism of N719 Sensitizer on Anatase TiO_2 Films for DSSC Applications Using Vibrational Spectroscopy and Confocal Raman Imaging* ,Langmuir 26(9575)(2010)

[8] Fillinger A., Parkinson B. A., *The Adsorption Behavior of a Ruthenium-Based Sensitizing Dye to Nanocrystalline TiO_2 Coverage Effects on the External and Internal Sensitization Quantum Yields*, J. Electrochem. 146 (12) (1999): 4559-4564, doi: 10.1149/1.1392674

[9] De Angelis F., Fantacci S., Selloni A., Nazeeruddin M. K., Gratzel M., *Influence of the Sensitizer Adsorption Mode on the Open-Circuit Potential of Dye-Sensitized Solar Cells*, J. Phys. Chem. C 114(6054) (2010)

[10] Hagberg D. P., Marinado T., Yum J., Karlsson K. M., Hagfeldt A., Lee H., Grätzel M., De Angelis F., Humphry-Baker, Sun L.,Nazeeruddin M. K., *Molecular Engineering of Organic Sensitizers R. for Dye-Sensitized Solar Cell Applications*, Journal of Am. Chemical Society. 130(2008): 6259–6266

[11] Bazzan, G.; Deneault, J. R.; Kang, T.-S.; Taylor, B. E.; Durstock, M. F., *Nanoparticle/ Dye Interface Optimization in Dye-Sensitized Solar Cell*s, Adv. Funct. Mater. 21 (2011): 3268-3274.

[12] Harms H. A., Tetreault N., Gusak V., Kasemo B., Grätzel M., *In situ investigation of dye adsorption on TiO_2 films using a quartz crystal microbalance with a dissipation technique*, Phys. Chem. Chem. Phys. 14 (2012): 9037–9040, doi: 10.1039/c2cp41268c

[13] Langhammer C., Larsson E. M., Kasemo B., Zoric´I, *Indirect Nanoplasmonic Sensing: Ultrasensitive Experimental Platform for Nanomaterials Science and Optical Nanocalorimetry*, Nano Lett. *10 (*2010): 3529–3538, doi: 10.1021/nl101727b

[14] Gusak V., Heiniger L.P., Graetzel M., Langhammer C., Kasemo B. *Time-resolved indirect nanoplasmonic sensing spectroscopy of dye molecule interactions with dense and mesoporous TiO_2 films,* Nano Lett. 12(5) (2012):2397-403. doi: 10.1021/nl3003842

[15] Grätzel M., *Recent Advances in Sensitized Mesoscopic Solar Cells*, Accounts of Chemical Research 11(42) (2009): 1788-1798

[16] Lee C., Kim H., Jang I., Im J., Park N., *Pseudo First-Order Adsorption Kinetics of N719 Dye on TiO_2 Surface*, ACS Appl. Mater. Interfaces 3 (2011): 1953–1957, dx.doi.org/10.1021/am2001696

[17] Lu Y., Choi D., Nelson J., Yang O., Parkinson B. A., *Adsorption, Desorption, and Sensitization of Low-Index Anatase and Rutile Surfaces by the Ruthenium Complex Dye N3*, Journal of The Electrochemical Society, 153 (8) (2006)E131-E137

[18] Larsson E. M., Syrenova S., Langhammer C., *Nanoplasmonic sensing for nanomaterials science* , Nanophotonics 1 (2012): 249–266 . doi 10.1515/nanoph-2012-0029

[19] Katoh R., Yaguchi K., Murai M., Watanabe S., Furube A., *Differences in adsorption behavior of N3 dye on flat and nanoporous TiO_2 surfaces*, Chemical Physics Letters 497 (2010) 48–51

[20] Fredriksson H., Alaverdyan Y., Dmitriev A., Langhammer C., Sutherland D. S.,Zäch, M. , Kasemo B., *Hole–Mask Colloidal Lithography*, Advanced . Materials 19 (2007) 4297–4302, doi: 10.1002/adma.200700680

[21]FredrikssonH. ,*Nanostructures of Graphite and Amorphous Carbon –Fabrication and Propreties*, PhD. Thesis, Chalmers University of Technology (2009)

[22] Tanemura S., Miao L., Wunderlich W., Tanemura M., Mori Y., Toh S., Kaneko K., *Fabrication and characterization of anatase/rutile –TiO_2 thin films by magnetron sputtering: a review*, Science and Technology of Advanced Materials 6 (2005) 11–17, doi:10.1016/j.stam.2004.06.002

[23] Marichy C., Bechelany M., Pinna N.,*Atomic Layer Deposition of Nanostructured Materials for Energy and Environmental Applications*, Advanced Materials *24 (*2012)1017–1032, doi: 10.1002/adma.201104129

[24] Wang, P.; Zakeeruddin, S. M.; Exnar, I.; Grätzel, M. *Chem. Commun.* 2002, 2972.

[25] Wang, P.; Zakeeruddin, S. M.; Humphry-baker, R.; Moser, J. E.; Grätzel, M. *Ad*V. *Mater. (Weinheim, Ger.)* 2003, *15*, 2101.

[26] Wang, P.; Zakeeruddin, S. M.; Moser, J. E.; Nazeeruddin, M. K.; Sekiguchi, T.; Grätzel, M. *Nat. Mater.* 2003, *2*, 498.

[27] Nazeeruddin M. K., Kay A., Rodicio I., Humphrybaker R., Muller E, Liska, P.,Vlachopoulos N, Gratzer M., Journal of the American Chemical Society 1993, 115 (14), 6382-6390

[28]Hirata N., Lagref J.J., Palomares E. J, Durrant J. R, Nazeeruddin M. K., Grätzel, M., Davide D., *Supramolecular control of charge-transfer dynamics on dye-sensitized nanocrystalline TiO_2 films*,Chem.Eur. J. 10(2004) 595- 602, doi: 10.1002/chem.200305408

[29] Wang P., Klein C., Humphry-Baker R., Zakeeruddin S. M., Grätzel M., A *High Molar Extinction Coefficient Sensitizer for Stable Dye-Sensitized Solar Cells*, Journal of American Chemical Society127 (2005) 808-809

[30] Fattori, A.; Peter, L. M.; McCall, K. L.; Robertson, N.; Marken, F., *Adsorption and redox chemistry of cis-RuLL'(SCN)(2) with L=4,4'-dicarboxylic acid-2,2'-bipyridine and L'=4,4'-dinonyl-2,2'-bipyridine (Z907) at FTO and TiO(2) electrode surfaces*. Journal of Solid State Electrochemistry **2010,** 14 (10), 1929-1936;

[31] L. S. Jung, C. T. Campbell, M. N. Mar, T. M. Chinowsky, S. S. Yee, Quantitative Interpretation of the Response of Surface Plasmon Resonance Sensors to Adsorbed Films, *Langmuir 14(1998)* 5636-5648

[32] Y. Pennec (UBC) ypennec@physics.ubc.ca, S. Burke (UBC) saburke@physics.ubc.ca, D. Bonn (UBC); W. Auwärter, J. Reichert, P. Feulner, J.V. Barth (TU Munich); A. Schiffrin, R. Kienberger (MPI for Quantum Optics), *Probing and controlling coherent charge dynamics at atomically engineered solid state interfaces*, on http://www.mpg-ubc.mpg.de/project9.html visited on 2013-10-29

Appendices

Appendix I: Plasmon Physics

I.a. Localized Plasmon – Drude Model

In the Drude-model, (which is in fact an overly simplified model of electrons in a metal), one considers an oscillating field $\vec{E}(\vec{r},t)$ interacting with the gold nanoparticles and provoke a displacement of light electrons compared to heavier lattice ions with a restoring force of $\vec{F}(\vec{r},t) = q\vec{E}(\vec{r},t)$. When charges are so separated, the coulomb attraction will impose a restoring force, and the resulting collective oscillatory behavior of the gas electron: the Plasmon.

Mathematically we can write the Maxwell's Equation for the displacement field $\vec{D}(\omega)$ as

$$\vec{D}(\omega) = \varepsilon_0 \varepsilon(\omega)\vec{E}(\omega) = \varepsilon_0 \vec{E}(\omega) + \vec{P}(\omega) \qquad \text{(I.1)}$$

$\varepsilon(\omega)$ is the dielectric function, ε_0 the vacuum permittivity and $\vec{P}(\omega)$ frequency depending on the polarization vector.

From a Drude-model which is purely classical, to be able to explain the quantum phenomenon of Plasmon, we introduced a quantum aspect in the model and then use the Drude-Sommerfeld model, where unbound electron moves in a periodic potential as a free electron in vacuum. The equation of motion of conduction electrons can be written as

$$m_e \frac{\partial^2 \vec{r}}{\partial t^2} + m_e \kappa \frac{\partial \vec{r}}{\partial t} = -q_e \vec{E}(t) \qquad \text{(I.2)}$$

where m_e is the electron mass, κ damping parameter and q_e is the electronic charge.

By doing the Fourier transformation in the time domain, and solve eq. (I.2), −the interested reader can find details in [I.1]* − one finds $\vec{r}$ in the frequency space as:

$$\vec{r}(\omega) = \frac{q_e / m_e}{\omega^2 + i\kappa\omega}\vec{E}(\omega)\text{, } i \text{ being the imaginary unit.} \qquad \text{(I.3)}$$

To this point we can express the polarization vector (=the how much dipole moment in a certain unit volume), $\vec{P}(\omega)$, previously found in eq. (I.1) as,

$$\vec{P}(\omega) = -\eta_e q_e \vec{r}(\omega) \qquad \text{(I.4)}$$

η_e being the density of electrons. By inserting (I.3) into (I.1) and use (I.4) we find

***[I.1] Folland G. B., Fourier analysis and its applications. Providence: American Mathematical Society; 1992**

$$\varepsilon_{free} = 1 - \frac{\omega_{plasma}^2}{\omega^2 + i\kappa\omega} \tag{I.5}$$

where ε_{free} is the free electron dielectric function, ω_{plasma} is the plasma frequency and

$\omega_{plasma} = \sqrt{\frac{\eta_e q_e^2}{\varepsilon_0 m_e}}$ is the plasma frequency. (I.6)

For lower energies (Novotny L. & Hecht B in their book about the principle of nano-optics [I.2]* they define low energies to be E< 2.26 eV or lambda>550nm) this Drude-Sommerfeld is an ideal model,(in noble metal such as gold, electrons are not really free) and also for the sake of measurements to be done in this project, mostly aimed to cover pretty much of the solar spectrum , which includes the higher energy regimes (E> 2.26 eV or lambda<550nm), then to the above described model we have to include the fact that some electrons in the bands below the conduction bands can be excited too [I.2]*. If so considered, the force term of the equation I.2 can be modified by including a certain nuclei potential term $\gamma\vec{r}$. The same algebra as shown above (the details about this can still be found in [I.2]*) will lead to the interband dielectric function $\vec{P}(\omega) = \varepsilon_{dielec}\wp(\omega)\vec{E}(\omega)$ to be expressed as

$$\varepsilon_{\text{int}} = 1 - \frac{\tilde{\omega}_{plasma}^2}{(\omega^2 - \omega_0^2) + i\alpha\omega} \tag{I.7}$$

where $\omega_0^2 = \frac{\gamma}{m_{eff}}$, α the damping factor for bound electrons and

$\tilde{\omega}_{plasma} = \sqrt{\frac{\tilde{\eta}_e q_e^2}{\varepsilon_0 m_{eff}}}$ the plasma frequency of bound electrons (I.8)

And on their turn, $\tilde{\eta}_e$ and m_{eff} are density of bound electrons and effective mass respectively.

As mentioned in the section 3.3 of Chapter 3, this phenomenon which is more likely to happen in the case of measurements connected with this thesis will be in the range of wavelengths starting to 510 nm up to 900nm (dye absorption at ~525 and Plasmon peak at ~900 in dye solution) which shows that this theory fits well with the experiment that we will look at in some details in chapter 4.

It is easy to notice that eq. I.7 can be easily rationalized and be written as,

$$\varepsilon_{\text{int}}(\omega) = 1 + \frac{\tilde{\omega}_{plasma}^2(\omega_0^2 - \omega^2)}{(\omega^2 - \omega_0^2)^2 + \alpha^2\omega^2} + i\frac{\alpha\tilde{\omega}_{plasma}^2\omega}{(\omega^2 - \omega_0^2)^2 + \alpha^2\omega^2} \tag{I.9}$$

And one has to notice that the real part of this interband dielectric function, ε_{int}, is negative at least for wavelengths in the region 400< λ< 1000 [I.2]* (which will be our region for dye absorption spectra ─ see figure 3.4). As this is related to the energy stored within the noble metal (Au in our case), and it shows that the light penetration depth in Au is very small, thus the name ***Localized Surface Plasmon (or LSP)***.

***[I.2] Novotny L and Hecht B., Principles of Nano-Optics. New York: Cambridge University Press; 2006**

I.b. Plasmonic in Spherical nanoparticles

In the rest of this report, it will be made clear that the Au nanoparticles to be used in the measurement samples are cylindrical, so, to establish their plasmonic theory, we start with the plasmonic in spherical nanoparticles. The interested reader can look in more details how Gustav Mie solved Maxwell's equations for the case of an incident plane electromagnetic wave interacting with a spherical particle in Kreibig and Vollmer, 1995 [I.3]* or Bohren C. and Huffman D., 1998 [I.4]# and see how for very small spherical particles (diameter < 30nm) we consider only the first term of the expansion- the dipolar term; This solution is what we call the "quasi-static or Rayleigh limit". As, in this case, the radius is very much smaller than the wavelength of used light, the polarizability $\wp(\omega)$ can be written as

$$\wp(\omega) = 4\pi R^3 \frac{\varepsilon(\omega) - \varepsilon_{dielec}}{\varepsilon(\omega) + 2\varepsilon_{dielec}} \qquad \text{(I.10)}$$

where R is the radius of the nanosphere and ε_{dielec} the dielectric function of the environment surrounding the nanoparticle. Now if the nanosphere is found in the isotropic medium (which means of constant ε_{dielec} at least for the visible spectrum), in that case there exist a frequency ω_0 that maximize the polarizability function $\wp(\omega)$, this maximum frequency can be found from eq. (I.10) when

$$\mathrm{Re}\,al\{\varepsilon(\omega)\} + 2\varepsilon_{dielec} = 0\,. \qquad \text{(I.11)}$$

Remember that even though we defined the dipole moment differently in eq. (I.4) but in fact eq. (I.1) shows that the dipole moment has the dimension [Permittivity × polarizability × Electric Field] which can be written as

$$\vec{P}(\omega) = \varepsilon_{dielec}\wp(\omega)\vec{E}(\omega) \qquad \text{(I.12)}$$

This eq. I.12 shows that ω_0 also maximize the dipole moment. So one can easily say that the incident light has, in this case, maximum probability of exciting the electron cloud (of the nanoparticle) with respect to the atomic nuclei to a phenomenon which is called ***Localized Surface Plasmon Resonance or LSPR.***

In the next section, there is a comment on how the LSPR conditions only change when there is only a change in the dielectric function of the metal of which the nanoparticle is made of, but the truth is that the LSPR conditions are strongly dependent on the geometry of the used nanoparticle. What are we to do as it has been mentioned before that Au nanoparticles to be used in the measurement samples are cylindrical?

I.c. Plasmonic in cylinder-like (spheroids) nanoparticles

The previous sub-section has shown the important results that we get from the geometry of

*** [I.3]Kreibig and Vollmer, 1995 U. Kreibig, M. Vollmer Optical Properties of Metal Clusters Springer-Verlag, Berlin (1995)**

 # [I.4] . Bohren C. and Huffuman D., Absorption and scattering of light by small particles. New York: John Wiley & Sons; 1998.

the spherical nanoparticle. As the nanoparticles used are cylindrical, we can approach it with a certain spheroid of $u = v > w$ with semi-axes $r_x = u$, $r_y = v$, $r_z = w$ and with a low aspect ratio c/a. The detail of this procedure can be found in Bohren C. and Huffman D., 1998 [I.4]*, but briefly, the result of applying this to eq. (I.6) gives now, the expression of the polarizability along an axis n, $n \in \{x, y, z\}$ to be

$$\wp_n(\omega) = V \frac{\varepsilon(\omega) - \varepsilon_{dielec}}{\varepsilon_{dielec} + L_n[\varepsilon(\omega) - \varepsilon_{dielec}]} \tag{I.13}$$

Where $V = \frac{4}{3}\pi uvw$ is the volume of a spheroid,

$$L_n = \frac{uvw}{2}\int_0^\infty \frac{d\ell}{(\ell + r_n^2)\sqrt{(\ell + u^2)(\ell + v^2)(\ell + w^2)}} \tag{I.14}$$

is the so-called the spheroid shape-factor.

(I.4) into (I.13) gives, after some mathematical manipulations,

$$\omega_{LSPR} = \frac{\omega_{plasma}}{\sqrt{1 + (1/L_n - 1)\varepsilon_{dielec}}} \tag{I.15}$$

which is an important theoretical result because, it shows that there will occur a shift in the LSPR when ε_{dielec} changes, in other words, when the refractive index changes, because,

$$\varepsilon_{dielec} = n_{dielec}^2 \tag{I.16}$$

if we take n_{dielec}^2 to be the refractive index of the dielectric.

***[I.4] . Bohren C. and Huffuman D., Absorption and scattering of light by small particles. New York: John Wiley & Sons; 1998.**

Appendix II: Plasmon Peak fitting procedure for the extinction spectroscopy

Chapter 2 explains the origin of the Plasmon peak from the nano-gold (sensors), then the set up that we have been using in our measurements (as depicted in the section3.4 of the third chapter) shows clearly how the plasmon peak is not static, but dynamic (it shifts), in time, due to the change of the environment (change of the refractive index), in the sensing volume. So, to be able to collect all these shifts (red-shift towards the long wavelengths, or blue—shift towards the short wavelengths) in time and be able to interpret the phenomena happening on the surface (see Chapter 4) it proved necessary to use a time-dependent fitting procedure for the obtention of the curve explaining the processes in the entire time interval.

To be able to fit this instantaneous data, Dahlin et al, 2006 [II.1]* define an algorithmic procedure (used in our case) consisting on calculating the centroid (or center of mass) of the peak and evaluate it on a high –degree polynomial fit to the data using the peak parameters shown on figure II.1.

Basically we start with the instantaneous or discrete extinction spectrum of which can be expressed (referring to equation 3.1) as

$$E(\lambda,t) = \log_{10}\left(\frac{reference(\lambda)}{counts(\lambda,t) - dark(t)}\right) \qquad \text{(II.1)}$$

where $counts(\lambda,t)$ is the raw data spectrum acquired from the detector at time t.

Then the continuous analytical expression of the resulting in tracking the extinction peak position is achieved by fitting, on a high-degree polynomial fit, of discrete data of the extinction spectra according to

$$E_{fitted}(\lambda,t) = \sum_{k=0}^{n} P_{k+1}\lambda^{k} \qquad \text{(II.2)}$$

* **[II.1]Andreas B. Dahlin, Jonas O. Tegenfeldt, and Fredrik Höök, Improving the Instrumental Resolution of Sensors Based on Localized Surface Plasmon Resonance, Anal. Chem. 2006, 78, 4416-4423**

Where n is the degree of the polynomial (in this cased n=20), P is the vector containing the parameters defining the polynomial. This polynomial fit was done using the built in MatLab© function *polyfit* which operates according to a least-square principle. To make the fit better, the λ vector has to be scaled by the subtraction of the mean wavelength value and divided by the standard deviation of the same λ vector; so that the P vector regenerates the spectral data from scaled wavelength values.

From the fact that the extinction spectrum resulting from this peak fitting suffer noise, the same paper (Dahlin et al, 2006[II.1]) propose an algorithm of for tracking the centroid (or center of mass) of the peak, with parameters defined in the figure1; Here down.

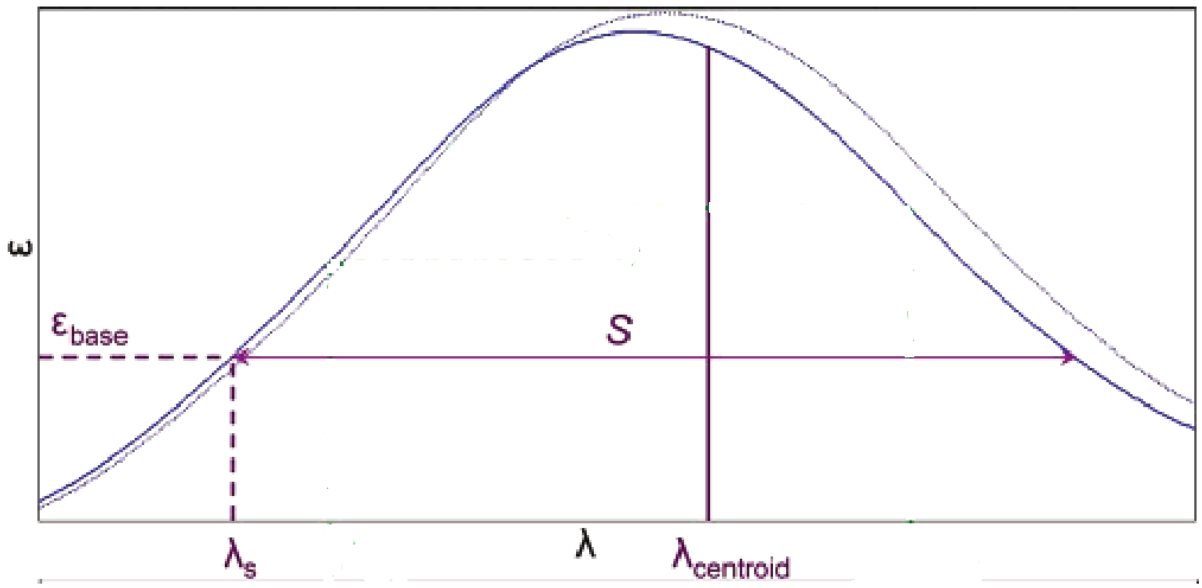

figureII. 1*: illustration of the parameters used in the algorithm the parameters used in calculation of* $\lambda_{centroid}$, S, λ_S *and* $E_{baseline}$ *are shown*

S is defined as the constant wavelength span which defines the region of the peak to be included in each centroid calculation. In the implementation, one has to start with $S_{initial}$ = full width at half-maximum of the peak, then apply this centroid tracking algorithm to the continuous function $E_{fitted}(\lambda)$ then avoid the discontinuities associated with end-point λ_S. In other words, S, is fitted to $E_{fitted}(\lambda)$
by solving the equation

$$E_{fitted}(\lambda) - E_{fitted}(\lambda + S) = 0 \qquad \text{(II.3)}$$

Remember to avoid a discontinuity at λ_S, thus providing a region f the spectrum of length S at the left of λ_S used to estimate the center of mass.
Knowing λ_S, we define the baseline value

$$E_{baseline} = E_{fitted} = E_{fitted}(\lambda_S + S) \qquad \text{(II.4)}$$

Then finally, the same calculation method as that done in eq. II.2 is used to express the centroid ($\lambda_{centroid}$) as,

$$\lambda_{centroid}(t) = \frac{\int_{\lambda_S}^{\lambda_S+S} \lambda(E_{fitted}(\lambda,t) - E_{baseline})d\lambda}{\int_{\lambda_S}^{\lambda_S+S} (E_{fitted}(\lambda,t) - E_{baseline})d\lambda} = \frac{\sum_{k=0}^{n}\left[\frac{P_{k+1}}{k+2}((\lambda_S+S)^{k+2} - \lambda_S^{k+2})\right] - \frac{E_{baseline}\times S}{2}(2\lambda_S+S)}{\sum_{k=0}^{n}\left[\frac{P_{k+1}}{k+1}((\lambda_S+S)^{k+1} - \lambda_S^{k+1})\right] - E_{baseline}\times S} \quad \text{(II.5)}$$

What is theoretically known is that the comparison between changes in $\lambda_{centroid}(t)$ and changes in the peak shift ($\Delta\lambda_{peak}$) to be obtained by the sign change of the derivative of the polynomial expressed in eq.II.3) are directly proportional with the proportionality constant~1.

It should to be noticed that in this report a choice was made to present experimental data using the shift in centroid of the Plasmon peak (due to its reduced noise) rather than the peak shift.

Appendix III: full-measurement-time of principal concentrations

The figures represented in this appendix are the 10 of 5 different concentrations: 0.1 mM , 0.05 mM, 0.01 mM and 0.001 mM, 0.0003mM. The shift in the centroid of Plasmon (in blues)and their absorbance (in green) together with their baseline to make sure of the stability in the system. For all these measurement, the system is NaZ907DMSO-ALD

For adsorption time= 30min

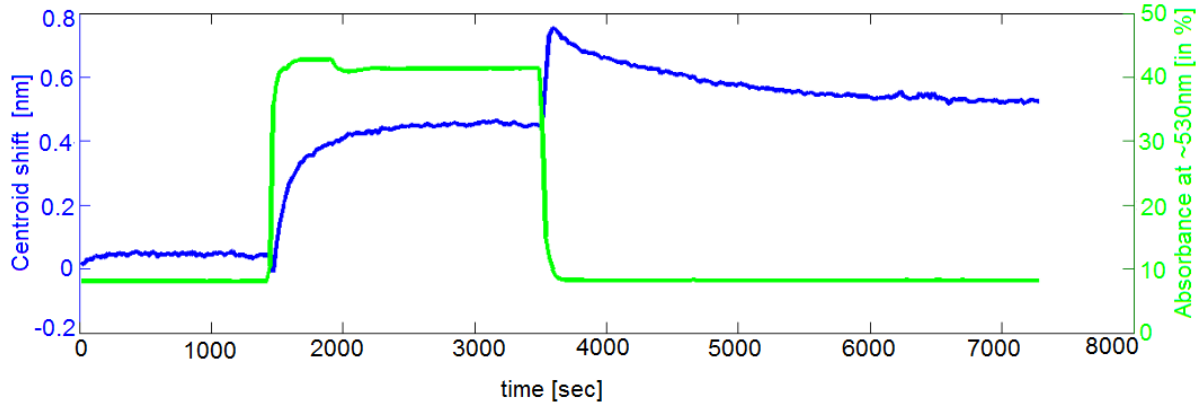

Figure III.1. *Concentration= 0.1 mM , adsorption time= 30min, desorption 60 min*

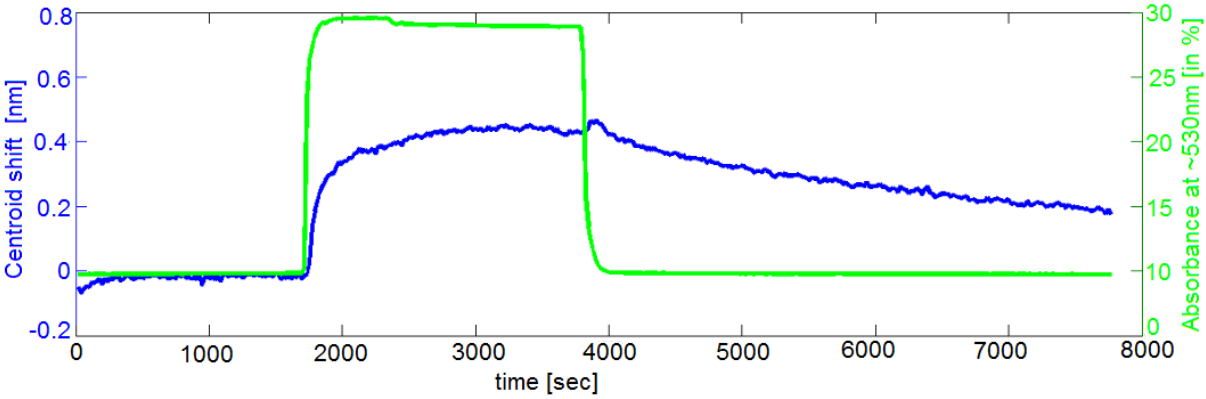

Figure III.2. *Concentration= 0.05 mM , adsorption time= 30min, desorption 60 min*

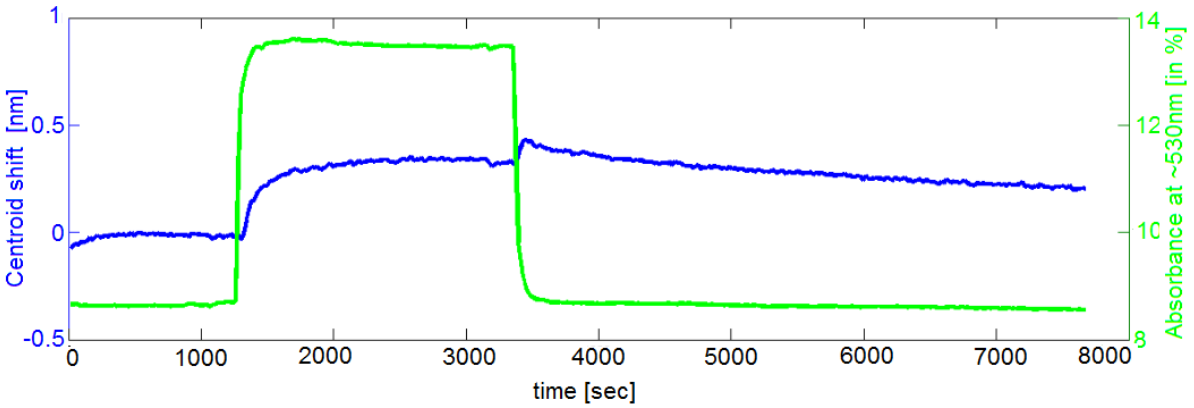

Figure III.3. *Concentration= 0.01 mM , adsorption time= 30min, desorption 60 min*

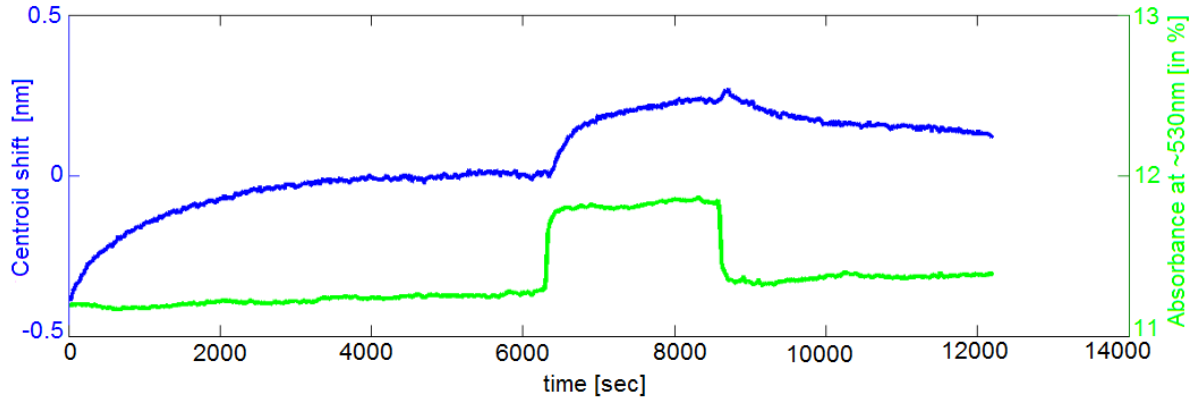

FigureIII.4. *Concentration= 0.001 mM, adsorption time= 30min, desorption 60 min*

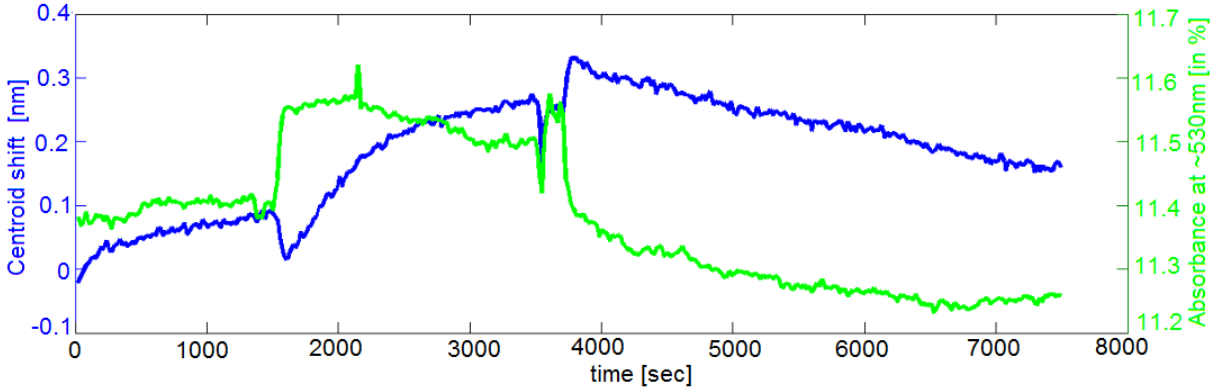

Figure III.5 *Concentration= 0.0003 mM, adsorption time= 30min desorption 60 min*

For adsorption time= 60min

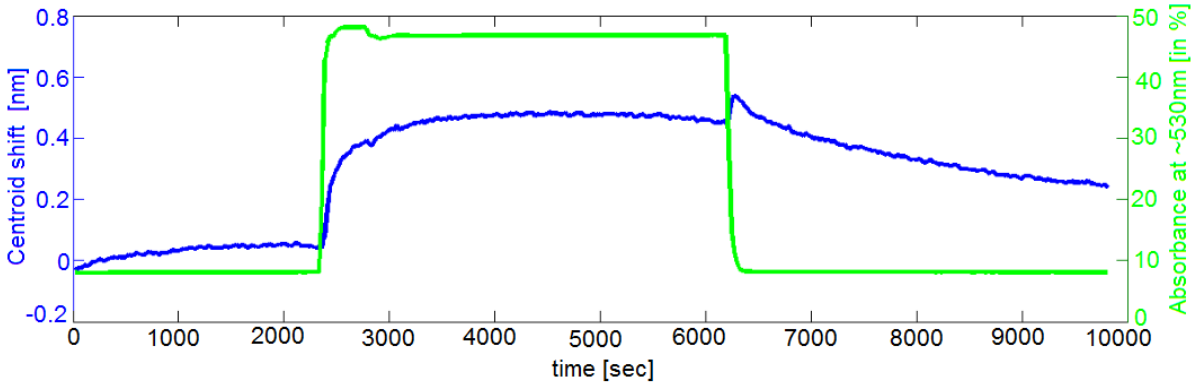

Figure III.6 *Concentration= 0.1 mM, adsorption time= 60min*

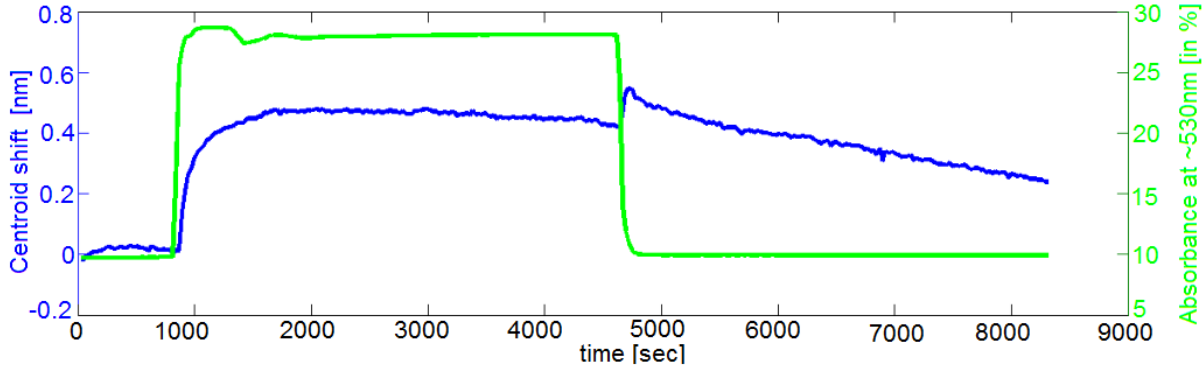

Figure III.7 *Concentration= 0.05 mM, adsorption time= 60min*

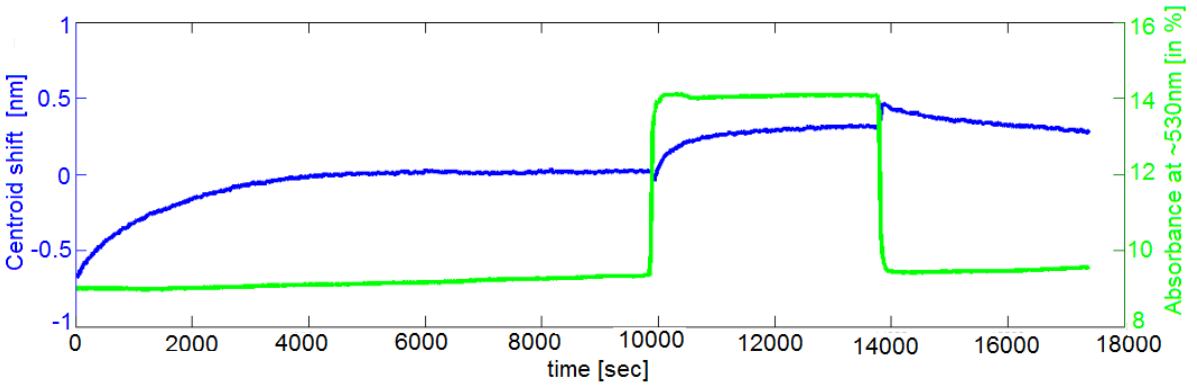

Figure III. 8 *Concentration= 0.01 mM, adsorption time= 60min*

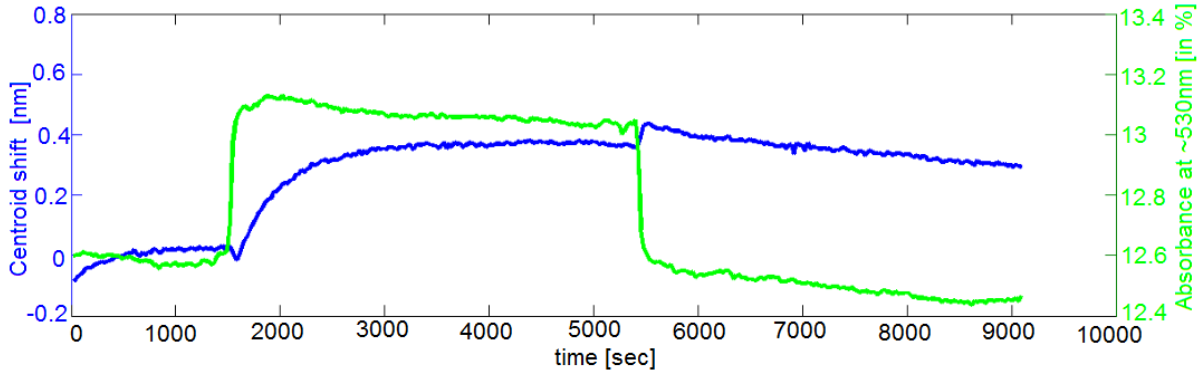

Figure III.9 *Concentration= 0.001 mM , adsorption time= 60min*

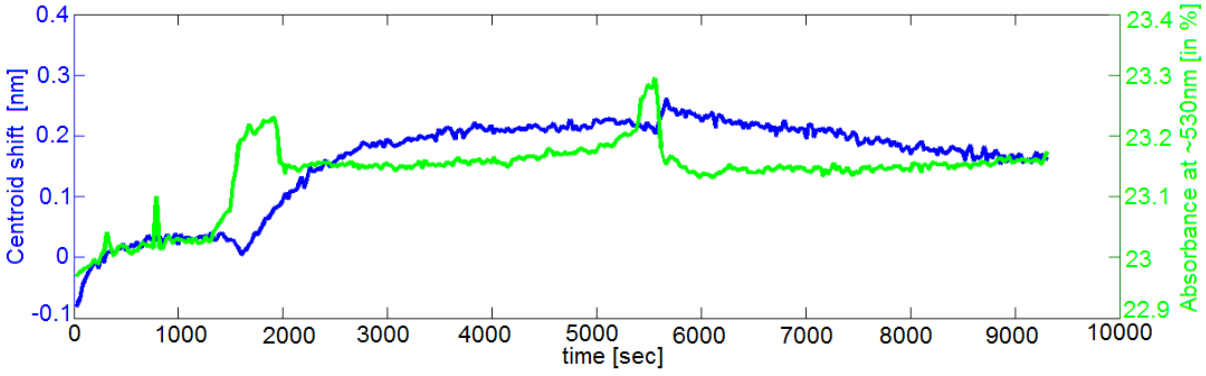

Figure III.10 *Concentration= 0.0003 mM , adsorption time= 60min*